

Development of a CRISPR/Cas9 gene editing system for *Fusarium oxysporum* and characterization of an extracellular superoxide dismutase and its contribution to pathogenicity on cotton

by

Qiang Wang

A dissertation submitted to the Graduate Faculty of
Auburn University
in partial fulfillment of the
requirements for the Degree of
Doctor of Philosophy

Auburn, Alabama
May 4, 2019

Keywords: CRISPR/Cas9, *F. oxysporum*,
Genome modifications, Gene knock-out, EGT, SOD

Copyright 2019 by Qiang Wang

Approved by

Jeffrey Coleman, Chair, Assistant Professor of Plant Pathology
Leonardo De La Fuente, Associate Professor of Plant Pathology
John Murphy, Professor of Plant Pathology
Kathy Lawrence, Professor of Plant Pathology
Tonia Schwartz, Assistant Professor of Biological Sciences

Abstract

The *Fusarium oxysporum* species complex (FOSC) is an important group of filamentous fungi that are able to infect both animals and plants. Based on its economic importance, an effort has been made to better understand the genetics and pathogenicity of members of the FOSC; however, efficient reverse genetic techniques including gene disruption/deletion methods have been limited. One aim of this research was to establish an efficient, stable CRISPR/Cas9 mediated genome editing system for investigating fungal genetics and pathogenicity. In Chapter 2, a transformation method based on Cas9 ribonucleoproteins was developed and used to obtain *URA3* and *URA5* mutants, proving that the Cas9 RNPs could be transferred into fungal protoplasts and function. In addition, the *FoBIK1* gene from a secondary metabolite biosynthetic cluster was mutated using this system and the maximum efficiency of this gene disruption was ~50%. In Chapter 3, the CRISPR/Cas9 system was used to carry out endogenous gene tagging (EGT) for the study of protein subcellular localization using two different integration strategies, homology-independent targeted integration (HITI) and homology-dependent recombination integration (HDRI). The HITI strategy was able to facilitate integration of a large DNA fragment, ~8 kb in length, into the genome of *F. oxysporum* at the sgRNA cleavage site, and was used to insert a C-terminal 3×*sGFP* tag to the *FoCHS5* gene and a N-terminal *mCherry* tag to the *FoSSO2* gene. The HDRI strategy was used to tag the paralogous gene, *FoSSO1*, with a C-terminal mCherry marker. In Chapter 4, an extracellular SOD protein (*FoSOD5*) from *F. oxysporum* was characterized. Expression of

FoSOD5 was dependent on external environmental stimuli and the protein was localized to various cellular structures in different environments, and a *lacZ* expression reporter strain indicated *FoSOD5* was induced in alkaline conditions. Importantly, a Δ *FoSOD5* strain was more sensitive to reactive oxygen species and has attenuated virulence on cotton. Above all, a stable and efficient CRISPR/Cas9 system has been developed for *F. oxysporum* genome editing and was used for investigating gene regulation and protein subcellular localization.

Acknowledgments

Here I sincerely express my appreciation to many people who have helped, supported, and encouraged me in the past four years. First, I would like to thank my advisor Dr. Jeffrey J Coleman for offering me this opportunity to work with him and for his patience, support, and guidance during my graduate study at Auburn University. I appreciate the time and energy he put in to review and provide important comments for my reports and manuscripts.

I would also like to thank my committee members, Dr. Leonardo De La Fuente (Associate Professor, Department of Entomology and Plant Pathology), Dr. John F. Murphy (Professor, Department of Entomology and Plant Pathology), Dr. Kathy Lawrence (Professor, Department of Entomology and Plant Pathology) and Dr. Tonia S. Schwartz (Assistant Professor, Department of Biology) for guidance during my graduate studies, research, and dissertation. In addition, I would like to thank Dr. Paul A. Cobine (Associate Professor, Department of Biology) for welcome guidance of the research and contributions to our paper.

I am thankful to our lab members, Laura Wendell, Yohannes Mehari, Sahar Hasim, Seungyeon Seo, Ambika Pokhrel, and Miranda Otero for your help and friendship. You made lab life wonderful! I love the environment. In addition, I also would like to thank Ni Xiang, Hongyu Chen, Bo Bi, Xiaoli Ma, and Xinyu Zhu for help in both life and research. I deeply appreciate the

assistance and help Dr. Ni Xiang and Hongyu Chen provided me when I arrived in the US in 2015. I would like to thank Bo Bi and Xiaoli Ma for teaching me to drive.

I am grateful for my parents who supported me in studying in the US. Your encouragement enabled me to pursue my dreams. In addition, I would like to thank my wife, Ya, for supporting and encouraging me, especially during my tough time during my graduate career. Although we have been separated for four years, I appreciate our short and cheerful get-togethers, and the memorable trips to beaches, mountains, and other sites.

Table of Contents

Abstract.....	ii
Acknowledgments.....	iv
List of Tables.....	ix
List of Illustrations.....	x
Chapter 1.....	1
Introduction and review of the literature	1
1.1 <i>Fusarium</i> spp.	1
1.2 Fusarium wilt of cotton caused by <i>F. oxysporum</i> f. sp. <i>vasinfectum</i>	2
1.3 <i>F. oxysporum</i> pathogenicity	3
1.4 ROS role for fungal developments and virulence.....	5
1.5 The working mechanism of the CRISPR/Cas9 system for genome editing.....	7
1.6 Various strategies for developing CRISPR/Cas9 tools in filamentous fungi.....	8
Reference	14
Chapter 2.....	18
Efficient genome editing in <i>Fusarium oxysporum</i> based on CRISPR/Cas9 ribonucleoprotein complexes	18
2.1 Introduction.....	18
2.2 Materials and methods	22

2.3 Results and Discussion	28
2.3.1 Identification of an efficient endogenous nuclear localization sequence (NLS) from <i>F. oxysporum</i>	28
2.3.2 Design and protein purification of NLS _{H2B} Cas9 and <i>in vitro</i> cleavage assay.....	29
2.3.3 A PEG-mediated transformation method can transfer NLS _{H2B} Cas9 RNPs into fungal protoplasts.....	29
2.3.4 Homology directed repair (HDR) can efficiently disrupt targeted genes by insertion of a dominant selectable marker.	31
2.3.5 Cas9 RNP-mediated disruption of a gene encoding a polyketide synthase in a secondary metabolite biosynthetic gene cluster.....	32
Reference	35
Chapter 3.....	51
CRISPR/Cas9-mediated endogenous gene tagging in <i>Fusarium oxysporum</i>	51
3.1 Introduction.....	51
3.2 Materials and methods	54
3.3 Results and Discussion	59
3.3.1 Identification of FoChs5, FoSso1, and FoSso2	59
3.3.2 HITI-mediated endogenous gene tagging at the C-terminus of <i>FoCHS5</i>	61
3.3.3 HDRI-mediated endogenous gene C-terminal tagging of <i>FoSSO1</i>	63
3.3.4 HITI-mediated endogenous gene tagging at the N-terminus of <i>FoSSO2</i>	64
Reference	68
Chapter 4.....	83
The extracellular superoxide dismutase Sod5 from <i>Fusarium oxysporum</i> is localized in response	

to external stimuli and contributes to fungal pathogenicity.....	83
4.1 Introduction.....	83
4.2 Materials and Methods.....	87
4.3 Result	98
4.3.1 Identification of an extracellular GPI SOD protein (FoSod5) from <i>F. oxysporum</i> ..	98
4.3.2 FoSod5 was a functional SOD protein.	99
4.3.3 <i>FoSOD5</i> is up-regulated during infection of cotton.	100
4.3.4 <i>FoSOD5</i> was required for full virulence of <i>Fov</i>	101
4.3.5 Expression of <i>FoSOD5</i> is regulated by various carbon sources and repressed in a nutrient rich-medium.	101
4.3.6 <i>FoSOD5</i> is rapidly induced under an alkaline environment.....	103
4.3.7 FoSod5 is only associated with fungal cells	104
4.3.8 Subcellular localizations of FoSod5	105
4.3.9 The GPI anchor is required for proper FoSod5 subcellular localization	106
4.3.10 FoSod5 could be re-localized to the cell wall and septum in the presence of ROS	106
4.3 Discussion.....	107
Reference	110

List of Tables

Table 2.1 Mutation frequencies of homolog directed repair using Cas9 RNPs	46
Table 2.2 The sequences of oligonucleotides used in Chapter 2	47
Table 2.3 The sgRNAs and associated target genes from <i>F. oxysporum</i> in Chapter 2	50
Table 3.1 The sgRNAs and associated transformants of <i>F. oxysporum</i> in Chapter 3.....	79
Table 3.2 The transformant amounts of the N-terminal tagging of <i>FoSSO2</i> gene.....	80
Table 3.3 The sequences of oligonucleotides used in Chapter 3	81
Table 4.1 Strains of <i>F. oxysporum</i> used in Chapter 4	124
Table 4.2 The sequences of oligonucleotides used in Chapter 4.....	125

List of Illustrations

Figure 1	CRISPR/Cas9 gene editing system and DNA repair mechanisms.	17
Figure 2.1	Determination of an endogenous NLS from the <i>F. oxysporum</i> histone <i>H2B</i> gene..	38
Figure 2.2	Protein purification and <i>in vitro</i> cleavage activity assay.	39
Figure 2.3	Disruption of two <i>F. oxysporum</i> genes, <i>URA5</i> and <i>URA3</i> , using the optimized Cas9 RNP transformation system.	40
Figure 2.4	The phenotypes of <i>ura5</i> and <i>ura3</i> mutants obtained by NHEJ and HDR methods.	41
Figure 2.5	<i>FoBIK1</i> gene encoding a polyketide synthase in a secondary metabolite biosynthetic cluster is the core enzyme responsible for the biosynthesis of a red pigment.....	42
Figure 2.6	Schematic diagram of Cas9 RNPs-directed delivery method to <i>F. oxysporum</i> protoplasts to efficiently generate gene disruptions/deletions.	43
Figure 2.7	Histone H2B amino acid sequence alignment of different <i>Fusarium</i> species.....	44
Figure 2.8	Analysis of the compounds in the supernatant of wild type (WT) and a $\Delta Fobik1$ transformant by mass spectrometry.	45
Figure 3.1	Identification of FoChs5, FoSso1 and FoSso2 proteins in <i>F. oxysporum</i>	70
Figure 3.2	<i>FoCHS5</i> gene C-terminal tagging with a 3×sGFP fluorescent marker based on the HITI strategy.	71
Figure 3.3	<i>FoSSO1</i> gene C-terminal tagging with a mCherry fluorescent marker based on the HDRI strategy.	72

Figure 3.4	<i>FoSSO2</i> gene tagging with a N-terminal <i>mCherry</i> fluorescent marker based on the HITI strategy.	73
Figure 3.5	Screen of the correct HITI transformants for generation of <i>FoCHS5-3×sGFP</i>	74
Figure 3.6	Screen of the correct HDRI transformants for generation of <i>FoSSO1-mCherry</i>	75
Figure 3.7	Each frame of the <i>FoChs5-3×sGFP</i> Z-series stack.	76
Figure 3.8	Each frame of the <i>FoSso1-mCherry</i> Z-series stack.	77
Figure 3.9	Each frame of the <i>mCherry-FoSso2</i> Z-series stack.	78
Figure 4.1	Bioinformatic analysis of <i>FoSod5</i> protein and stress assay.	113
Figure 4.2	<i>FoSOD5</i> gene was up-regulated during the infection and <i>FoSod5</i> was a functional SOD protein.	114
Figure 4.3	CRISPR/Cas9 RNPs-based transformant generation.	115
Figure 4.4	<i>lacZ</i> as a suitable reporter gene was used for <i>in vivo</i> analysis of <i>FoSOD5</i> expressions under different environments in <i>F. oxysporum</i>	116
Figure 4.5	<i>FoSod5C2</i> subcellular localizations under the confocal microscopy.	117
Figure 4.6	GPI site was required for <i>FoSod5</i> subcellular localizations and ROS treatments allowed <i>FoSod5</i> to localize to cell walls and septum in YG media.	118
Figure 4.7	The pathogenicity analysis of <i>FoSOD5</i> gene on the natural host.	119
Figure 4.8	Amino acid multiple sequence alignment of the SOD domain from <i>FoSod5</i> , <i>CaSod5</i> , <i>CaSod1</i> (<i>C. albicans</i>), <i>FoSod1</i> and <i>ScSod1</i> (<i>Saccharomyces cerevisiae</i>).	120
Figure 4.9	The <i>FoSOD5</i> gene replacement and complementation.	121
Figure 4.10	The DNA sequences of target regions of <i>FoSod5C1</i> , <i>FoSod5C2</i> and <i>FoSod5C3</i> transformants.	122
Figure 4.11	The Z-stacks analysis of <i>FoSod5C2</i> on M-100 medium under the confocal microscopy.	123

Chapter 1.

Introduction and review of the literature

1.1 *Fusarium* spp.

Fusarium is a diverse genus with at least 20 species complexes of filamentous fungi that are widely spread in our environment, especially in the soil (Geiser et al., 2013). Although most species are saprobes and rarely cause infections, several *Fusarium* species are important pathogens of humans, animals, and plants. One of the best studied *Fusarium* spp. is *F. graminearum* the predominant agent causing Fusarium head blight (FHB), a devastating disease of wheat and barley. The fungus rapidly causes premature bleaching symptoms on wheat spikelets after infection and produces the well-known mycotoxin deoxynivalenol which can lead to strong emetic effects after consumption (Goswami and Kistler, 2004).

The *F. oxysporum* species complex contains more than 100 formae speciales with a wide range of hosts including plants and humans (Michielse and Rep, 2009). Unlike *F. graminearum*, *F. oxysporum* has no known sexual life cycle. Several well-known formae speciales are responsible for vascular wilt diseases (Table 1.1); for example, *F. oxysporum* f. sp. *cubense* causes Fusarium wilt of banana (Panama disease) and is widely distributed in Africa, Asia, and South America while *F. oxysporum* f. sp. *lycopersici* causes wilt disease on tomato (Ploetz, 2006). The symptoms of Fusarium wilt disease includes browning of the xylem tissue, leaf

yellowing, chlorosis, necrosis, stunting, and wilting. Besides infecting plants, some species can infect humans and cause invasive fusariosis, in particular infecting immunocompromised patients (Nucci and Anaissie, 2007). Although some forma speciales are considered agricultural or human pathogens, several are used as biological agents to control other plant diseases. Nonpathogenic *F. oxysporum* strains could effectively inhibit Fusarium or Verticillium wilts in suppressive soils (Fravel et al., 2003; Veloso and Diaz, 2012). For instance, the nonpathogenic isolate *F. oxysporum* 47 (Fo47) induces expression of plant resistance genes and significantly reduces disease symptoms (Veloso and Diaz, 2012). Increasing evidence has demonstrated that strains of *F. oxysporum* and *F. solani*, and not other Fusarium species, are able to more efficiently establish the suppressive property in soils (Fravel et al., 2003).

1.2 Fusarium wilt of cotton caused by *F. oxysporum* f. sp. *vasinfectum*

F. oxysporum f. sp. *vasinfectum* (FOV) is a soil-borne pathogen that causes Fusarium wilt of cotton and threatens cotton production throughout the world. The disease was first identified in 1892 in cotton growing areas of Alabama in the United States, and subsequently appeared in Egypt, India, Brazil, China, and Australia (Chakrabarti et al. 2011, Holmes et al. 2009). Eight races of FOV have been identified based on their pathogenicity on different cotton cultivars or alternative host plants (Skovgaard et al., 2001). However, this classification system is time consuming, unstable, and influenced by environmental conditions. More recent research has focused on identifying genetic markers associated with each “race” of FOV, which may provide a simple and more reproducible method for identification (Assigbetse et al., 1994; Skovgaard et al., 2001).

Multiple factors can lead to cotton yield losses within a region. When planting susceptible cultivars, farmers may experience high yield losses, and in California there have been reports of total cotton crop loss in some regions. The variability in virulence of FOV populations has an influence on the development of cotton in the field. In addition, factors such as climate conditions, soil fertility, soil type, and interactions with nematodes also contribute to high yield losses (Davis et al., 2006).

FOV initially infects the plant through the root system, enters the vascular tissue via the cortex, and spreads rapidly within the host. It is able to infect cotton at any stage of development (Davis et al., 2006). In the cotton seedling stage, infection results in uneven stands, causing problems for cotton production throughout the season. After infection, older cotton plants show various symptoms such as wilting, chlorosis, leaf necrosis, and dieback (Davis et al. 2006, Chakrabarti et al. 2011). However, it is difficult to distinguish this disease from only these symptoms since the symptoms between Fusarium wilt and Verticillium wilt, another vascular disease of cotton caused by a different pathogen, are similar.

1.3 *F. oxysporum* pathogenicity

Several *F. oxysporum* genomes have been sequenced in recent years (Ma et al., 2010; Schmidt et al., 2016), and revealed these fungi carry mobile chromosomes that contain a high proportion of transposable elements and are involved in pathogenicity. These chromosomes are capable of being transferred horizontally among isolates of *F. oxysporum*, allowing a non-pathogenic isolate to become pathogenic on a particular host plant (Ma et al., 2010).

Plant pathogens may secrete small proteins or chemicals into the host cells to facilitate

infection. *F. oxysporum* is able to secrete numerous proteins into the host xylem tissue, many of which have been identified and referred to as SIX (secreted in xylem) proteins and some have been shown to function as effectors. Fourteen Six proteins have been identified in xylem sap after infection with *F. oxysporum* (Houterman et al., 2007), and among them, Six1, Six3, Six5, and Six6 showed involvement in fungal pathogenicity (Gawehns et al., 2014; Rep et al., 2004). Many of the *SIX* genes including *SIX5*, *SIX6*, and *SIX7* reside on the mobile chromosomes, suggesting these effector encoding genes can be transferred horizontally to other isolates of *F. oxysporum*, potentially leading to the observed host range expansion (Ma et al., 2010). Besides the Six proteins, *F. oxysporum* secretes a plant alkalizing peptide to alter the extracellular pH, ultimately promoting fungal growth during infection and contributing to fungal pathogenesis (Masachis et al., 2016).

F. oxysporum can synthesize some key secondary metabolites involved in fungal virulence. Fusaric acid (FA) was shown to be involved in virulence on both plant and animal hosts (Lopez-Diaz et al., 2018). FA is able to interfere with the water balance in banana leaves, accelerating development of Fusarium wilt symptoms (Ding et al., 2018; Dong et al., 2012). In addition, *F. oxysporum* is able to secrete siderophores, a small, membrane-transmissible, high-affinity iron-chelating compound, which can regulate fungal growth and enhance fungal virulence in low iron conditions (Leal et al., 2013). Some strains of *F. oxysporum* are also able to produce isoleucine- and leucine-conjugated jasmonate (JA-Ile/Leu) and use these compounds to promote infection of the root (Cole et al., 2014).

1.4 ROS role for fungal developments and virulence

Reactive oxygen species (ROS) such as peroxides, superoxide, and hydroxyl radical have long been known as a natural byproduct of normal metabolism and play an important role in cell signaling. The importance of ROS was first recognized as part of the innate immune system of animals where large quantities of ROS, referred to as the 'oxidative burst', can be rapidly released by phagocytes and used for killing invasive microbes (Rada and Leto, 2008). Increasing evidence has shown fungi can regulate ROS levels intercellularly and intracellularly for growth development and virulence (Heller and Tudzynski, 2011).

NADPH-dependent oxidases (Nox) and superoxide dismutases (SOD) are the main enzymes that contribute to the balance of ROS levels. Nox, the most important enzymatic ROS generating class of enzymes, are found in a wide range of organisms. For example, the mammalian *Nox2* gene is responsible for the neutrophil oxidative burst defense response. In fungi, the Nox gene family is composed mainly of three distinct clusters, NoxA, NoxB, and NoxC (Tudzynski et al., 2012). Nox genes are involved in regulating sexual development in filamentous fungi, as in *Aspergillus nidulans* NoxA was required for the development of cleistothecia while the homologous gene was necessary for perithecia development in *Neurospora crassa* (Lara-Ortiz et al., 2003). Additionally, Nox proteins participate in the regulation and development of specific fungal structures including sclerotia and appressoria. Loss of these fungal structures lead to a reduction in fungal survival or virulence (Tudzynski et al., 2012). In *Botrytis cinerea*, two copies of Nox genes, *NoxA* and *NoxB*, were necessary for the development of sclerotia, a compact mass of hardened fungal mycelium that enable fungi to survive in extreme environments (Segmuller et al., 2008).

Since large amounts of ROS can cause various types of cellular damage, superoxide dismutase (SOD) plays a key antioxidant role and is an important enzyme responsible for partitioning superoxide into either oxygen or hydrogen peroxide which can be catalyzed by cellular catalases. Based on the protein folding of the SOD and the required metal cofactors, these proteins can be categorized into three types, Cu/Zn-SOD, Fe/Mn-SOD, and Ni-SOD.

Fungal SOD proteins, primarily the Cu/Zn-SOD and Fe/Mn-SOD types, have been shown to contribute to pathogenicity during fungal infections. In the medically important basidiomycete yeast *Cryptococcus neoformans*, disruption of the Cu/Zn-SOD-encoding gene (*SOD1*) lead to decreased cellular SOD activity and high sensitivity to ROS *in vitro*. The *sod1* mutant was significantly less virulent than the wide-type strain (Cox et al., 2003). Similarly, the homologous *SOD1* genes serve as virulence factors in the phytopathogenic fungi, *F. graminearum* and *S. sclerotiorum* (Veluchamy et al., 2012; Yao et al., 2016). Fe/Mn SODs mainly localize to the mitochondria where endogenous superoxide accumulation occurs (Miller, 2012). The *sod2* mutants (Fe/Mn Sod) in *A. fumigatus* have a reduced growth rate when cultured at high temperatures, while in *C. neoformans var. gattii* *SOD2*, rather than *SOD1*, was shown to be essential for survival during the stationary phase of growth (Lambou et al., 2010; Narasipura et al., 2005).

Recently, a class of extracellular Cu/Zn-SODs have been described that are involved in pathogenesis during fungal infections. These SOD enzymes, containing GPI anchors that allow them to be attached to the fungal cell wall, are regulated by the external environment. Interestingly, some extracellular SODs, like Sod5 from *Candida albicans*, only binds Cu instead of Zn but maintains strong SOD activity. In addition, they can reduce host-derived

superoxide and promote virulence in animal models (Broxton and Culotta, 2016; Frohner et al., 2009).

1.5 The working mechanism of the CRISPR/Cas9 system for genome editing

CRISPR (clustered regularly interspaced short palindromic repeats) is a family of DNA repeats found in ~50% of the sequenced bacterial genomes and ~90% of the archaeal genomes (Hille et al., 2018), and these repeats are homologous to some regions of viruses or other invasive genetic elements. These sequences (pre-crRNAs) are transcribed and later cleaved into short CRISPR RNAs (crRNAs) by one of the Cas proteins. The tracrRNAs, trans-activating crRNAs, direct the maturation of crRNAs by the activities of the widely conserved endogenous RNase III and the CRISPR-associated Csn1 protein (Deltcheva et al., 2011). Cas9, a DNA endonuclease enzyme, can form a simple bacterial immune system with the guide of a crRNA/tracrRNA hybrid to recognize, bind, and ultimately cleave the foreign DNA (Jinek et al., 2012). The crRNA/tracrRNA hybrid was later engineered into a single guide RNA which facilitated experimental design (Jinek et al., 2012).

The recognition of a DNA target region depends on a PAM (protospacer adjacent motif) which is located at the 3'-terminus of a 20 bp target sequence. Once the CRISPR/Cas9 complex recognizes the target DNA sequence, it will generate a double strand break (DSB) at the DNA target region between the final third and fourth nucleotides which will activate the host DNA repair process. Two cellular DNA repair mechanisms, non-homologous end joining (NHEJ) and homologous recombination (HR), play essential roles in precise genome editing and gene manipulation. NHEJ was usually viewed as an error-prone repair mechanism that generates

short insertions or deletions of nucleotides in close proximity to the DSB site(s) (Rodgers and McVey, 2016). If these short insertions or deletions exist in a gene coding region or within a portion of the promoter involved in recruiting proteins involved in transcription, the function of the endogenous gene will be disrupted. Consequently, this procedure is widely used for generating gene knock-outs. However, increasing evidence indicated that NHEJ was not always error-prone (Betermier et al., 2014). Recently, a homology independent targeted integration (HITI) strategy was devised and allowed fragments to be integrated into the genome by NHEJ repair mechanisms. Interestingly, the integration can occur in both dividing and non-dividing cells with a high probability of perfect DNA repair at the gRNA cleavage site (Guo et al., 2018; Suzuki et al., 2016). The second well-known DSB repair pathway is based on homologous recombination (HR). In HR where a template exists, DSBs will be repaired based on the templates, allowing the foreign DNA fragments to be precisely integrated into the host genome. However, HR-mediated DSB repair only occurs in dividing cells, limiting the application of this method to a broad range of uses (Fig 1).

1.6 Various strategies for developing CRISPR/Cas9 tools in filamentous fungi

Unlike animal cell lines, fungi have thick cell walls and can have a complicated genetic background as it is not uncommon for fungi to have many duplicated loci, have undergone whole genome duplications, or harbor supernumerary chromosomes. Transformation of filamentous fungi usually requires the remove all of the cell wall generating protoplasts or utilizes electrical shock. Consequently, various versions of CRISPR/Cas9 tools have been

developed for fungi and each of these methods may be the preferred methods for a particular fungus. The yeast *Saccharomyces cerevisiae* was the first fungus that CRISPR/Cas9 was used to genetically modify the genome (DiCarlo et al., 2013), and the ability of this fungus to stably maintain plasmids facilitated CRISPR/Cas9 tool development. Usually these plasmids contain the Cas9 gene under constitutive expression, and when coupled with transient gRNA cassette transformation, generates DSBs thereby increasing homologous recombination rates (DiCarlo et al., 2013). Previously, gene manipulation in the clinically relevant yeast *C. albicans* was tedious as the fungus is a diploid; however development of a CRISPR/Cas9 method provided an efficient way to generate homozygous mutations and facilitated genome engineering in this organism (Vyas et al., 2015).

Based on these initial CRISPR/Cas9 developments with yeasts, this gene editing tool was adapted to filamentous fungi, in which several methods currently exist for both model and non-model fungi. A CRISPR/Cas9 system was first established in the filamentous fungus *Trichoderma reesei* using a codon-optimized *Cas9* gene that was introduced into the genome using *Agrobacterium tumefaciens*-mediated transformation (Liu et al., 2015). When the expression of *Cas9* was under the control of either a constitutive or inducible promoter, there was obvious alteration in the function of other proteins as observed by fungal morphology and various other phenotypes. The successful integration of *Cas9* into the fungal genome generated a strain (a 'Cas9' strain) that requires only the sgRNA for genome editing through protoplast transformation, providing a method to rapidly target multiple genes simultaneously (Liu et al., 2015).

The random integration of the *Cas9* gene into the host genome may induce undesired

mutations, and obtaining a ‘Cas9’ fungal strain may require screening several transformants or optimizing the codon usage of the *Cas9* gene due to different codon preference for each species. Another caveat is the constitutive expression of *Cas9* and/or the long-time retention in host cells may generate off-target effects (Kuscu et al., 2014). To overcome these limitations, transient expression systems of the *Cas9* gene and gRNA in filamentous fungi have been utilized. A transient expression CRISPR/Cas9 system was developed in the model filamentous fungus, *N. crassa* (Matsu-Ura et al., 2015), where the *Cas9* gene was engineered with the *trpC* constitutive promoter from *A. nidulans*, and the Small Nucleolar RNA 52 (SNR52) promoter from *S. cerevisiae* was used to drive gRNA expression. The editing efficiency gradually increased with increasing number of copies of *Cas9* and quantity of gRNA plasmids. The replacement of the endogenous promoter of the *clr-2* gene with the β -*tubulin* promoter and the insertion of a codon optimized firefly luciferase cassette suggested that this strategy was feasible and efficient in filamentous fungi (Matsu-Ura et al., 2015).

A CRISPR/Cas9 gene editing tool for the multinucleate filamentous phytopathogenic fungus *Sclerotinia sclerotiorum* has been reported (Li et al., 2018). Cas9 and gRNA are able to be transiently expressed in the protoplasts and function properly. Interestingly, plasmid fragments of various lengths are integrated into the Cas9/sgRNA cleavage site by the NHEJ repair pathway, generating mutants with large insertions of the plasmid (Li et al., 2018). Using this tool, the *Ssoah1* gene which is involved in the accumulation of oxalic acid was disrupted, and the Δ *Ssoah1* strain was unable to acidify the growth medium and change the pH indicator (Li et al., 2018).

Although filamentous fungi cannot stably maintain most plasmids, several chromosomal

replicators, including AMA1 and MATE elements, have provided a possible mechanism for extrachromosomal maintenance of plasmids in filamentous fungi (Aleksenko and Clutterbuck, 1997). AMA1 plasmids can significantly enhance transformation efficiency, and are able to be easily lost after transformation without selection, allowing the dominant selectable marker(s) to be reused for additional transformation procedures. In addition, the *Cas9-sgRNA* gene cassette on the AMA1 plasmids is less likely to be inserted into the fungal genome during transformation. Based on these advantages, several CRISPR/Cas9 systems utilize AMA1 plasmids for filamentous fungi (Nielsen et al., 2017; Nodvig et al., 2015; Pohl et al., 2016). In one of the first studies using this method, Nodvig et al. successfully induced mutagenesis of the *yA* gene in *A. nidulans*, which was responsible for producing the yellow color of conidia (Nodvig et al., 2015). In this study, the expressions of the *gRNA* depended on two key components, an intrinsic hammerhead (HH) ribozyme and a hepatitis delta virus (HDV) ribozyme. Both can be self-cleaved and allowed the precise initiation of *gRNA* (Nodvig et al., 2015). In addition, Pohl et al. knocked out a polyketide synthetase (*pks17*) from *Penicillium chrysogenum*, which was involved in formation of a green pigment in spores, resulting in a mutant where the colony color changed from green to white (Pohl et al., 2016).

All of these CRISPR/Cas9 systems in filamentous fungi require a functional host transcription or translation system for the expression of the foreign Cas9 gene and *gRNA* transcription. Appropriate promoters must be chosen for both the Cas9 and *gRNA* expression, requiring various promoters to be attempted and perhaps optimized for Cas9 gene expression in different filamentous fungi. In addition, the synthesis of *gRNA* is controlled by the RNA polymerase III (Pol III) promoters like the U6 promoter and requires precise transcription

initiation. A considerable amount of time and effort is necessary for optimizing a plasmid-based Cas9/gRNA delivery method. Consequently, more recent attempts have used a Cas9 RNP-based delivery method for genome editing in different species, including Arabidopsis, fruit fly, zebrafish, and human cell lines. Cas9 RNPs consist of the purified Cas9 protein and *in vitro* transcribed gRNA, and both components are assembled *in vitro* into a complex and directly transfected to the host cells for gene editing. Compared to plasmid-based delivery, the Cas9 RNPs-based delivery has several advantages including: 1) the expression of the *Cas9* gene and transcription of the gRNA does not rely on host machinery, and therefore the precise transcription initiation of the gRNA is not a concern; 2) the assembled Cas9 RNPs have immediate cleavage activity and can be directly delivered into the host cells to target the specified DNA locus without having to express Cas9 or transcribe the gRNA; 3) the cleavage efficiency of the different gRNAs can be evaluated *in vitro*, allowing a more optimal gRNA to be chosen for further experiments; 4) Cas9 RNPs will be removed over a short timeframe from host cells by protein degradation pathways, reducing the possibility of off-target activity of Cas9.

Cas9 RNPs-based delivery methods have been used in filamentous fungi. The well-established polyethylene glycol (PEG)-mediated protoplast transformation technique has been used for Cas9 RNP delivery, in which protoplasts are generated and the Cas9 RNPs added to the recipient fungal protoplasts for genome manipulations. Cas9 RNP is a large ribonucleoprotein, but despite their size Cas9 RNPs can be transferred into fungal protoplasts by PEG-mediated transformation. A simple and universal CRISPR/Cas9 system based on *in vitro*-assembled Cas9 RNPs has been reported in *A. fumigatus* (Al Abdallah et al., 2017), where

two strains, the WT and a *ΔakuB* (disrupting the NHEJ pathway), were used in a study on the CRISPR/Cas9-mediated HR repair mechanism to disrupt *pksP*, a gene responsible for the green color of the conidia. The hygromycin resistance cassette flanked with two microhomology sequences (35~50 bp) at both ends of the cassette would serve as both the selective marker and the donor template for insertion into the Cas9 RNP cleavage sites. With the *ΔakuB* laboratory strain, up to 97% of the colonies showed the desired phenotypes regardless of using a 35 bp or 50 bp homology sequence while in the WT strain, the efficiency was 40~74%, and the length of microhomology directly influenced the integration efficiency (Al Abdallah et al., 2017).

Reference

- Al Abdallah, Q., et al., 2017. A Simple and Universal System for Gene Manipulation in *Aspergillus fumigatus*: In Vitro-Assembled Cas9-Guide RNA Ribonucleoproteins Coupled with Microhomology Repair Templates. *mSphere*. 2.
- Aleksenko, A., Clutterbuck, A. J., 1997. Autonomous plasmid replication in *Aspergillus nidulans*: AMA1 and MATE elements. *Fungal Genet Biol.* 21, 373-87.
- Assigbetse, K. B., et al., 1994. Differentiation Of *Fusarium-Oxysporum* F Sp *Vasinfectum* Races on Cotton by Random Amplified Polymorphic DNA (Rapid) Analysis. *Phytopathology*. 84, 622-626.
- Betermier, M., et al., 2014. Is Non-Homologous End-Joining Really an Inherently Error-Prone Process? *Plos Genetics*. 10.
- Broxton, C. N., Culotta, V. C., 2016. SOD Enzymes and Microbial Pathogens: Surviving the Oxidative Storm of Infection. *Plos Pathogens*. 12.
- Cole, S. J., et al., 2014. Host perception of jasmonates promotes infection by *Fusarium oxysporum* formae speciales that produce isoleucine- and leucine-conjugated jasmonates. *Molecular Plant Pathology*. 15, 589-600.
- Cox, G. M., et al., 2003. Superoxide dismutase influences the virulence of *Cryptococcus neoformans* by affecting growth within macrophages. *Infection And Immunity*. 71, 173-180.
- Davis, R. M., et al., 2006. *Fusarium* wilt of cotton: Population diversity and implication for management. *Plant Disease*. 90, 692-703.
- Deltcheva, E., et al., 2011. CRISPR RNA maturation by trans-encoded small RNA and host factor RNase III. *Nature*. 471, 602-7.
- DiCarlo, J. E., et al., 2013. Genome engineering in *Saccharomyces cerevisiae* using CRISPR-Cas systems. *Nucleic Acids Research*. 41, 4336-4343.
- Ding, Z. J., et al., 2018. Fusaric acid is a virulence factor of *Fusarium oxysporum* f. sp *cubense* on banana plantlets. *Tropical Plant Pathology*. 43, 297-305.
- Dong, X., et al., 2012. Fusaric acid is a crucial factor in the disturbance of leaf water imbalance in *Fusarium*-infected banana plants. *Plant Physiology And Biochemistry*. 60, 171-179.
- Fravel, D., et al., 2003. *Fusarium oxysporum* and its biocontrol. *New Phytologist*. 157, 493-502.
- Frohner, I. E., et al., 2009. *Candida albicans* cell surface superoxide dismutases degrade host-derived reactive oxygen species to escape innate immune surveillance. *Molecular Microbiology*. 71, 240-252.
- Gawehns, F., et al., 2014. The *Fusarium oxysporum* Effector Six6 Contributes to Virulence and Suppresses I-2-Mediated Cell Death. *Molecular Plant-Microbe Interactions*. 27, 336-348.
- Geiser, D. M., et al., 2013. One Fungus, One Name: Defining the Genus *Fusarium* in a Scientifically Robust Way That Preserves Longstanding Use. *Phytopathology*. 103, 400-408.
- Goswami, R. S., Kistler, H. C., 2004. Heading for disaster: *Fusarium graminearum* on cereal crops. *Molecular Plant Pathology*. 5, 515-525.
- Guo, T., et al., 2018. Harnessing accurate non-homologous end joining for efficient precise deletion in CRISPR/Cas9-mediated genome editing. *Genome Biol*. 19, 170.
- Heller, J., Tudzynski, P., 2011. Reactive oxygen species in phytopathogenic fungi: signaling, development, and disease. *Annu Rev Phytopathol*. 49, 369-90.
- Hille, F., et al., 2018. The Biology of CRISPR-Cas: Backward and Forward. *Cell*. 172, 1239-1259.
- Houterman, P. M., et al., 2007. The mixed xylem sap proteome of *Fusarium oxysporum*-infected tomato plants. *Mol Plant Pathol*. 8, 215-21.

- Jinek, M., et al., 2012. A programmable dual-RNA-guided DNA endonuclease in adaptive bacterial immunity. *Science*. 337, 816-21.
- Kuscu, C., et al., 2014. Genome-wide analysis reveals characteristics of off-target sites bound by the Cas9 endonuclease. *Nature Biotechnology*. 32, 677-+.
- Lambou, K., et al., 2010. Functional analysis of the superoxide dismutase family in *Aspergillus fumigatus*. *Molecular Microbiology*. 75, 910-923.
- Lara-Ortiz, T., et al., 2003. Reactive oxygen species generated by microbial NADPH oxidase NoxA regulate sexual development in *Aspergillus nidulans*. *Mol Microbiol*. 50, 1241-55.
- Leal, S. M., et al., 2013. Targeting Iron Acquisition Blocks Infection with the Fungal Pathogens *Aspergillus fumigatus* and *Fusarium oxysporum*. *Plos Pathogens*. 9.
- Li, J., et al., 2018. Introduction of Large Sequence Inserts by CRISPR-Cas9 To Create Pathogenicity Mutants in the Multinucleate Filamentous Pathogen *Sclerotinia sclerotiorum*. *MBio*. 9.
- Liu, R., et al., 2015. Efficient genome editing in filamentous fungus *Trichoderma reesei* using the CRISPR/Cas9 system. *Cell Discovery*. 1.
- Lopez-Diaz, C., et al., 2018. Fusaric acid contributes to virulence of *Fusarium oxysporum* on plant and mammalian hosts. *Molecular Plant Pathology*. 19, 440-453.
- Ma, L. J., et al., 2010. Comparative genomics reveals mobile pathogenicity chromosomes in *Fusarium*. *Nature*. 464, 367-373.
- Masachis, S., et al., 2016. A fungal pathogen secretes plant alkalizing peptides to increase infection. *Nature Microbiology*. 1.
- Matsu-Ura, T., et al., 2015. Efficient gene editing in *Neurospora crassa* with CRISPR technology. *Fungal Biol Biotechnol*. 2, 4.
- Michielse, C. B., Rep, M., 2009. Pathogen profile update: *Fusarium oxysporum*. *Molecular Plant Pathology*. 10, 311-324.
- Miller, A. F., 2012. Superoxide dismutases: ancient enzymes and new insights. *FEBS Lett*. 586, 585-95.
- Narasipura, S. D., et al., 2005. Characterization of *Cryptococcus neoformans* variety *gattii* SOD2 reveals distinct roles of the two superoxide dismutases in fungal biology and virulence. *Molecular Microbiology*. 55, 1782-1800.
- Nielsen, M. L., et al., 2017. Genes Linked to Production of Secondary Metabolites in *Talaromyces atrovirens* Revealed Using CRISPR-Cas9. *Plos One*. 12.
- Nodvig, C. S., et al., 2015. A CRISPR-Cas9 System for Genetic Engineering of Filamentous Fungi. *Plos One*. 10.
- Nucci, M., Anaissie, E., 2007. *Fusarium* infections in immunocompromised patients. *Clin Microbiol Rev*. 20, 695-704.
- Ploetz, R. C., 2006. *Fusarium* wilt of banana is caused by several pathogens referred to as *Fusarium oxysporum* f. sp. *cubense*. *Phytopathology*. 96, 653-656.
- Pohl, C., et al., 2016. CRISPR/Cas9 Based Genome Editing of *Penicillium chrysogenum*. *Acs Synthetic Biology*. 5, 754-764.
- Rada, B., Leto, T. L., 2008. Oxidative innate immune defenses by Nox/Duox family NADPH oxidases. *Contrib Microbiol*. 15, 164-87.
- Rep, M., et al., 2004. A small, cysteine-rich protein secreted by *Fusarium oxysporum* during colonization of xylem vessels is required for I-3-mediated resistance in tomato. *Molecular Microbiology*. 53, 1373-1383.
- Rodgers, K., McVey, M., 2016. Error-Prone Repair of DNA Double-Strand Breaks. *J Cell Physiol*. 231, 15-24.
- Schmidt, S. M., et al., 2016. Comparative genomics of *Fusarium oxysporum* f. sp. *melonis* reveals the secreted protein recognized by the Fom-2 resistance gene in melon. *New Phytologist*. 209, 307-318.

- Segmuller, N., et al., 2008. NADPH oxidases are involved in differentiation and pathogenicity in *Botrytis cinerea*. *Mol Plant Microbe Interact.* 21, 808-19.
- Skovgaard, K., et al., 2001. Evolution of *Fusarium oxysporum* f. sp. *vasinfectum* Races Inferred from Multigene Genealogies. *Phytopathology.* 91, 1231-7.
- Suzuki, K., et al., 2016. In vivo genome editing via CRISPR/Cas9 mediated homology-independent targeted integration. *Nature.* 540, 144-+.
- Tudzynski, P., et al., 2012. Reactive oxygen species generation in fungal development and pathogenesis. *Curr Opin Microbiol.* 15, 653-9.
- Veloso, J., Diaz, J., 2012. *Fusarium oxysporum* Fo47 confers protection to pepper plants against *Verticillium dahliae* and *Phytophthora capsici*, and induces the expression of defence genes. *Plant Pathology.* 61, 281-288.
- Veluchamy, S., et al., 2012. The CuZn superoxide dismutase from *Sclerotinia sclerotiorum* is involved with oxidative stress tolerance, virulence, and oxalate production. *Physiological And Molecular Plant Pathology.* 78, 14-23.
- Vyas, V. K., et al., 2015. A *Candida albicans* CRISPR system permits genetic engineering of essential genes and gene families. *Science Advances.* 1.
- Yao, S. H., et al., 2016. A cytoplasmic Cu-Zn superoxide dismutase SOD1 contributes to hyphal growth and virulence of *Fusarium graminearum*. *Fungal Genetics And Biology.* 91, 32-42.

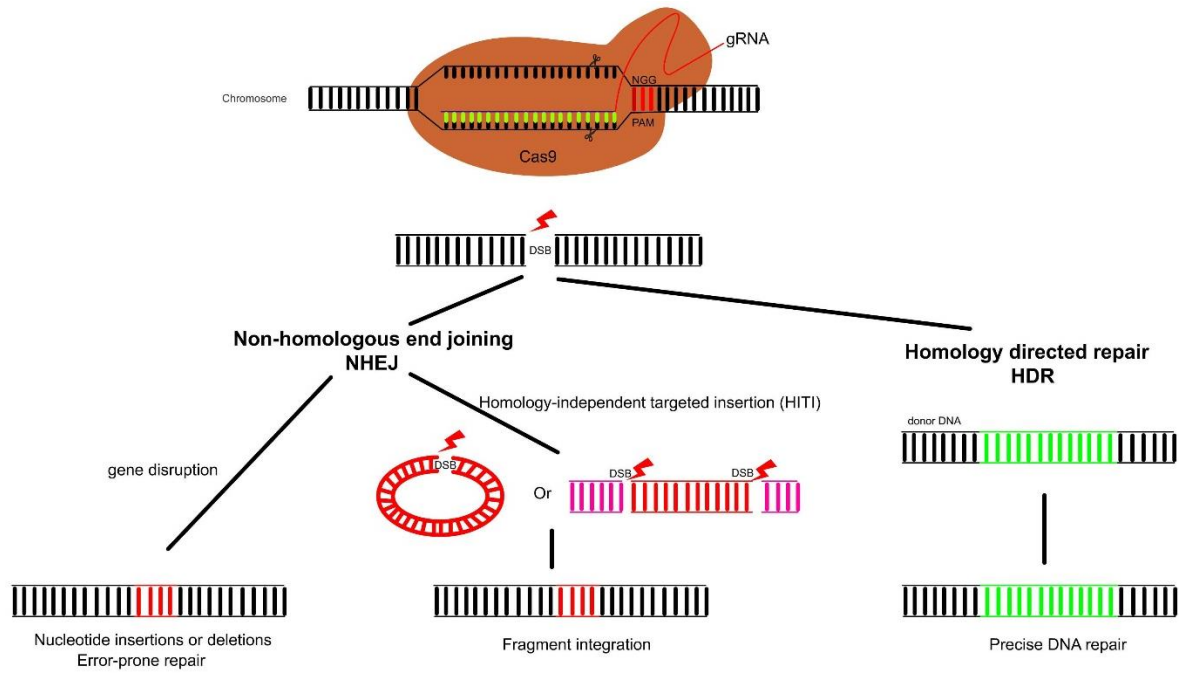


Figure 1 CRISPR/Cas9 gene editing system and DNA repair mechanisms.

With the gRNA, Cas9 can cleave double stranded DNA (inducing dsDNA breaks, DSBs) at specific sites, activating the host DNA repair mechanism. Two well-known DNA repair pathways, NHEJ and HDR, were utilized for host genome modifications. NHEJ could disrupt the desired genes due to an error in the DNA repair or integration of fragments into the genome by HDR and precise DNA repair.

Chapter 2.

Efficient genome editing in *Fusarium oxysporum* based on CRISPR/Cas9 ribonucleoprotein complexes

This chapter has been published (Wang et al., 2018).

2.1 Introduction

Fungi in the genus *Fusarium* originated during the Cretaceous period and are currently represented by at least 20 species complexes containing isolates that are able to cause diseases in plants, animals, and humans (Geiser et al., 2013; O'Donnell et al., 2013). They are well known to produce a diverse array of secondary metabolites including mycotoxins that contaminate food and poison livestock leading to reduced production (Geiser et al., 2013; Hansen et al., 2012; O'Donnell et al., 2013). One of these groups, the *Fusarium oxysporum* species complex (FOSC), are soil-borne filamentous fungi that have an extensive host range from plants to animals. These isolates carry small supernumerary chromosomes that harbor host-specific virulence factors that are capable of being horizontally transferred to other FOSC isolates and increase host range (Ma et al., 2010; van Dam et al., 2017). In agriculture, *F. oxysporum* is an important plant pathogen that is able to cause significant economic damage on various plant species including tomato, banana, legumes, and cotton (Michielse and Rep, 2009). This fungus infects the root system of a susceptible host and eventually colonizes the

xylem system, where it blocks the translocation of water and nutrients, resulting in chlorosis, necrosis, stunting, and wilting. Clinically, members of the FOOSC are responsible for ~20% of the disseminated *Fusarium* infections termed fusariosis (Muhammed et al., 2013; Nucci and Anaissie, 2007) and have been implicated in several disease outbreaks such as nosocomial infections due to contaminated water supplies and contact lens associated keratitis (Chang et al., 2006; Edel-Hermann et al., 2016; O'Donnell et al., 2004).

Reverse genetic approaches utilizing gene deletion/disruption technologies have played an essential role in studies identifying the function of a gene. Recently, the CRISPR (clustered regularly interspaced short palindromic repeats)-Cas9 system, derived from the bacterial and archaeal immune system, has been developed into a powerful gene editing tool (Doudna and Charpentier, 2014; Hsu et al., 2014; Ran et al., 2013). Based on the highly efficient gene targeting editing and low off-target rates, this tool has become popular and has been widely used in model or non-model organisms such as fruit fly, zebrafish, *Arabidopsis*, yeast, mouse, and human cell cultures (Bassett et al., 2014; Jacobs et al., 2014; Jiang et al., 2013; Li et al., 2016; Platt et al., 2014; Shalem et al., 2014). The simple gene editing system includes two components, a single chimeric guide RNA (sgRNA) and the Cas9 endonuclease enzyme. The sgRNA consists of a protospacer sequence which targets the expected DNA region by base pairing, and is able to interact with Cas9 to become a stable complex. Once the base pairing has occurred, Cas9 cuts the double-stranded DNA *in vivo*, subsequently activating DNA repair mechanisms. One method of DNA repair involves random insertion or deletion of nucleotides at the DNA cleavage site (Non-Homologous End Joining, NHEJ). The NHEJ mechanism tends to repair the DNA incorrectly, and if this repair occurs in a gene coding region, the associated

gene is likely to be inactivated. In contrast, when a template with homologous sequence is present, the cleaved DNA region could be repaired using the homologous sequence as a template. The main benefits of this gene disruption/deletion system are accurate gene modification and highly successful mutation rates (Doudna and Charpentier, 2014; Ran et al., 2013).

The development of CRISPR/Cas9 genome editing tools for fungal research has facilitated functional studies. Several gene deletion systems based on CRISPR/Cas9 have been developed in *Saccharomyces cerevisiae*, *Candida albicans*, *Trichoderma*, *Aspergillus*, *Alternaria* and *Neurospora* (DiCarlo et al., 2013; Liu et al., 2015; Matsu-Ura et al., 2015; Nodvig et al., 2015; Vyas et al., 2015; Wenderoth et al., 2017). While these cases showed successful gene disruptions, some limitations still exist. *Trichoderma reesei* was the first filamentous fungus used for CRISPR/Cas9 research, where *Agrobacterium*-mediated fungal transformation was used to insert a codon-optimized Cas9 gene randomly into the genome leading to a potential unintended mutation. Other CRISPR tools have been developed for filamentous fungi that are highly dependent on AMA1-derived plasmids (Nodvig et al., 2015; Pohl et al., 2016; Wenderoth et al., 2017). The AMA1 element is an inverted duplication of a sequence derived from *Aspergillus nidulans*, and it is able to enhance fungal transformation efficiency (Aleksenko and Clutterbuck, 1997). However, experimental evidence has shown that AMA1 plasmid integration occurred in some filamentous fungi and could lead to long-time retention in fungal transformants (Fierro et al., 1996). Additionally, after successful transformation positive colonies may have to be treated with single spore isolation for several rounds to remove the residual AMA1 plasmids (Nodvig et al., 2015; Wenderoth et al., 2017).

Using the Cas9 protein/sgRNA ribonucleoproteins (RNPs) to perform genome editing has several advantages compared with plasmid transformation and Cas9 mRNA/sgRNA transformation. A major advantage is transformation of Cas9 RNPs alleviates the possibility of integration of genetic material to a non-targeted region of the genome. Additionally, Cas9 and sgRNA are able to form a stable ribonucleoprotein *in vitro*, so there is less likelihood of RNA degradation compared with Cas9 mRNA/sgRNA transformation. Furthermore, this method is able to evaluate the target cleavage efficiency of different sgRNA *in vitro*, so a highly efficient sgRNA can be selected for research. This method has been widely used in different organisms such as mouse, human, grape, apple, tobacco, and *Arabidopsis* (Kim et al., 2014; Malnoy et al., 2016; Woo et al., 2015). In plants, an efficient protoplast transformation method for Cas9 RNPs has been developed and mutant individuals can be generated from the Cas9 RNP-modified protoplasts (Woo et al., 2015); however, few studies involving Cas9 RNP transformation for filamentous fungi have been published.

In this study, we developed and optimized a Cas9 RNP transformation procedure for gene editing in the ascomycete fungus, *Fusarium oxysporum*. A PEG-mediated transformation method was used to transfer Cas9 RNPs, which efficiently target the locus of interest, into fungal protoplasts. Several genes that have been well characterized in other fungi were disrupted in *F. oxysporum* with a hygromycin gene cassette using this system, generating mutants displaying strong expected phenotypes based on characterization of orthologous genes. As a proof of concept, the gene encoding the polyketide synthase PKS4 was disrupted using this system and demonstrated this enzyme is responsible for production of the red pigment bikaverin, and in keeping with the established nomenclature of other *Fusarium* spp., refer to it

as *FoBIK1* (Wiemann et al., 2009).

2.2 Materials and methods

2.2.1 Fungal isolate and culture media.

All experiments were conducted using *F. oxysporum* f. sp. *vasinfectum* obtained from the Fungal Genetics Stock Center (FGSC #10442) (McCluskey et al., 2010). This fungus was cultured in Potato Dextrose Broth (PDB), PDB with agar, and minimal medium (M-100) agar plates (Stevens, 1974). All mutants were strictly determined on M-100 agar plates with a hygromycin concentration of 75 µg/mL or a 5-FOA concentration of 1.5 g/L. The wild type and mutant strains were cultured at room temperature (25 °C).

2.2.2 Sequence analysis and fluorescence microscopy.

Amino acid multiple sequence alignment analysis was conducted using Clustal Omega (Sievers et al., 2011), and the nuclear localization signal prediction accomplished using NLStradamus (Nguyen Ba et al., 2009). The subcellular localization of NLS_{H2B}-eGFP was carried out using a Zeiss Axiovert 200 fluorescence microscope. The transformant containing NLS_{H2B}-eGFP was cultured in PDB medium on a rotary shaker (160 rpm) at room temperature for three days. Before microscopic examination, the hyphae were stained with 4',6-diamidino-2-phenylindole (DAPI) at a concentration of 1 µg/mL for 20 min in the dark. The excitation for the DAPI dye was 405 nm while the value for eGFP was 488 nm.

2.2.3 Plasmid construction.

The donor template DNA loci containing the hygromycin cassette were constructed using a NEBuilder® HiFi DNA Assembly Master Mix kit. All template plasmids were constructed

in the background of the pUC19 plasmid with HindIII and BamHI restriction sites. For the construction of the pExFO-NLS_{H2B}eGFP plasmid, the basic plasmid pExFO was constructed in the background of pGEM-T where three fragments, the hygromycin cassette including *pgpdA* promoter amplified from the plasmid pCWHyg1, the *trpC* promoter amplified from the plasmid pII99, and the *tefl* terminator amplified from the plasmid pFFC332, were simultaneously inserted into the SphI and SacI enzyme sites in pGEM-T. Between the *trpC* promoter and the *tefl* terminator, a multiple cloning site (MCS, HindIII-KpnI-NotI-PacI-Sall-SpeI-XbaI) were inserted. The NLS sequence from histone H2B and eGFP sequence were inserted into this MCS region for the construction of pExFO-NLS_{H2B}eGFP. The assembled plasmids were sequenced to confirm they were correct and plasmids were extracted with the E.Z.N.A.[®] plasmid DNA maxi kit (OMEGA, bio-tek) for PEG-mediated transformation.

The plasmid construction for the *E.coli* protein expression and purification was performed with the pHis-parallel1 plasmid (Sheffield et al., 1999). First, the nuclear localization sequence from the H2B gene of *F. oxysporum* was cloned from genomic DNA using primers NLS_{H2B}_BamHIF and NLS_{H2B}_SalIR and inserted into the BamHI and SallI enzyme sites of the pHis-parallel1 plasmid (pHis-parallel1-NLS_{H2B}). The Cas9 gene was cloned from the plasmid pFFC332, and subsequently inserted between the SallI and HindIII sites of the pHis-parallel1-NLS_{H2B} plasmid with the NEBuilder[®] HiFi DNA Assembly Master Mix kit. The plasmids were sequenced to confirm no mutations for inserted fragments. All the primers used for plasmid constructions and sequencing in this study are listed in Table 2.2.

2.2.4 Cas9 protein purification.

The plasmid pHis-parallel1-NLS_{H2B}Cas9 was transformed into Rosetta[™](DE3) strain

which is able to highly express genes containing rare codons. The correctly transformed *E. coli* isolate was determined by PCR using with primers DetCas9F and DetCas9R (Table 2.2). High expression of this protein in the *E. coli* containing the pHis-parallel1-NLS_{H2B}Cas9 plasmid was obtained by first culturing in 50 mL LB liquid medium for 14 h at 37 °C with 100 µg/mL ampicillin. The cultured *E. coli* was used to inoculate 1.5 L of fresh LB liquid medium at a dilution of 1:100. When the OD₆₀₀ value of the *E. coli* cell culture concentration reached 0.6, IPTG was added to a final concentration of 0.3 mM and the culture incubated for an additional 5 h at room temperature (25 °C) at 160 rpm on a rotary shaker. After determining the proper protein expression using a SDS-PAGE gel, the culture was centrifuged at 13000 rpm for 15 min and the pellet suspended in 30 mL lysis buffer (20 mM NaH₂PO₄, 300 mM NaCl, 1 mM imidazole, 1% TritonX-100, 1 mM PMSF, pH 7.5) and lysed in an ultrasonic bath (15 s + 15 s, 10 min). The mixture was centrifuged at 13000 rpm, 4 °C for 15 min, and the supernatants were filtered with a 0.22 µm filter, and subsequent protein purification conducted using HisPur™ Ni-NTA Chromatography Cartridges (Thermo Fisher Scientific). The eluted Cas9 protein was further dialyzed against the Cas9 buffer (20 mM NaH₂PO₄, 300 mM NaCl, 10% glycerol, pH 7.5) for 6-8 h. The dialyzed Cas9 protein was centrifuged and the associated undissolved protein was removed. The Cas9 protein was further concentrated with a 100 K centrifugal filter to a final concentration of 4 mg/mL. The Cas9 nuclease cleavage assay *in vitro* should be conducted immediately. The final purified Cas9 protein was aliquoted into PCR tubes and stored at -30°C for future use. There was no significant difference in cleavage activity of the purified Cas9 protein after a year at -30°C.

2.2.5 sgRNA design and *in vitro* Cas9 nuclease assay.

The sgRNA for gene mutation was designed with the following parameters: 1) the sgRNA cleavage site was located close to the 5' end of the gene coding region; 2) the protospacer and PAM sequence was (N)₂₀NGG, and if the beginning nucleotide of the target sequence lacked a G, at least one G was added after the T7 promoter; 3) similarity to the protospacer and PAM sequence was searched by BLASTn to the *F. oxysporum* genome to avoid cleavage at other loci; and 4) the sgRNA forward primer (T7 promoter-(N)₂₀-GTTTTAGAGCTAGAAATAGCAAG) and the sgRNA universal primer (Table 2.2) were used to generate the sgRNA templates by PCR using the EnGen® sgRNA Synthesis kit (New England Biolabs).

For the *in vitro* cleavage assay mediated by Cas9 with different sgRNAs, a PCR fragment ranging from 1000 bp to 3000 bp was first amplified and purified from the agarose gel with E.Z.N.A® Gel Extraction Kit (OMEGA, bio-tek). The purified Cas9 protein was diluted to a concentration of 200 ng/μL. The cleavage assay was conducted in a system with 20 μL total volume (1 μL diluted purified Cas9 protein, 40 ng sgRNA, 1× Cas9 Nuclease Reaction Buffer, 3 μL 20 nM PCR fragment, DEPC-treated water). All items were added together and incubated 37 °C for 1 h. The final products were analyzed on a 0.8% agarose gel and the associated cleavage efficiency was evaluated with the software, ImageJ (<https://imagej.nih.gov/ij/>). All sgRNAs and the associated targeted genes used in this study are listed in Table 2.3.

2.2.6 PEG-mediated fungal transformation.

PEG-mediated fungal transformation was conducted according as previously described with slight modifications (Coleman et al., 2011b). About 10⁷ conidia were inoculated into 100 mL fresh PDB liquid medium and allowed to germinate at 28 °C at 160 rpm overnight. The

fungal germlings were collected and treated with a mixture of 10 mg/mL Driselase (Sigma) and 15 mg/mL β -Glucanase (Sigma) suspended in 0.7M NaCl for 2-3 h. Fungal protoplasts were collected and washed twice with SuTC buffer. The fungal protoplasts were diluted into a concentration of 2×10^7 per mL with SuTC buffer, and 200 μ L of the protoplast solution was used for each transformation.

The Cas9 RNPs or template donor DNA was prepared during generation of the protoplasts where the Cas9 RNPs were made as follows: a 1:1 mole ratio of Cas9: sgRNA was added into a 50 μ L total volume with 5 μ L 10 \times Cas9 Nuclease Reaction Buffer and DEPC-treated water. This mixture was incubated in a 37 $^{\circ}$ C water bath for 20 min. 200 μ L of fungal protoplasts were mixed with 50 μ L Cas9 RNPs or donor DNA (template) at room temperature for 20 min. An equal volume of 60 % PEG was added into the above system and incubated at room temperature for 20 min. The total system was transferred into a 15 mL tube containing 5 mL TB3 and placed on a rotary shaker (160 rpm at room temperature) for 18-24 h. The regenerated fungal protoplasts were mixed with the selective medium and poured into sterile plates. For screening *ura3* and *ura5* mutants with only Cas9 RNPs transformation, the selective plates with uracil, uridine, and 2 g/L 5-FOA were used. For the *ura5* mutant generation with Cas9 RNPs and donor DNA transformation, the selective plates contained uracil, uridine, and a final concentration of 150 μ g/mL hygromycin. The *Fobik1* mutant selection was accomplished using selective plates with 150 μ g/mL hygromycin. All transformants were visible in 3 ~ 5 days after plating on selective media. The transformants were then transferred onto the minimum nutrient agar medium (M100) with the associated antibiotics for further determination.

Three pairs of primers were used to detect the hygromycin cassette location for HR-

directed mutant determination. The first pair ($H_{in}F + H_{in}R$) was used to detect the presence of the hygromycin phosphotransferase gene. For HR-directed *ura5* mutants, three pairs of primers ($H_{out}F + FoURA5TR$, $FoURA5TF + H_{out}R$ and $FoURA5TF + FoURA5TR$) were used to determine the insertion location of the hygromycin phosphotransferase gene. Similarly, $Det_bik1g1F + Det_bik1g1R$ and $H_{out}F + Det_bik1g2R$ were used to determine HR-directed *Fobik1* gene mutants.

2.7 HPLC and MS analysis.

The wild type and *Fobik1* mutants were inoculated into the fresh PDB liquid medium and grown on a rotary shaker (160 rpm) at room temperature for 7 days. The culture was centrifuged at 13000 rpm for 10 min to remove conidia and hyphae. The supernatant was treated with a 0.22 μ m filter. The supernatant medium from wild type and the *Fobik1* mutant was fractionated on a Sonoma phenyl-hexyl 10- μ m 100-Å (25 cm x 4.6 mm) HPLC column (ES Industries, West Berlin, NJ, USA) which was equilibrated in 1% formic acid and acetonitrile (ACN). The HPLC programs were set as follows: a linear gradient from 20% to 50% ACN was applied over 15 minutes, and a linear gradient from 50% to 75% ACN was used over 5 minutes. The column was washed with 100% ACN for 5 minutes and then was re-equilibrated as above. Fractions were collected and submitted to MS analysis which was performed on a Bruker Micro-TOF MS with flow injection.

2.3 Results and Discussion

2.3.1 Identification of an efficient endogenous nuclear localization sequence (NLS) from *F. oxysporum*.

The Cas9 RNPs must enter into the nucleus in order to bind to the targeted DNA regions. The classical nuclear localization sequence (NLS) SV40 has been shown to be functional in many organisms (Liu et al., 2015), however this NLS was not suitable for *F. oxysporum* and was unable to efficiently translocate GFP into the nucleus (data not shown), similar to observed results with other organisms such as *Phytophthora sojae* (Fang and Tyler, 2016). In order to facilitate Cas9 entering the *F. oxysporum* nucleus, the endogenous nuclear localization sequence from histone H2B was fused to the N-terminus of Cas9. Histone H2B is conserved in eukaryotes and involved in the assembly of the nucleosomes (Mosammamarast et al., 2001). The histone H2B NLS amino acid sequence was highly conserved among *Fusarium* spp., which indicates that this system may be applicable for use in other *Fusarium* species (Fig. 2.7).

Bioinformatic analysis revealed the *F. oxysporum* histone H2B contained a NLS at its N-terminus (NLS_{H2B}, aa: 6-45). The middle and C-terminus amino acids of histone H2B were highly conserved among a diverse group of organisms including other fungi, plants, and metazoans, but the NLS sequences of these organisms has evolved divergently (Fig. 2.1A). In order to confirm the predicted NLS of histone H2B was sufficient to localize a protein to the nucleus of *F. oxysporum*, the first 54 amino acids including the entire NLS sequence were fused to the N-terminus of eGFP under the constitutive promoter of *trpC* (pExFO-NLS_{H2B}eGFP). Transformants of *F. oxysporum* expressing the NLS_{H2B}-eGFP construct contained eGFP

localized to the nuclei of the cells (Fig. 2.1B), indicating the NLS_{H2B} was suitable to engineer a protein to be translocated into the nucleus.

2.3.2 Design and protein purification of NLS_{H2B}Cas9 and *in vitro* cleavage assay.

The endogenous NLS from the *F. oxysporum* histone H2B gene was fused to the N-terminus of the Cas9 gene and cloned into an *E. coli* protein expression plasmid (pHis parallel1-NLS_{H2B}Cas9) which was subsequently transformed into the *E. coli* RosettaTM (DE3) strain for protein expression and purification. The resulting recombinant protein with a molecular weight of approximately 165 kDa was soluble in water and reached a yield at least 4 mg per liter of bacterial culture (Fig. 2.2A). The ability of the purified Cas9 protein to efficiently cleave at a specified target site was evaluated *in vitro*. A ~2.1 kb PCR fragment containing the coding region of the *F. oxysporum* *URA5* gene was mixed with a single guide RNA targeting this locus and the Cas9 protein. The NLS_{H2B}Cas9-FoURA5sgRNA complex was able to cleave almost all of the template *in vitro* within an hour and the lengths of cleaved fragments were of the expected size, supporting that the NLS_{H2B} sequence fusion had no significant influence on the Cas9 endonuclease cleavage activity (Fig. 2.2B).

2.3.3 A PEG-mediated transformation method can transfer NLS_{H2B}Cas9 RNPs into fungal protoplasts.

Recently, Cas9 RNPs have been transferred into plant protoplasts for gene-editing (Malnoy et al., 2016; Woo et al., 2015). This system has at least two advantages in filamentous fungi 1) fungal protoplasts are easier to be regenerated into individual transformants (compared to

plants) and 2) Cas9 RNPs will be degraded in the protoplasts, which further minimizes the potential influence from the Cas9 RNPs being maintained in the cell. A RNP mediated transformation method has been developed for two fungi, *Aspergillus fumigatus* and *Penicillium chrysogenum* (Al Abdallah et al., 2017; Pohl et al., 2016). A PEG-mediated transformation method was developed for the *F. oxysporum* optimized NLS_{H2B}Cas9. The *URA5* gene encoding orotate phosphoribosyltransferase involved in pyrimidine biosynthesis was initially targeted, as mutants of the ortholog in *S. cerevisiae* and other fungi generates uracil auxotrophs and allows for direct selection on media containing 5-fluoro-orotic acid (5-FOA) (de Montigny et al., 1989). Protoplasts transformed with the NLS_{H2B}Cas9-FoURA5sgRNA RNPs should result in cleavage at the target site in the *URA5* coding region and subsequent inactivation of the gene due to NHEJ repair. Seven transformants were generated that were able to grow on 5-FOA selective media containing uracil and uridine. As Cas9 RNPs cleave the dsDNA between the last third and fourth nucleotide at the region targeted by the protospacer element, this region was sequenced to characterize the resulting mutations in the transformants. All these *ura5* mutants contained short nucleotide deletions ranging in size from a single nucleotide to -123 bp in the target region of the guide RNA (Fig. 2.3). The *ura5* mutants were uracil auxotrophs and are able to grow on media containing 5-FOA (Fig. 2.4).

In order to further confirm that PEG-mediated transformation of Cas9 RNPs can be used in *F. oxysporum* protoplasts another sgRNA was generated that targets the homologous gene of *URA3* encoding orotidine 5'-phosphate decarboxylase. This gene is involved in de novo UMP biosynthesis and, similar to *ura5* mutants, *ura3* mutants are uracil auxotrophs and can grow on minimum media containing 5-FOA (Fig. 2.4) (Boeke et al., 1984). The targeted locus of two

randomly selected *ura3* transformants were sequenced and contained short deletions at the Cas9 cleavage site (Fig. 2.3C). Overall, the PEG-mediated transformation of Cas9 RNPs into *F. oxysporum* protoplasts was successful and the transformed particles can cleave the genomic DNA at the target site generating a mutation via an error-prone DNA repair mechanism. Interestingly, among the sequenced transformants, several of the mutants generated using this gene editing tool contained a single nucleotide deletion instead of double or four nucleotide deletions, which suggests the NHEJ repair system of *F. oxysporum* prefers the removal of a single nucleotide at the cleavage site causing a frame-shift mutation in the coding sequence.

2.3.4 Homology directed repair (HDR) can efficiently disrupt targeted genes by insertion of a dominant selectable marker.

To further extend the protocol, experiments were conducted to assess whether donor DNA containing a selective marker and the NLS_{H2B}Cas9 RNPs are able to promote CRISPR–Cas9 induced homologous recombination. The NLS_{H2B}Cas9-FoURA5sgRNA transformation system used for NHEJ mutation above (Fig. 2.3) was selected as it was previously confirmed to have activity at the specified target site in *URA5*. The donor DNA contained the gene encoding hygromycin phosphotransferase (*hph*), conferring resistance to hygromycin, and had ~ 600 bp of homologous sequence flanking both sides of the cleavage site in the *URA5* gene (Fig. 2.3D). Mutants should grow on the selective medium including uracil, uridine, and hygromycin (Fig. 2.4). Of the 14 transformants generated, three contained the *hph* cassette integrated at the gRNA target site (21.4%; Table 2.1). The *ura5* mutants are unable to grow on minimal medium containing hygromycin without uracil and uridine and were resistant to 5-FOA, supporting the

integration of the hygromycin resistance cassette at the targeted cleavage site in the *F. oxysporum* *URA5* gene (Fig. 2.4).

2.3.5 Cas9 RNP-mediated disruption of a gene encoding a polyketide synthase in a secondary metabolite biosynthetic gene cluster.

Some filamentous fungi including *Aspergillus*, *Penicillium*, and *Alternaria*, produce a pigment on certain agar medium during the early growth phase (Nodvig et al., 2015; Pohl et al., 2016; Wenderoth et al., 2017), and detection of these pigments have been used as a marker for the rapid development of CRISPR methodologies in these fungi. *F. oxysporum* is able to produce red pigmented compounds during the later stages of growth. While the gene cluster responsible for the pigment production has not been functionally characterized in *F. oxysporum*, the biosynthetic genes responsible for a red pigment (bikaverin) biosynthesis in the closely related fungus *Fusarium fujikuroi* are encoded in a large secondary metabolite gene cluster (Wiemann et al., 2009). Bioinformatic analysis showed that there is a similar secondary metabolite cluster that may be involved in the synthesis of bikaverin in *F. oxysporum*. This secondary metabolite cluster is composed of six genes, where the ortholog to the *BIK1* gene encodes a putative polyketide synthase that could be essential for the biosynthesis of bikaverin. As this method can mediate donor DNA and NLS_{H2B}Cas9 RNPs to enter *F. oxysporum* protoplasts and trigger the CRISPR–Cas9 induced homology directed repair, the *bik1* gene was selected for optimizing our CRISPR system.

In order to confirm whether the putative *BIK1* gene from *F. oxysporum* (FOTG_08225) was involved in bikaverin synthesis, a sgRNA site was chosen with a location close to the 5'-

terminus of the coding region in the first exon (Fig. 2.5A). The PCR template cleavage efficiency was close to 100% *in vitro*, demonstrating the chosen sgRNA had high cleavage activity with NLS_{H2B}Cas9 (Fig. 2.5B). In order to optimize this CRISPR system various concentrations of the assembled NLS_{H2B}Cas9-Fobik1sgRNA RNPs were used for transformation. In the absence of the Cas9 RNPs in the transformation system, no *bik1* *F. oxysporum* mutants were generated; however, using concentrations of Cas9/sgRNA between 10/2 (µg/µg) and 15/3 (µg/µg) resulted in generation of Δ *bik1* transformants of approximately 50% (Table 2.1). Using a Cas9/sgRNA concentration higher than 15/3 (µg/µg) was unable to further increase the frequency of desired mutants. Six randomly selected *Fobik1* mutants were unable to produce the red pigment when cultured in conducive conditions such as PDB medium for 7 days (Fig. 2.5C), supporting this secondary metabolite gene cluster is responsible for the synthesis of the red pigment. The identity of the red pigment of *F. oxysporum* was confirmed to be bikaverin by fractionation on HPLC using a phenyl hexyl column and mass spectrometry (MS). The HPLC profile monitoring absorbance at 400 nm indicated the wide-type isolate contained multiple peaks with one major peak at a retention time (R_T) of 22 minutes, that appeared different to two large peaks seen under highly similar conditions in *F. fujikuroi* (Fig. 2.5D, Fig. 8). Previous results showed *F. fujikuroi* synthesized two similarly structured compounds, nor-bikaverin and bikaverin (Wiemann et al., 2009). The peak at $R_T \sim 22$ min from the medium of the wild-type isolate and the associated region from the medium of *Fobik1* mutant were collected for MS analysis. A large peak with a molecular weight of 383 was present in the extract of the wild-type *F. oxysporum* isolate, which was absent in the fraction from the *Fobik1* mutant (Fig. 8). The exact mass determination and isotope ratio suggest a best

fit to C₂₀H₁₄O₈ corresponded to bikaverin and initial MS/MS fragmentation of the molecule confirmed the identity as bikaverin (ESI-MS m/z 383: MS/MS (40 eV) m/z (%): 270 (100), 340 (70), 256 (60), 297 (25)). This identification combined with the absence of this secondary metabolite in the mutant demonstrates the disrupted gene (*FoBIK1*) is responsible for the synthesis of bikaverin in *F. oxysporum*.

This CRISPR/Cas9 RNP transformation system is an additional molecular tool to study members of the FOOSC. Unlike currently used transformation procedures such as the *Agrobacterium tumefaciens*-mediated and protoplast transformation methods (Coleman et al., 2011a; Mullins et al., 2001), when utilizing the CRISPR/Cas9 RNP system only short flanking sequences are required for homologous recombination, thereby bypassing the need to construct vectors with >1 kb of homologous sequence flanking the selectable marker. Additionally, this system has the potential to be used to target multiple copies of a single gene if the entire PAM sequence and a significant proportion of the protospacer region between the copies are conserved. While the NLS_{H2B}Cas9 protein needs to be expressed and purified *in vitro* prior to transformation, the advantage of using the purified Cas9 protein is it does not rely on the integration and expression of the Cas9 gene within the fungal nucleus, and therefore there is less of a chance of unforeseen effects due to the random integration of the Cas9 gene within the fungal genome.

In summary, we have developed an approach to transfer Cas9 RNPs and/or donor DNA into fungal protoplasts for gene editing as demonstrated by generating several mutants having the expected phenotypes (Fig. 2.6). In addition, we showed experimental evidence that the red-pigmented compound produced by *F. oxysporum* is bikaverin. This is the first report of a

CRISPR system that could be efficiently used to generate mutations in genes of interest in a member of the FOOSC and may facilitate functional studies concerning the broad host range, secondary metabolite production, and supernumerary chromosomes of these fungi. Importantly, the high degree of similarity of the NLS_{H2B} sequence between all the fusaria and the NLS_{H2B} sequence that was fused to the Cas9 protein suggests this transformation system may be applicable to the other members within the genus *Fusarium*.

Reference

- Al Abdallah, Q., et al., 2017. A Simple and Universal System for Gene Manipulation in *Aspergillus fumigatus*: In Vitro-Assembled Cas9-Guide RNA Ribonucleoproteins Coupled with Microhomology Repair Templates. *mSphere*. 2.
- Aleksenko, A., Clutterbuck, A. J., 1997. Autonomous plasmid replication in *Aspergillus nidulans*: AMA1 and MATE elements. *Fungal Genet Biol.* 21, 373-87.
- Bassett, A. R., et al., 2014. Highly efficient targeted mutagenesis of *Drosophila* with the CRISPR/Cas9 system. *Cell Rep.* 4, 220-228.
- Boeke, J. D., et al., 1984. A positive selection for mutants lacking orotidine-5'-phosphate decarboxylase activity in yeast: 5-fluoro-orotic acid resistance. *Mol. Gen. Genet.* 197, 345-6.
- Chang, D. C., et al., 2006. Multistate outbreak of fusarium keratitis associated with use of a contact lens solution. *JAMA.* 296, 953-963.
- Coleman, J. J., et al., 2011a. Characterization of the gene encoding pisatin demethylase (*FoPDA1*) in *Fusarium oxysporum*. *Mol. Plant-Microbe Interact.* 24, 1482-1491.
- Coleman, J. J., et al., 2011b. An ABC transporter and a cytochrome P450 of *Nectria haematococca* MPVI are virulence factors on pea and are the major tolerance mechanisms to the phytoalexin pisatin. *Mol. Plant-Microbe Interact.* 24, 368-376.
- de Montigny, J., et al., 1989. Structure and expression of the *URA5* gene of *Saccharomyces cerevisiae*. *Mol. Gen. Genet.* 215, 455-462.
- DiCarlo, J. E., et al., 2013. Genome engineering in *Saccharomyces cerevisiae* using CRISPR-Cas systems. *Nucleic Acids Res.* 41, 4336-4343.
- Doudna, J. A., Charpentier, E., 2014. Genome editing. The new frontier of genome engineering with CRISPR-Cas9. *Science.* 346, 1258096.
- Edel-Hermann, V., et al., 2016. A clonal lineage of *Fusarium oxysporum* circulates in the tap water of different French hospitals. *Appl. Environ. Microbiol.* 82, 6483-6489.
- Fang, Y., Tyler, B. M., 2016. Efficient disruption and replacement of an effector gene in the oomycete *Phytophthora sojae* using CRISPR/Cas9. *Mol. Plant Pathol.* 17, 127-39.
- Fierro, F., et al., 1996. Autonomously replicating plasmids carrying the AMA1 region in *Penicillium chrysogenum*. *Curr. Genet.* 29, 482-489.
- Geiser, D. M., et al., 2013. One fungus, one name: defining the genus *Fusarium* in a scientifically robust way that

- preserves longstanding use. *Phytopathol.* 103, 400-408.
- Hansen, F. T., et al., 2012. Quick guide to polyketide synthase and nonribosomal synthetase genes in *Fusarium*. *Int. J. Food Microbiol.* 155, 128-136.
- Hsu, P. D., et al., 2014. Development and applications of CRISPR-Cas9 for genome engineering. *Cell.* 157, 1262-78.
- Jacobs, J. Z., et al., 2014. Implementation of the CRISPR-Cas9 system in fission yeast. *Nat. Commun.* 5, 5344.
- Jiang, W. Z., et al., 2013. Demonstration of CRISPR/Cas9/sgRNA-mediated targeted gene modification in *Arabidopsis*, tobacco, sorghum and rice. *Nucleic Acids Res.* 41, e188.
- Kim, S., et al., 2014. Highly efficient RNA-guided genome editing in human cells via delivery of purified Cas9 ribonucleoproteins. *Genome Res.* 24, 1012-1019.
- Li, M. Y., et al., 2016. Zebrafish genome engineering using the CRISPR-Cas9 system. *Trends Genet.* 32, 815-827.
- Liu, R., et al., 2015. Efficient genome editing in filamentous fungus *Trichoderma reesei* using the CRISPR/Cas9 system. *Cell Discov.* 1, 15007.
- Ma, L.-J., et al., 2010. Comparative genomics reveals mobile pathogenicity chromosomes in *Fusarium*. *Nature.* 464, 367-373.
- Malnoy, M., et al., 2016. DNA-free genetically edited grapevine and apple protoplast using CRISPR/Cas9 ribonucleoproteins. *Front. Plant Sci.* 7, 1904.
- Matsu-Ura, T., et al., 2015. Efficient gene editing in *Neurospora crassa* with CRISPR technology. *Fungal Biol. Biotechnol.* 2, 4.
- McCluskey, K., et al., 2010. The Fungal Genetics Stock Center: a repository for 50 years of fungal genetics research. *J. Biosci.* 35, 119-126.
- Michielse, C. B., Rep, M., 2009. Pathogen profile update: *Fusarium oxysporum*. *Mol. Plant Pathol.* 10, 311-324.
- Mosammaparast, N., et al., 2001. Nuclear import of histone H2A and H2B is mediated by a network of karyopherins. *J. Cell Biol.* 153, 251-262.
- Muhammed, M., et al., 2013. *Fusarium* infection: report of 26 cases and review of 97 cases from the literature. *Medicine (Baltimore).* 92, 305-16.
- Mullins, E. D., et al., 2001. Agrobacterium-mediated transformation of *Fusarium oxysporum*: an efficient tool for insertional mutagenesis and gene transfer. *Phytopathol.* 91, 173-180.
- Nguyen Ba, A. N., et al., 2009. NLStradamus: a simple Hidden Markov Model for nuclear localization signal prediction. *BMC Bioinformatics.* 10, 202.
- Nodvig, C. S., et al., 2015. A CRISPR-Cas9 System for Genetic Engineering of Filamentous Fungi. *PLoS One.* 10, e0133085.
- Nucci, M., Anaissie, E., 2007. *Fusarium* infections in immunocompromised patients. *Clin Microbiol Rev.* 20, 695-704.
- O'Donnell, K., et al., 2013. Phylogenetic analyses of *RPB1* and *RPB2* support a middle Cretaceous origin for a clade comprising all agriculturally and medically important fusaria. *Fungal Genet. Biol.* 52, 20-31.
- O'Donnell, K., et al., 2004. Genetic diversity of human pathogenic members of the *Fusarium oxysporum* complex inferred from multilocus DNA sequence data and amplified fragment length polymorphism analyses: evidence for the recent dispersion of a geographically widespread clonal lineage and nosocomial origin. *J. Clin. Microbiol.* 42, 5109-5120.
- Platt, R. J., et al., 2014. CRISPR-Cas9 Knockin Mice for Genome Editing and Cancer Modeling. *Cell.* 159, 440-455.
- Pohl, C., et al., 2016. CRISPR/Cas9 Based Genome Editing of *Penicillium chrysogenum*. *Acs Synthetic Biology.* 5, 754-764.

- Ran, F. A., et al., 2013. Genome engineering using the CRISPR-Cas9 system. *Nature Protocols*. 8, 2281-2308.
- Shalem, O., et al., 2014. Genome-scale CRISPR-Cas9 knockout screening in human cells. *Science*. 343, 84-87.
- Sheffield, P., et al., 1999. Overcoming expression and purification problems of RhoGDI using a family of “parallel” expression vectors. *Protein Expr. Purif.* 15, 34-39.
- Sievers, F., et al., 2011. Fast, scalable generation of high-quality protein multiple sequence alignments using Clustal Omega. *Mol. Syst. Biol.* 7, 539.
- Stevens, R. B., 1974. *Mycology Guidebook*. University of Washington Press, Seattle.
- van Dam, P., et al., 2017. A mobile pathogenicity chromosome in *Fusarium oxysporum* for infection of multiple cucurbit species. *Sci Rep.* 7, 9042.
- Vyas, V. K., et al., 2015. A *Candida albicans* CRISPR system permits genetic engineering of essential genes and gene families. *Science Advances*. 1.
- Wang, Q., et al., 2018. Efficient genome editing in *Fusarium oxysporum* based on CRISPR/Cas9 ribonucleoprotein complexes. *Fungal Genet Biol.* 117, 21-29.
- Wenderoth, M., et al., 2017. Establishment of CRISPR/Cas9 in *Alternaria alternata*. *Fungal Genet. Biol.* 101, 55-60.
- Wiemann, P., et al., 2009. Biosynthesis of the red pigment bikaverin in *Fusarium fujikuroi*: genes, their function and regulation. *Mol. Microbiol.* 72, 931-46.
- Woo, J. W., et al., 2015. DNA-free genome editing in plants with preassembled CRISPR-Cas9 ribonucleoproteins. *Nat. Biotechnol.* 33, 1162-4.

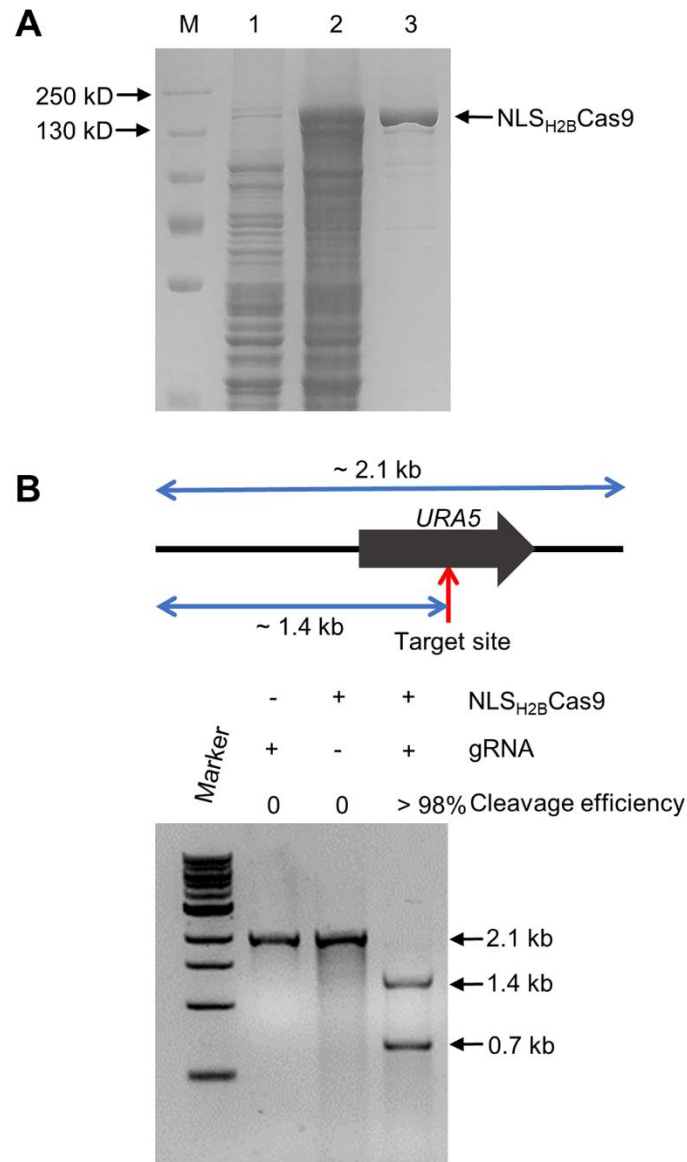


Figure 2.2 Protein purification and *in vitro* cleavage activity assay.

(A) SDS-PAGE gel depicting protein expression and purification conditions. Lane 1 represents total protein before inducing; Lane 2 total protein after addition of 0.3 mM IPTG for 5 h; Lane 3 represents about 5 μ g purified NLS_{H2B}Cas9 protein. (B) Top: diagram depicting the template length, the sgRNA cleavage site, and the lengths of expected fragments after cleavage with Cas9; Bottom: assessment of the cleavage efficiency by gel electrophoresis after incubation at 37 °C for one hour.

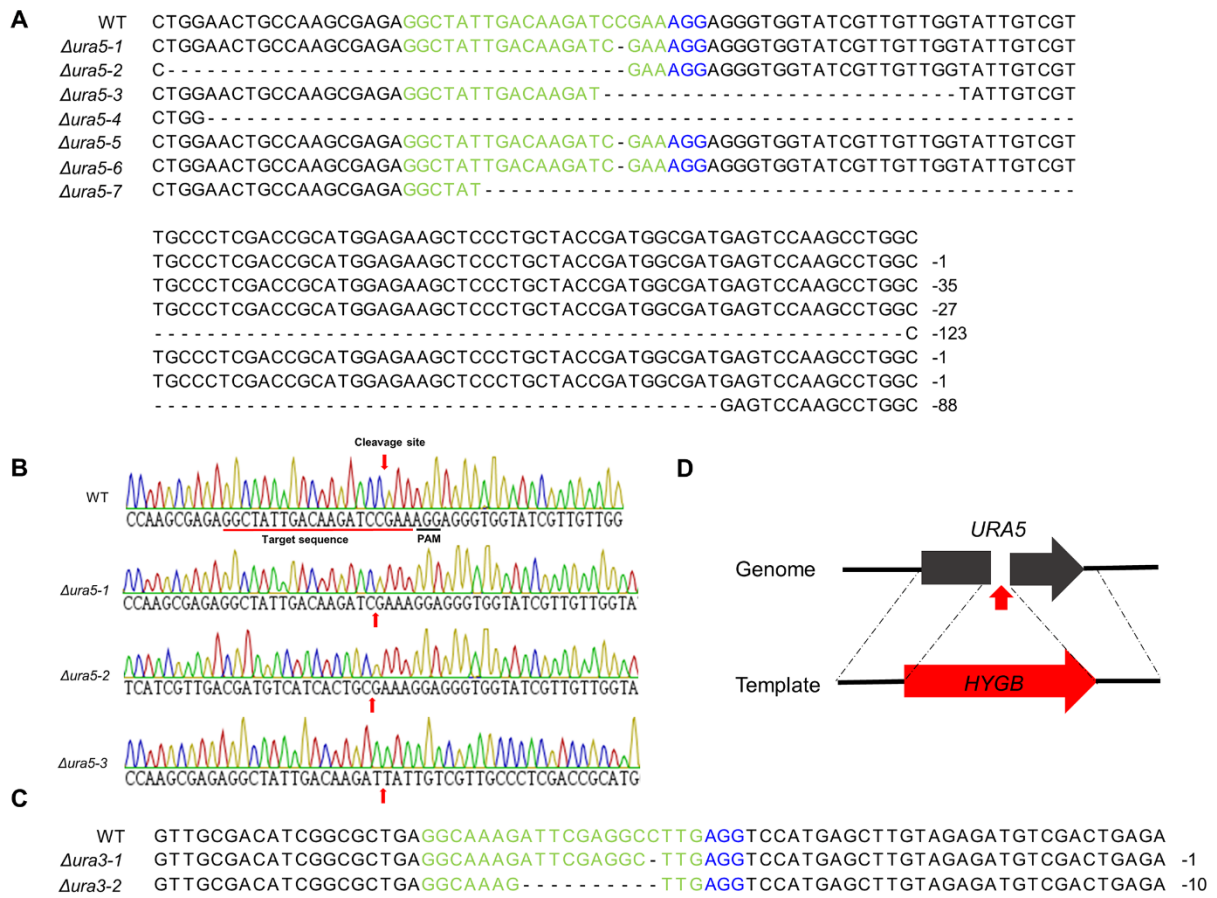


Figure 2.3 Disruption of two *F. oxysporum* genes, *URA5* and *URA3*, using the optimized Cas9 RNP transformation system.

(A-C) characterization of individual NHEJ-mediated mutants (A) The multiple sequence alignment of target regions of seven randomly chosen *ura5* mutants is shown. (B) DNA sequences of the wild-type isolate and three *ura5* mutants. (C) The multiple sequence alignment of target regions of two randomly chosen *ura3* mutants is shown. (D) *URA5* homologous-directed repair disruption chart depicting insertion site of hygromycin phosphotransferase.

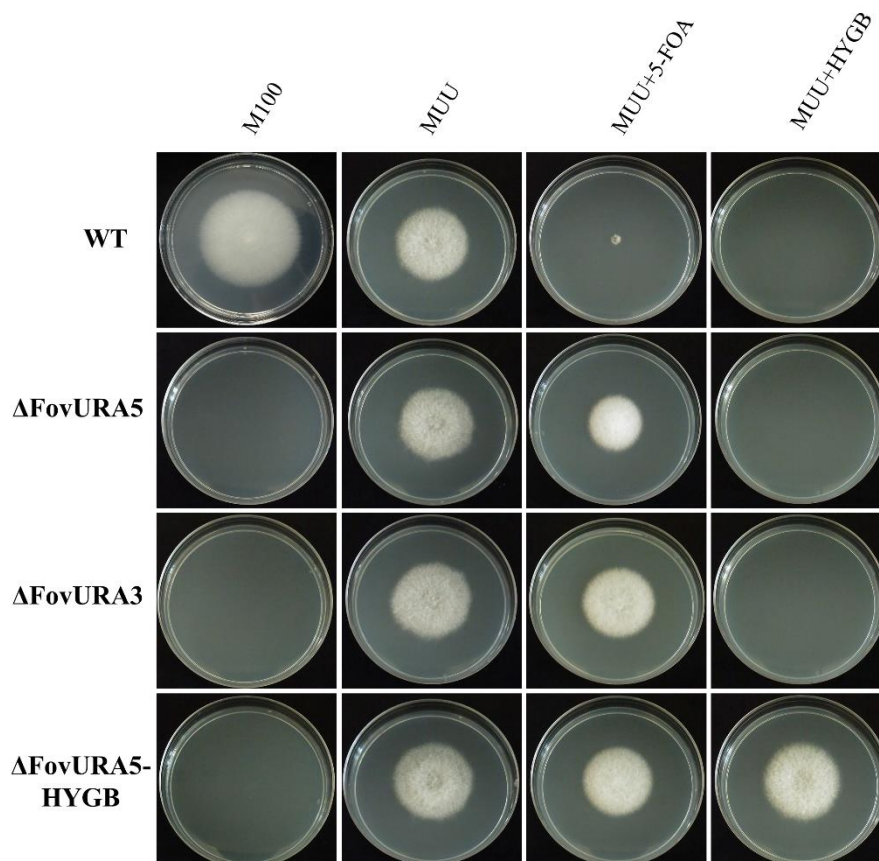


Figure 2.4 The phenotypes of *ura5* and *ura3* mutants obtained by NHEJ and HDR methods.

About 200 conidia were positioned onto the center of the plates, which were cultured at room temperature. The phenotypes were evaluated after six days. MUU represents M100 medium supplemented with uracil and uridine. The concentrations of 5-FOA and hygromycin are 1.5 g/L and 100 μ g/mL, respectively.

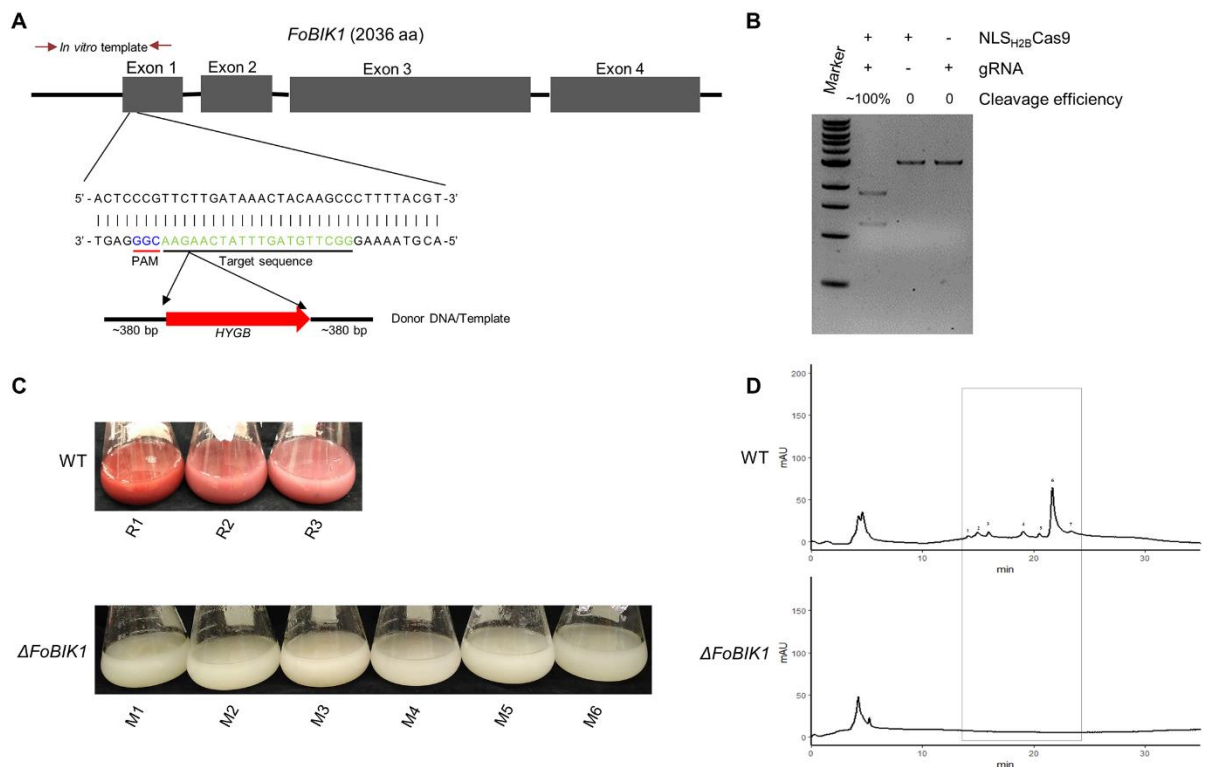


Figure 2.5 *FoBIK1* gene encoding a polyketide synthase in a secondary metabolite biosynthetic cluster is the core enzyme responsible for the biosynthesis of a red pigment. (A) The *BIK1* gene structure, the location of the sgRNA in exon 1, and the construction of the associated HDR template. (B) The cleavage efficiency of the sgRNA for *bik1* *in vitro* after incubation at 37 °C for one hour. (C) The phenotypes of three replicative wild type and six randomly chosen *bik1* mutants cultured for seven days. (D) HPLC-DAD analysis of red pigment production between wild type and *bik1* mutants.

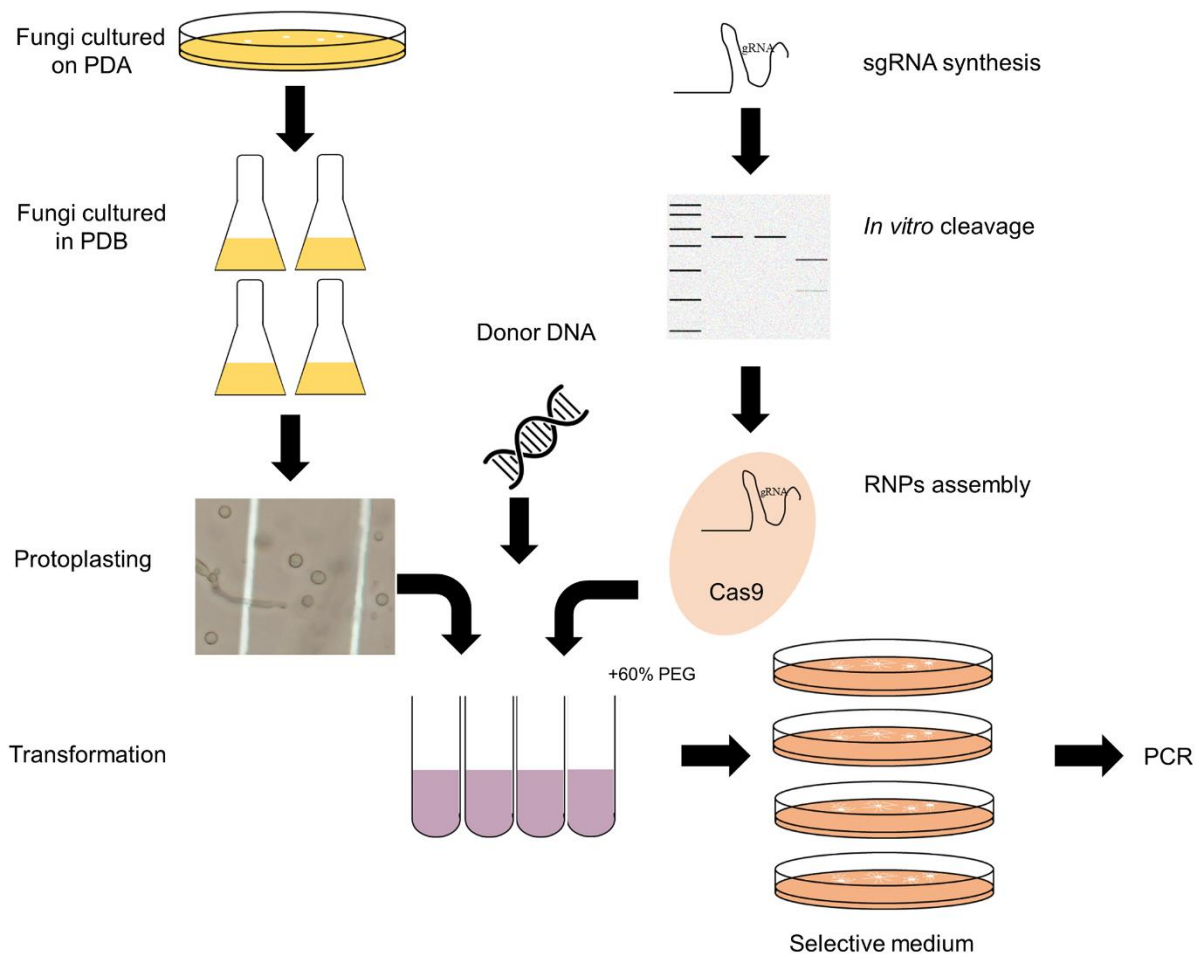


Figure 2.6 Schematic diagram of Cas9 RNPs-directed delivery method to *F. oxysporum* protoplasts to efficiently generate gene disruptions/deletions.

Fa	MAPKAADKKE	ASKAPATASKAP	EKKDAGKKTAAAGDKKKRSK	TRKETYSYIYKVLKQVHPDTGISNRAM	ILNSFVNDIFERVA	GEASKLAAYNKKS	98
Fs	MPKAADKKE	ASKAPATASKAP	EKKDAGKKTAAAGDKKKRSK	TRKETYSYIYKVLKQVHPDTGISNRAM	ILNSFVNDIFERVA	SEASKLAAYNKKS	98
Fv	MAPKAADKKE	ASKAPATASKAP	EKKDAGKKTAAAGDKKKRSK	TRKETYSYIYKVLKQVHPDTGISNRAM	ILNSFVNDIFERVA	SEASKLAAYNKKS	99
Fo	MAPKAADKKE	ASKAPATASKAP	EKKDAGKKTAAAGDKKKRSK	TRKETYSYIYKVLKQVHPDTGISNRAM	ILNSFVNDIFERVA	SEASKLAAYNKKS	98
Fj	MAPKAADKKE	ASKAPATASKAP	EKKDAGKKTAAAGDKKKRSK	TRKETYSYIYKVLKQVHPDTGISNRAM	ILNSFVNDIFERVA	SEASKLAAYNKKS	98
Fpse	MAPKAADKKE	ASKAPATASKAP	EKKDAGKKTAAAGDKKKRSK	TRKETYSYIYKVLKQVHPDTGISNRAM	ILNSFVNDIFERVA	SEASKLAAYNKKS	98
Flan	MAPKAADKKE	ASKAPATASKAP	EKKDAGKKTAAAGDKKKRSK	TRKETYSYIYKVLKQVHPDTGISNRAM	ILNSFVNDIFERVA	SEASKLAAYNKKS	98
Fman	MAPKAADKKE	ASKAPATASKAP	EKKDAGKKTAAAGDKKKRSK	TRKETYSYIYKVLKQVHPDTGISNRAM	ILNSFVNDIFERVA	SEASKLAAYNKKS	98
Fpro	MAPKAADKKE	ASKAPATASKAP	EKKDAGKKTAAAGDKKKRSK	TRKETYSYIYKVLKQVHPDTGISNRAM	ILNSFVNDIFERVA	SEASKLAAYNKKS	98
Fpoa	MAPKAADKKE	ASKAPATASKAP	EKKDAGKKTAAAGDKKKRSK	TRKETYSYIYKVLKQVHPDTGISNRAM	ILNSFVNDIFERVA	SEASKLAAYNKKS	99
Fg	MAPKAADKKE	ASKAPATASKAP	EKKDAGKKTAAAGDKKKRSK	TRKETYSYIYKVLKQVHPDTGISNRAM	ILNSFVNDIFERVA	SEASKLAAYNKKS	98
Fa	TISSREIQTSVRLILPGELAKHAVSEGTKAVTKYSSSTK						137
Fs	TISSREIQTSVRLILPGELAKHAVSEGTKAVTKYSSSTK						137
Fv	TISSREIQTSVRLILPGELAKHAVSEGTKAVTKYSSSTK						138
Fo	TISSREIQTSVRLILPGELAKHAVSEGTKAVTKYSSSTK						137
Fj	TISSREIQTSVRLILPGELAKHAVSEGTKAVTKYSSSTK						137
Fpse	TISSREIQTSVRLILPGELAKHAVSEGTKAVTKYSSSTK						137
Flan	TISSREIQTSVRLILPGELAKHAVSEGTKAVTKYSSSTK						137
Fman	TISSREIQTSVRLILPGELAKHAVSEGTKAVTKYSSSTK						137
Fpro	TISSREIQTSVRLILPGELAKHAVSEGTKAVTKYSSSTK						137
Fpoa	TISSREIQTSVRLILPGELAKHAVSEGTKAVTKYSSSTK						138
Fg	TISSREIQTSVRLILPGELAKHAVSEGTKAVTKYSSSTK						137

Figure 2.7 Histone H2B amino acid sequence alignment of different *Fusarium* species. Abbreviations for specific species are as follows: Fo, *F. oxysporum*; Fg, *F. graminearum*; Fv, *F. verticillioides*; Ff, *F. fujikuroi*; Fa, *F. acuminatum*; Fs, *F. solani*; Fpse, *F. pseudograminearum*; Flan, *F. langsethiae*; Fman, *F. mangiferae*; Fpro, *F. proliferatum*; and Fpoa, *F. poae*.

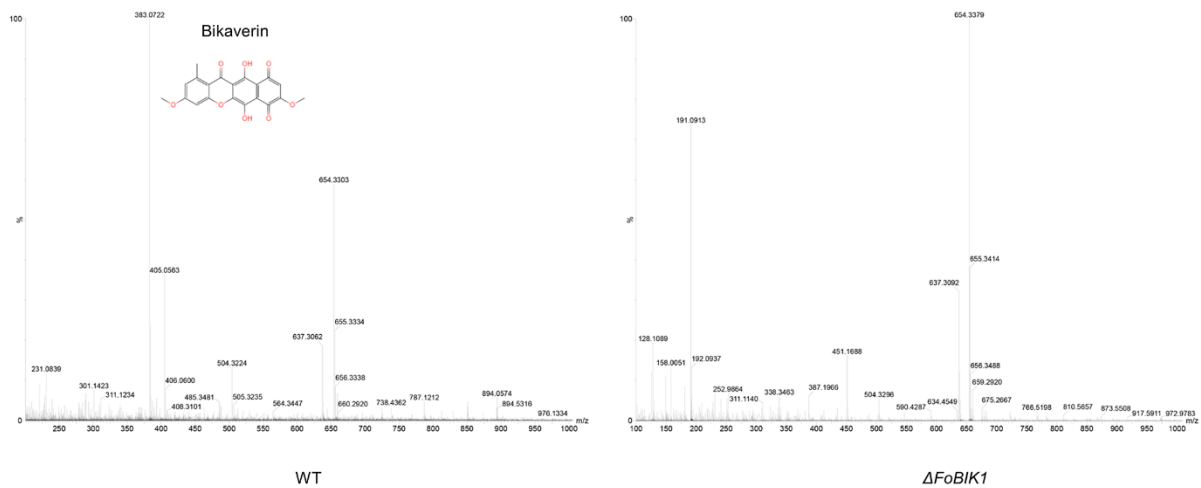


Figure 2.8 Analysis of the compounds in the supernatant of wild type (WT) and a $\Delta Fobik1$ transformant by mass spectrometry.

The major peak found in the WT at 383.0722 corresponds to bikaverin and is absent in the *Fobik1* mutant profile.

Table 2.1 Mutation frequencies of homolog directed repair using Cas9 RNPs

Gene	Donor DNA ^a	Cas9/sgRNA ^a	Pick No.	Positive No.	Frequency (%)
<i>URA5</i>	6	0/0	32	0	0
	6	10/2	14	3	21.4
<i>bik1</i>	6	0/0	27	0	0
	6	5/1	20	4	20
	6	10/2	13	7	53.8
	6	15/3	25	12	48
	6	20/4	21	2	9.5

^a represent that the unit is μg

Table 2.2 The sequences of oligonucleotides used in Chapter 2

Primer names	Oligomer sequences	Usage
Inf_HygB_F	TTGGGCCCGACGTCGCATGTATATTAATG GAAGGGTATATAACCACGC	
Inf_HygB_XhoI_R	CTCGAGCCTCTAAACAAGTGTACCTGTG	The construction of the plasmid pExFO (MCS: HindIII-KpnI-NotI-PacI-Sall-SpeI-XbaI)
Inf_trpC_F	TTGTTTAGAGGCTCGAGTCCATCACCGGG TCTGGCGTT	
Inf_trpC_R	ATCGATGCTTGGGTAGAATAGG	
Inf_MCS_Tef1_1F	ATTAAGGGTTCGACGACTAGTCTCTAGAGC GGACATTCGATTTATGCC	
Inf_MCS_Tef1_2F	AAGCTTGGTACCTTGCGGCCGCAACCTTA ATTAAGGGTTCGACGACTAGTCTC	
Inf_MCS_Tef1_3F	TCTACCCAAGCATCGATAAGCTTGGTACC TTGCGGCC	
Inf_Tef1_R	ATCCAACGCGTTGGGAGCTGTATTGGGAT GAATTTTGTATGCAC	
HindIII-NLS_F	CCCAAGCTTATGGCTCCCAAGGCTGCTGA CA	pExFO-NLS _{H2B} eGFP
NLS_KpnI_R	CGGGGTACCCTTGTAGATGTAAGAAGAGT AGG	
KpnI_eGFP_F	CGGGGTACCATGGTGAGCAAGGGCGAGG A	
eGFP_XbaI_R	GCTCTAGATTACTTGTACAGCTCGTCCAT G	
NLS _{H2B} _BamHIF	CGCGGATCCGATGGCTCCCAAGGCTGCTG	pHis parallel1-NLS _{H2B} Cas9
NLS _{H2B} _SalIR	ACGCGTCGACCTTGTAGATGTAAGAAGA GT	
Cas9expSalIF	CATCTACAAGGTCGACATGGACAAGAAG TATAGCATCGG	
Cas9expHindIIIR	GTGCGGCCGCAAGCTTTCAGACCTTGCG CTTCTTC	
DetCas9F1	CGCGAGCGGATGAAGCGGAT	Cas9 gene detection
DetCas9R1	CGCAGTTCCCACGACTGCGT	
Seq_Case9_1	GCCCAAATCGGTGACCAGTAC	Cas9 gene sequencing
Seq_Case9_2	GGCTATCGTCGATTTGCTTTTTTA	
Seq_Case9_3	ATGGACGCGACATGTACGTC	
Seq_Case9_4	GCATGCCGCAAGTCAATATCG	
DeteGFPF	ATGGTGAGCAAGGGCGAGGAGC	eGFP gene detection
DeteGFPR	TACTTGTACAGCTCGTCCATG	
FoURA5TF	AAATGGTCGGCATCGTAGAG	URA5 <i>in vitro</i> cleavage template
FoURA5TR	TCAAAGACCTTGGCCCAAGC	
FoURA5sgRNA1	TTCTAATACGACTCACTATAGGCTATTGAC AAGATCCGAAGTTTTAGAGCTAGAAATAG	URA5 sgRNA DNA synthesis

	CAAG	
sgRNA_universal	AAAAGCACCGACTCGGTGCCACTTTTTTC AAGTTGATAACGGACTAGCCTTATTTTAA CTTGCTATTTCTAGCTCTAAAAC	
FoURA5_S_F	GTCAAAGCGCATCTCACCT	DNA Sequencing for the
FoURA5_S_R	TAGTCGCTGGCCTTGTACTTG	targeted <i>URA5</i> region
FoURA3sgRNA1	TTCTAATACGACTCACTATAGGCAAAGAT TCGAGGCCTTGGTTTTAGAGCTAGAAATA GCAAG	FoURA3 sgRNA DNA synthesis
FoURA3_S_F	TACGCCTCACATCGGACGAC	DNA Sequencing for the
FoURA3_S_R	CTCGTTGTCTGAACGCTCGC	targeted <i>URA3</i> region
pUC19URA5upF	AGTGAATTCGAGCTCGGTACCCGGGTGA ACCACCCGAAGGGTC	
pUC19URA5upR	TACCCTTCCATTAGGATCTTGTCAATAGCC TCTCG	HR template construction
pUC19URA5hygb F	ATTGACAAGATCCTAATGGAAGGGTATAT ACCACGC	PUC19- <i>URA5</i>
pUC19URA5hygb R	CCACCCTCCTTTCAGGGTTGCGAGGTCCA ATG	
pUC19URA5down F	ACCTCGCAACCCTGAAAGGAGGGTGGTA TCG	
pUC19URA5down R	AACAGCTATGACCATGATTACGCCATGGT CCTAAGAGAAAGAC	
Fobik1sgRNA1	AAGCTAATACGACTCACTATAGGCTTGTA GTTTATCAAGAAGTTTTAGAGCTAGAAAT AGCAAG	<i>FoBIK1</i> sgRNA DNA synthesis
Fobik1TF	GCTGTCAAGTCCGTGCTCGT	<i>FoBIK1</i> <i>in vitro</i> cleavage
Fobik1TR	GGGTACCGATTCCGTCAGCG	template
pUC19bik1g1upF	AGTGAATTCGAGCTCGGTACCCGGGCGC CACCCTAGCAGTTTC	
pUC19bik1g1upR	TTCCATTAATATAGAACGGGAGTGCTTTG ATC	HR template construction
pUC19hygbik1g1_ F	AGCACTCCCGTTCTATATTAATGGAAGGG TATATACCACGC	pUC19-bik1
pUC19hygbik1g1_ R	TGTAGTTTATCAAAGGGTTGCGAGGTCCA ATG	
pUC19bik1g1down F	ACCTCGCAACCCTTTGATAAACTACAAGC CCTTTTACG	
pUC19bik1g1down R	AACAGCTATGACCATGATTACGCCACATC TTTCGCGCAGCTGAC	
Det_bik1g1F	ATGAGATAGCCCCGGCAGTG	
Det_bik1g1R	CGAACGCCCTCCAAAAGCAA	HRD bik1 mutant
Det_bik1g2R	ATCGGAAAGCAACAGTAGCA	detection

H _{in} F	AACTCACCGCGACGTCTGTC	Detection of HYGB cassette
H _{in} R	TTGTCCGTCAGGACATTGTT	
H _{out} F	GTCGATGCGACGCAATCGT	HRD mutant detection
H _{out} R	GGTCGAGCGTGGTGGCTTGA	

Table 2.3 The sgRNAs and associated target genes from *F. oxysporum* in Chapter 2

sgRNA	PAM	Targeted gene	Gene No.	Gene Function
GGCTATTGACA AGATCCGAA	AGG	<i>URA5</i>	FOTG_04865	Orotate phosphoribosyltransferase
GGCAAAGATT CGAGGCCTTG	AGG	<i>URA3</i>	FOTG_02245	Orotidine 5'-phosphate decarboxylase
GGCTTGTAGTT TATCAAGAA	CGG	<i>FoBIK1</i>	FOTG_08225	Predicted bikaverin synthesis gene

Chapter 3.

CRISPR/Cas9-mediated endogenous gene tagging in *Fusarium oxysporum*

This chapter has been published (Wang and Coleman, 2019).

3.1 Introduction

Members of the *Fusarium oxysporum* species complex (FOSC) are soil-borne pathogens which pose a serious threat to agricultural production and human health (Gordon, 2017). In agriculture, *F. oxysporum* is capable of causing several diseases, most notably Fusarium wilt resulting from colonized plant xylem tissue. Infected plants show a range of symptoms including chlorosis, necrosis, stunting, and wilting (Gordon, 2017). In addition, these fungi can be opportunistic human pathogens infecting immunocompromised patients with high mortality rates (Muhammed et al., 2013; Nucci and Anaissie, 2007).

Rapid improvement of high-throughput DNA and RNA sequencing techniques has facilitated researchers to investigate fungal pathogenicity based on a large scale of whole genome and/or transcriptome analysis. Currently, several high-quality, well-annotated *F. oxysporum* genomes are publicly available, and enable further exploration of fungal pathogenesis and disease control (Ma et al., 2010; van Dam et al., 2017). Experimental evidence has shown that horizontal transfer could have contributed to the genetic diversity

among FOSC isolates, as mobile chromosomes harboring virulence factor genes were able to expand the host range of the recipient and increase their environmental nich(es) (Ma et al., 2010; Vlaardingerbroek et al., 2016).

Molecular manipulation of genes and proteins are essential to fully understand the role they have in an organism, and some of the more common techniques to elucidate cellular functions include gene deletion, RNAi knockdown, ectopic gene expression, and protein subcellular localization. The subcellular localization of a protein influence on the function, as improperly localized proteins, including those that have lost their subcellular localization peptides, may result in decreased or abolished protein activity (Scott et al., 2005). Several studies have indicated that cellular location of a fungal protein is critical for proper function inside the cell. For example, the well characterized calcineurin-regulated transcription factor Crz1 which ultimately controls transcription of several stress response genes and cell wall integrity in most fungi (Lev et al., 2012; Schumacher et al., 2008; Spielvogel et al., 2008). Upon an increase in intracellular calcium levels, Crz1 is dephosphorylated resulting in rapid localization into the nucleus activating the expression of downstream genes.

Studies of fungal protein subcellular localization may rely on several methods, where the most commonly employed method is the use of fluorescent markers including GFP, eGFP, RFP, YFP, and mCherry. These fluorescent proteins are usually fused in frame with the coding sequence of the gene of interest and randomly inserted into the fungal genome under the control of a constitutive or native promoter (Gupta et al., 2015; Schuster et al., 2016). Based on different excited marker fluorescence, protein subcellular localization can be determined and protein translocation can be dynamically tracked (Schuster et al., 2016). While this method

enables the protein subcellular localization to be detected or translation of the protein monitored, some limitations still exist including: 1) native promoters may not have been accurately predicted upstream of the coding regions, resulting in no or altered expression of the protein fused with tags; 2) protein expression that is driven by constitutive promoters might cause inaccurate protein subcellular localization, as constitutive expression may disrupt post-translational regulation; 3) ectopic insertion may disrupt other genes or important regions in the fungal genome, resulting in inaccurate protein subcellular localization or dynamic gene expression, necessitating multiple transformants to be assessed. While antibody-based immunofluorescence approaches to determine the subcellular localization of proteins exist (Rasmussen and Glass, 2005), the difficulty in obtaining an antibody with high specificity, compounded by the time required to generate the antibody, have limited the application of this approach.

As molecular methods to generate gene fusions are an important component for functional studies, a rapid and efficient endogenous gene tagging system (EGT) in *F. oxysporum* was developed based on a CRISPR/Cas9 ribonucleoprotein complex transformation method (Wang et al., 2018). With this system, we could not only localize the protein encoded by the endogenous genes of interest, but also detect the relative protein abundance at various fungal structures. Different fluorescent markers were integrated prior to the start/stop codon of the gene, allowing gene fusions to be generated with the gene under its native promoter, at the usual location within the genome, and containing the gene introns. Two strategies, a homology-independent targeted integration (HITI) and homology-dependent recombination integration (HDRI), were used in the development of the EGT system with

fluorescent markers including *sGFP* (a variant of *eGFP*) and *mCherry*. The HITI strategy was initially developed based on the non-homologous end joining (NHEJ) DNA repair approach (Suzuki et al., 2016). We used this strategy to tag endogenous genes at either the N- terminus or the C-terminus, and generated FoChs5-3×sGFP (C-terminus tagging) and mCherry-FoSso2 (N-terminus) transformants. The protein subcellular localization showed FoChs5 in *F. oxysporum* was present in both conidia and hyphae where a majority accumulated at the hyphal tips although some existed in the septum. FoChs5 was largely found on the surface of newly formed germling tubes, suggesting Chs5 plays an important role in cell wall modelling. The HDRI strategy was used to tag the plasma membrane syntaxin 1 SNARE protein FoSso1 with a mCherry marker at the C-terminus. FoSso1-mCherry was localized to the cell plasma membrane (PM) of hyphae and the septum in conidia while mCherry-FoSso2 showed strong PM localizations in conidia, germlings, fungal tips, hyphae, and phialides. Overall, this CRISPR/Cas9 mediated EGT system was highly efficient and stable for use in protein subcellular localization studies and could provide a genetic engineering reference for gene tagging in other filamentous fungi.

3.2 Materials and methods

3.2.1 Strains and culture conditions.

The *Fusarium oxysporum* f.sp. *vasinfectum* strain (FGSC #10442) was used in this study (McCluskey et al., 2010), and was cultured in PDB (Potato Dextrose Broth), YG (1% yeast extract, 3% glucose) or M-100 (minimum medium). All transformants in this study were isolated on M-100 agar plates containing 75 µg/mL hygromycin B before observation by

confocal microscopy. All transformed strains generated in this study are listed in Table 3.1.

3.2.2 Homologous gene identification.

Two well-annotated *CHS5* genes from *Neurospora crassa* (NCU04352) and *Ustilago maydis* (UM03204.1) were used as query sequences to identify the Chs5 homologous sequence in *F. oxysporum* with blastp software in the EnsembleFungi database (<https://fungi.ensembl.org/index.html>). Several previously identified syntaxin 1 SNARE proteins from *Saccharomyces cerevisiae* (SSO1: YPL232W and SSO2: YMR183C), *N. crassa* (SSO1: XP_961235.1) and *Zymoseptoria tritici* (SSO1: XP_003857391.1) were used as the blastp queries against the homologous sequences in the above database. Since these genes perform similar functions during fungal development, their amino acid sequences were hypothesized to be conserved. To determine the sequence identity or splice variants, the potential homologous genes were compared with the associated genes in closely-related filamentous fungal pathogens including *Fusarium oxysporum* f. sp. *lycopersici* 4287, *Magnaporthe oryzae* 70-15, *Fusarium graminearum* PH1, and *Fusarium solani* (*Nectria haematococca* MPVI 77-13-4), which had well-annotated genomes. The protein domains were predicted using PFAM (Finn et al., 2016). Multiple sequence alignments were conducted using the online bioinformatic program TCOFFEE (Notredame et al., 2000). The phylogenetic tree was generated using online PhyML 3.1 with the maximum likelihood algorithm and 500 bootstraps (http://www.phylogeny.fr/one_task.cgi?task_type=phyml) (Dereeper et al., 2008). All accession numbers of predicted genes in this study are listed in Table 3.1.

3.2.3 The evaluation of fusion protein topology and plasmid construction.

Since the integrated location of the different fluorescent protein markers may alter the

original protein topology, the TMHMM v. 2.0 analysis software (<http://www.cbs.dtu.dk/services/TMHMM/>) was used to compare the differences of protein topology between the WT proteins and the fusion proteins. All plasmids were maintained, propagated, and stored in DH5 α *E. coli*. All tagging plasmid constructs were based on a pUC19 plasmid, and cloned fragments were inserted between two enzyme sites, BamHI and HindIII, with the NEBuilder[®] HiFi DNA Assembly Master Mix kit (NEB). For the *CHS5* gene tagging vector construction (HITI), the initial vector was first constructed by amplifying the following three fragments by PCR: 1) 1 \times *sGFP* from the plasmid pCT74 (Lorang et al., 2001), 2) the *Tef-1* terminator from the plasmid pFFC332, and 3) the hygromycin cassette from the plasmid pCWHyg1. These three fragments were simultaneously inserted between the BamHI and HindIII sites in the pUC19 vector in the following order 1 \times *sGFP-Tef-1-HYGB* generating the primary vector pUC19-1 \times *sGFP-Tef-1-HYGB*. The final *CHS5* HITI vector was constructed as follows: 1) a ~700 bp coding sequence prior to the stop codon of *FoCHS5* was cloned as a bait sequence which contained a sgRNA cleavage site; 2) to construct a triple *sGFP* in the vector, the first copy of *sGFP* (1st *sGFP*) was cloned with the addition of a 3'-terminus marker sequence (nt: GACTACAAGGACGAC, aa: DYKDD) while the second copy of *sGFP* (2nd *sGFP*) was cloned with the addition of the 3'-terminus marker sequence (nt: AGCGCTGGCGCTTAC, aa: SAGAY); 3) the fragment of 1 \times *sGFP-Tef-1-HYGB* was cloned from the above primary plasmid; and 4) these four fragments were simultaneously inserted into the pUC19 plasmid to generate the final HITI plasmid containing the triple *sGFP* tag, which was named as pUC19-HITI-*FoCHS5*-3 \times *sGFP*. The detailed N-terminal *FoSSO2* gene tagging vector for HITI was constructed as follows: 1) a ~800 bp sequence in front of the *FoSSO2* gene start codon was

cloned with a sgRNA site; 2) 1 × mCherry was cloned from plasmid ss3591; 3) the *FoSSO2* coding sequence including introns and a ~ 450 bp 3-UTR region were amplified from genomic DNA; 4) the hygromycin cassette was obtained from plasmid pCWHyg1; 5) the above four fragments were simultaneously inserted into the pUC19 plasmid, which was later labeled as pUC19-HITI-*mCherry-FoSSO2*.

The *FoSSO1* C-terminal tagging plasmids contained a *mCherry* tag fused with a *Tef-1* terminator and hygromycin resistance cassette. The detailed HDRI vector construction was carried out as follows: 1) a ~400 bp DNA template fragment prior to the gene stop codon was cloned from the genomic DNA (upstream sequence); 2) the other DNA fragment after the sgRNA cleavage site, ~400bp in length, was obtained using PCR (downstream sequence); 3) the mCherry was cloned from the plasmid ss3591 and the *Tef-1* terminator fused with hygromycin cassette was cloned from pUC-HITI-*FoCHS5-3×sGFP* as constructed above; 4) these four fragments were assembled in the following order, upstream sequence, mCherry, *Tef-1* fused with the hygromycin cassette, and downstream sequence, into pUC19 (pUC19-HDRI-*FoSSO1-mCherry*). All primers used in this study are listed in Table 3.3.

3.2.4 sgRNA selection and in vitro Cas9 nuclease assay.

The sgRNA sites were located after the stop codon between 0 and 200 bp for the HDRI strategy (*FoSSO1-mCherry*), while those for C-terminal tagging of the *FoCHS5* gene and N-terminal tagging of the *FoSSO2* gene were located prior to the gene stop or start codon, respectively. A ~2kb fragment was cloned for use as a template for the *in vitro* Cas9 nuclease assay to confirm the Cas9 endonuclease cleavage activity. The *in vitro* Cas9 nuclease assay was performed as previously described (Wang et al., 2018). In brief, a mixture of 200 ng Cas9, ~40

ng sgRNA, 1×Cas9 Nuclease Reaction Buffer and ~ 75 ng DNA template in a 20 µL total volume was incubated at 37°C for 1 h. The cleaved products were evaluated on a 1% agarose gel. All sgRNA were able to effectively cleave PCR fragments with the Cas9 nuclease (Figs. 3.5C and 3.6B).

3.2.5 Fungal transformation and transformant identification.

Transformation of *F. oxysporum* was carried out as previously described (Wang et al., 2018). For the HDRI strategy, donor PCR fragments were amplified from the donor plasmids (pUC19-HDRI-*FoSSO1-mCherry* and pUC19-HDRI-*FoSSO2-mCherry*) with the primers, NA_FoSSO1upF/ NA_FoSSO1downR and NA_FoSSO2upF/ NA_FoSSO2downR, and used to conduct the transformations. The desired transformants will contain the gene of interest fused with the different marker tags under the native promoter, and were screened by three PCR reactions to determine the location of the integrated fragment in the fungal genome. Detailed illustrations of correct transformants are shown in Fig. 3.5A and 3.6A. The first pair of primers, Tf and Tr, were used to assess the full length near the sgRNA cleavage site after the fragments were integrated. Another two pairs of primers were used to determine the upstream and downstream sequences of the inserted fragments. All primers used are listed in Table 3.3.

3.2.6 Confocal microscopy observation.

Transformant hyphae were picked and inoculated into 50 mL YG media and cultured for 4 days at room temperature on a rotary shaker at 150 rpm. The 500 µL hyphae-conidia mixture of the *F. oxysporum* transformants were inoculated into 50 mL fresh YG media and incubated on a shaker at 18°C at 220 rpm for 16 h. One mL of the fungal culture was centrifuged at 13,000 rpm for 1 min and the supernatant removed. The resulting pellet was suspended in 500 µL of

4% paraformaldehyde and the mixture was incubated at room temperature at least 15 min, followed by at least two washes of PBS, pH 7.4. Transformants were suspended in a final volume of 300 μ L of PBS, pH 7.4 and imaged by confocal microscopy using an inverted agar method under 60 \times oil magnification (Nikon A1 Confocal Microscopy) (Hickey and Read, 2009). For live cell imaging, the fungus was cultured in a four-chambered coverglass (Thermo Scientific™ Nunc™ Lab-Tek™ Chambered Coverglass) or the live fungal cells were dispensed on the surface of a 0.5 cm \times 0.5 cm piece of agar on a slide and covered with the coverglass. The sGFP fluorescent marker was excited at 488 nm while the mCherry fluorescent marker was excited at 561 nm.

3.3 Results and Discussion

3.3.1 Identification of FoChs5, FoSso1, and FoSso2

Orthologs to several well-characterized genes in other filamentous fungi were selected in *F. oxysporum* to develop an EGT system to study subcellular localization. The well characterized localization of the transmembrane chitin synthases (CHSs) and their importance in production of the fungal cell wall component chitin, make this group of enzymes ideal to use in the development of an EGT system. Nine CHS genes reside in the *F. oxysporum* genome and the presence of multiple copies of CHSs suggest functional complexity exists in regards to chitin biosynthesis in these fungi (Kong et al., 2012). Among these CHSs, the class V CHS (CHS5) usually contain several protein domains including a Myosin head, Cyt-b5, Chitin_synth_2, and DEK C domains (Fig. 3.1A); importantly, this class of CHS enzymes have been shown to be involved in pathogenesis and vesicle transportation (Madrid et al., 2003;

Treitschke et al., 2010). Among these domains, the myosin domain is involved in traversing on actin filaments and microtubules while the chitin synthase domain participates in chitin synthesis (Schuster et al., 2016; Treitschke et al., 2010). To characterize the subcellular localization of FoChs5 in different fungal structures and stages of development, the orthologous gene (FOTG_09933) in the *F. oxysporum* genome was identified based on the *CHS5* genes from other fungi. FoChs5 shares 83.3% and 52.8% amino acid similarity to Chs5 in *N. crassa* and Mcs1 in *U. maydis*, respectively; supporting Chs5 performs similar functions among these fungi.

In addition to *FoCHS5*, we chose the duplicated genes *SSO1* and *SSO2*, that encode homologues of syntaxin 1, as representative genes to develop this EGT system based on their known localization to membranes (Kienle et al., 2009). Syntaxins are Qa SNARE transmembrane proteins that play essential roles in membrane fusion events (Salaun et al., 2004). In the yeast *S. cerevisiae*, the *SSO1* and *SSO2* genes are involved in the fusion between secretory vesicles and the plasma membrane. Deletion of *SSO1* halted vesicle fusion and decreased sporulation efficiency, while mutation of *SSO2* resulted in increased sensitivity to chemicals and temperature (Jantti et al., 2002; Nakanishi et al., 2006). Syntaxin 1 and its homologues contain, in their cytosolic region, an N-terminal syntaxin domain followed by a TMD-proximal SNARE domain (Fig. 3.1A), and the syntaxin Sso1 has been used for characterization of the plasma membrane in some fungi (Kilaru et al., 2017; Schuster et al., 2016; Taheri-Talesh et al., 2008; Valkonen et al., 2007). To identify the homologous genes of syntaxin 1, several previously described syntaxin 1 genes from *S. cerevisiae*, *U. maydis*, and *Z. tritici* were used as a query for the *FoSSO1* and *FoSSO2* gene sequences (Kilaru et al., 2017).

FoSso1 and FoSso2 contained the two typical domains (syntaxin and SNARE) and shared ~44% amino acid sequence similarity between the two proteins. Although some strains of *Aspergillus* species only contain a single copy of the *SSO* genes (Kienle et al., 2009), phylogenetic analysis revealed that a majority of the ascomycete fungi encode two copies of the *SSO* genes, and can be resolved into two distinct phylogenetic clades suggesting that these two genes diverged some time ago and have since evolved to function differently (Fig. 3.1B). Both copies of the *SSO* genes were highly conserved among *Fusarium* spp. and were clustered in the phylogenetic tree supporting that the presence of two *SSO* genes is ancestral in this genus.

3.3.2 HITI-mediated endogenous gene tagging at the C-terminus of *FoCHS5*

A homology-independent targeted integration (HITI) strategy was developed utilizing CRISPR/Cas9 technology (Wang et al., 2018), which enables long DNA fragments to be inserted into the genome using the NHEJ repair mechanism. The main advantage of HITI is that it can occur in non-dividing cells, and has been validated in many cell types including human cell lines and zebrafish (Auer et al., 2014; Suzuki et al., 2016). The HITI strategy was used to insert a 3×*sGFP* (a variant of *eGFP*) tag before the *FoCHS5* stop codon (C-terminal tagging), generating a fusion protein consisting of FoChs5 and a strong green fluorescent signal for protein subcellular localization. The donor plasmid DNA was composed of the following: a ~700 bp homologous fragment containing the sgRNA cleavage site before the *FoCHS5* stop codon was fused with a 3×*sGFP* sequence, a *Tef-1* terminator sequence, and the hygromycin resistance cassette sequence (Fig. 3.2A). During the transformation, both the genome and donor plasmid sequences can be simultaneously cleaved by the Cas9 RNPs. The activated DNA repair

mechanism allows “cross-ligation” between the chromosome and the donor plasmid at some frequency (C1--P2 and P1--C2, Fig. 3.2A). The desired transformants will contain the complete *FoCHS5* endogenous gene sequence fused in frame with the 3×sGFP tag followed by the remaining portion of the donor plasmid containing the hygromycin resistance cassette for selection of the desired transformants (Fig. 3.2A).

Previous evidence showed the HITI strategy allowed perfect repair of DNA at a higher frequency, and that error-prone DNA repair occurred infrequently (Auer et al., 2014; Suzuki et al., 2016). We hypothesized if the Cas9 RNP transformation of *F. oxysporum* protoplasts only allowed a miniscule amount of the Cas9 RNPs into the cell and the Cas9 RNPs carried out the cleavage a short time before their degradation, some proportion of the transformants would have perfect DNA repair occurring between the cleavage sites of the chromosome and donor plasmid. After transformation, two of the four transformants were used for PCR analysis to confirm that the whole plasmid (~ 8 kb) was inserted into the genome at the sgRNA cleavage site (Fig. 3.5D). In theory, the HITI-mediated gene editing may generate short losses or additions of nucleotides at the repair sites (Auer et al., 2014; Suzuki et al., 2016). However, sequencing of the sgRNA target sequence site of the two transformants showed identical nucleotide sequence with the wide-type strain (Fig. 3.5B), demonstrating that the NHEJ DNA repair mechanism for some *F. oxysporum* protoplast cells would be error free, which was consistent with previous publications (Auer et al., 2014; Suzuki et al., 2016).

The subcellular localization of FoChs5 revealed that the protein had variable distribution and accumulated in some areas (Fig. 3.2B). In conidia, FoChs5-3×sGFP accumulated at both ends of the spore; however in *F. oxysporum* germlings FoChs5-3×sGFP was distributed in the

cell membrane primarily at the newly formed hyphal tips emerging from the conidium showing that FoChs5, as a class V myosin chitin synthase, was strongly polarized. In addition, confocal microscopy showed that FoChs5 localized to the hyphal tips and septa (Mov. 1, Fig 3.7). As FoChs5 is polarized and contains a myosin motor domain, it may have a similar function with *U. maydis* Mcs1 and participate in the transportation of vesicles (Treitschke et al., 2010).

3.3.3 HDRI-mediated endogenous gene C-terminal tagging of *FoSSOI*

Our previous study showed Cas9 RNPs significantly improved the efficiency of homologous recombination (Wang et al., 2018). *FoSSOI* was tagged with a *mCherry* peptide at the 3'-terminus of the genes by a homology-dependent recombination integration (HDRI) strategy. The sgRNA site was located after the gene stop codons (Fig 3.3A). The donor DNA was constructed by the following: an upstream homologous fragment, ~400 bp in length, prior to the gene stop codon was cloned and fused with the mCherry-*Tef-1-HYGB* and a ~400 bp downstream homologous fragment after the sgRNA cleavage site. During the transformation with the donor DNA fragments and Cas9 RNPs, two homologous recombination events were expected to occur at the sgRNA cleavage site (Fig. 3.2B). The desired transformants will express the Sso-mCherry fusion protein and can be selected for by hygromycin resistance.

Since the transformation efficiency was significantly increased with the CRISPR/Cas9 RNPs (Wang et al., 2018), three potential *FoSSOI-mCherry* transformants were randomly selected for further analysis. All of the transformants possessed the desired fusion (Fig. 3.6C) and fluorescence signal when excited at a wavelength of 561 nm under confocal microscopy. The previous study showed when the donor plasmid was directly used for the protoplast

transformation, the maximum correct integrated frequency was ~50% (Wang et al., 2018). However, all our selected HDRI transformants contained the correctly integrated fragments at the expected sites, suggesting that PCR fragment transformation might have a higher integration efficiency in *F. oxysporum* than transformation with plasmid donors. In conidia, FoSso1-mCherry primarily accumulated at the septum and the cell plasma membrane (Fig 3.3B, a and b). FoSso1-mCherry had no specific accumulation except for the septum in the germinating conidia and showed a weak signal in the newly-formed hyphal tip (Fig 3.3B, c and d). Conversely, FoSso1-mCherry accumulated in well-formed hyphae distant from the fungal tips, instead of newly formed hyphae and fungal tips (Fig 3.3B e and f). To further confirm the FoSso1-mCherry subcellular localization results, the Z-series scanning function on the confocal microscopy was used to observe the fungus at a fluorescent range of 3.2 μm with a step of 0.4 μm (Mov. 2, Fig 3.8). The Z-series stack indicated that all three fungal tips showed weak fluorescent signals while the septa and hyphae distal from the fungal tips had strong fluorescence accumulation.

3.3.4 HITI-mediated endogenous gene tagging at the N-terminus of *FoSSO2*

Previous studies have tagged SSO2 orthologs at the N-terminus to avoid the fluorescent protein residing in the lumen of exocytic vesicles, which can result in improper folding of the protein tag (Taheri-Talesh et al., 2008; Valkonen et al., 2007). To further confirm the subcellular localizations of FoSso2 proteins, we conducted with N-terminal tagging to *FoSSO2* gene using the HITI strategy. The donor DNA was composed of a ~800 bp fragment prior to the *FoSSO2* start codon containing a sgRNA cleavage site which was fused with the mCherry coding

sequence fused in frame with the *FoSSO2* coding sequence, including the introns and the 3'-UTR sequence, followed by the hygromycin resistance cassette (Fig 3.4A). During the transformation the entire plasmid is intended to be integrated at the sgRNA cleavage site, and the desired transformants will contain an intact endogenous *FoSSO2* gene fused with a *mCherry* marker gene at the N-terminus (Fig 3.4A). The number of transformant colonies generated using the Cas9 RNPs was much greater than those without the Cas9 RNPs (Fig 3.4B, Table 3.2), indicating that the addition of the Cas9 RNPs significantly enhanced transformation efficiency. A total of 49 independent colonies were selected and screened for detection of mCherry fluorescence, and only five transformants failed to produce any detectable fluorescent signal under confocal microscopy (positive fluorescent efficiency was ~90% (44/49)). Nine randomly selected mCherry-FoSSO2 transformants were further assessed for precise integration at the expected site in the genome by PCR results (data not shown) and sequencing the locus. Sequencing revealed eight of the transformants were correct, having the desired mCherry-FoSSO2 gene fusion, while one transformant contained a 3-bp nucleotide deletion at the sgRNA cleavage site, although the resulting transformant was still fluorescent.

The mCherry fluorescent marker for FoSso2 indicated that the Qa SNARE protein was localized to the fungal plasma membrane (Fig 3.4C). To further investigate the mCherry-FoSso2 plasma membrane localization, confocal microscopy Z-series stacks of live cells were used to further observe key structures involved in *F. oxysporum* conidiation (Fig 3.4C d, Fig 3.9). mCherry-FoSso2 was localized to an extensive array of fungal structures including conidia, phialides, septa, germlings, hyphae, and fungal tips (Fig 3.4C). The localization of FoSso2 to the plasma membrane of a broad range of fungal structures indicates it may serve as

a better marker for the characterization of the plasma membrane than FoSso1.

Clearly the differences in subcellular localization between FoSso1 and FoSso2 indicate divergence during their evolution. While FoSso1-mCherry showed a weak fluorescent signal in germlings and at subapical regions of the hyphae, mCherry-FoSso2 showed strong plasma membrane localization in conidia, fungal germlings, and in hyphae at the apical fungal tips. Qa SNARE proteins encode a single type II transmembrane domain which allows it to be localized to the plasma membrane (Sharpe et al., 2010). Previously, the single Qa SNARE protein SSOA from *Aspergillus nidulans* was shown to localize to the plasma membrane of the hyphal tip with some accumulation at the apical plasma membrane (Taheri-Talesh et al., 2008). Alternatively, in the fungus *Trichoderma reesei* the site of SNARE complex formation between SNCI and SSOI or SSOII was spatially segregated (Valkonen et al., 2007). Both Qa SNARE proteins from *T. reesei* was localized to the plasma membrane; however the SNCI-SSOII complexes were mainly localized to the growing hyphal apical regions while SSOI and SNCI co-localized to subapical regions.

This EGT system is a rapid and efficient method for fungal protein subcellular localization studies. There are several advantages of this system over traditional methods including: 1) conventional methods for protein subcellular localization in fungi required cloning and fusing the promoter region with the gene coding region and fluorescent marker sequences (Kilaru et al., 2015). However, in this CRISPR/Cas9-based EGT system, one or two short homologous fragments around the sgRNA sites were cloned. This avoids the usually time-consuming process to clone large gene coding regions such as the FoCHS5 gene from cDNA; 2) this method does not require the promoter region of a gene to be predicted to generate a construct,

which avoids inaccurate promoter prediction or incorrect expression; 3) the HITI strategy allows a large DNA fragment to be integrated into the fungal genome. This is a potential advantage to simultaneously expressing multiple genes from plasmids in fungi, to be tested in the future; 4) the EGT system could accurately insert DNA fragments at the desired site(s) in the genome, and has a clear advantage over traditional transformation methods since it limits the frequency of random insertion; 5) the desired transformant(s) can be obtained from a small quantity of transformants due to the high efficiency of the system. Despite these advantages, using this EGT system might be difficult for genes with low expression under the native promoter due to low fluorescent signal detection during microscopy.

In this study, we used two different strategies for tagging endogenous genes *in situ* with fluorescent markers in the plant pathogenic filamentous fungus *F. oxysporum*. Both methods allowed the gene of interest to be expressed with a fluorescent signal under the control of the native promoter. The HITI strategy allowed a long DNA fragment to be inserted into the fungal chromosome and was used for the C-terminal tagging of *FoCHS5* and the N-terminal tagging of *FoSSO2*. In addition, the other Qa SNARE syntaxin 1 homologous gene, *FoSSO1*, was tagged by an HDRI strategy. All these tagging transformants carried the desired fluorescent signals. Overall, this CRISPR/Cas9 RNP-mediated transformation method for EGT may facilitate the study of genetic engineering and the elucidation of gene function(s) in *F. oxysporum* and other fungi.

Reference

- Auer, T. O., et al., 2014. Highly efficient CRISPR/Cas9-mediated knock-in in zebrafish by homology-independent DNA repair. *Genome Res.* 24, 142-53.
- Dereeper, A., et al., 2008. Phylogeny.fr: robust phylogenetic analysis for the non-specialist. *Nucleic Acids Res.* 36, W465-W469.
- Finn, R. D., et al., 2016. The Pfam protein families database: towards a more sustainable future. *Nucleic Acids Research.* 44, D279-D285.
- Gordon, T. R., 2017. *Fusarium oxysporum* and the Fusarium Wilt Syndrome. *Annu Rev Phytopathol.* 55, 23-39.
- Gupta, Y. K., et al., 2015. Septin-Dependent Assembly of the Exocyst Is Essential for Plant Infection by *Magnaporthe oryzae*. *Plant Cell.* 27, 3277-3289.
- Hickey, P. C., Read, N. D., 2009. Imaging living cells of *Aspergillus* in vitro. *Med Mycol.* 47 Suppl 1, S110-9.
- Jantti, J., et al., 2002. Characterization of temperature-sensitive mutations in the yeast syntaxin 1 homologues Sso1p and Sso2p, and evidence of a distinct function for Sso1p in sporulation. *J Cell Sci.* 115, 409-20.
- Kienle, N., et al., 2009. Phylogeny of the SNARE vesicle fusion machinery yields insights into the conservation of the secretory pathway in fungi. *BMC Evol Biol.* 9.
- Kilaru, S., et al., 2015. A gene locus for targeted ectopic gene integration in *Zymoseptoria tritici*. *Fungal Genet Biol.* 79, 118-24.
- Kilaru, S., et al., 2017. Fluorescent markers of various organelles in the wheat pathogen *Zymoseptoria tritici*. *Fungal Genet Biol.* 105, 16-27.
- Kong, L. A., et al., 2012. Different chitin synthase genes are required for various developmental and plant infection processes in the rice blast fungus *Magnaporthe oryzae*. *PLoS Pathog.* 8.
- Lev, S., et al., 2012. The Crz1/Sp1 transcription factor of *Cryptococcus neoformans* is activated by calcineurin and regulates cell wall integrity. *PLOS ONE.* 7, e51403.
- Lorang, J. M., et al., 2001. Green fluorescent protein is lighting up fungal biology. *Applied And Environmental Microbiology.* 67, 1987-1994.
- Ma, L. J., et al., 2010. Comparative genomics reveals mobile pathogenicity chromosomes in *Fusarium*. *Nature.* 464, 367-73.
- Madrid, M. P., et al., 2003. Class V chitin synthase determines pathogenesis in the vascular wilt fungus *Fusarium oxysporum* and mediates resistance to plant defence compounds. *Mol Microbiol.* 47, 257-66.
- McCluskey, K., et al., 2010. The Fungal Genetics Stock Center: a repository for 50 years of fungal genetics research. *J Biosci.* 35, 119-26.
- Muhammed, M., et al., 2013. *Fusarium* infection: report of 26 cases and review of 97 cases from the literature. *Medicine (Baltimore).* 92, 305-16.
- Nakanishi, H., et al., 2006. Phospholipase D and the SNARE Sso1p are necessary for vesicle fusion during sporulation in yeast. *J Cell Sci.* 119, 1406-1415.
- Notredame, C., et al., 2000. T-Coffee: A novel method for fast and accurate multiple sequence alignment. *J Mol Biol.* 302, 205-217.
- Nucci, M., Anaissie, E., 2007. *Fusarium* infections in immunocompromised patients. *Clin Microbiol Rev.* 20, 695-704.
- Rasmussen, C. G., Glass, N. L., 2005. A rho-type GTPase, rho-4, is required for septation in *Neurospora crassa*. *Eukaryot Cell.* 4, 1913-1925.
- Salaun, C., et al., 2004. Plasma membrane targeting of exocytic SNARE proteins. *Biochim Biophys Acta.* 1693, 81-9.

- Schumacher, J., et al., 2008. Calcineurin-responsive zinc finger transcription factor CRZ1 of *Botrytis cinerea* is required for growth, development, and full virulence on bean plants. *Eukaryotic Cell*. 7, 584-601.
- Schuster, M., et al., 2016. Co-delivery of cell-wall-forming enzymes in the same vesicle for coordinated fungal cell wall formation. *Nat Microbiol*. 1, 16149.
- Scott, M. S., et al., 2005. Refining protein subcellular localization. *PLoS Comput Biol*. 1, e66.
- Sharpe, H. J., et al., 2010. A comprehensive comparison of transmembrane domains reveals organelle-specific properties. *Cell*. 142, 158-69.
- Spielvogel, A., et al., 2008. Two zinc finger transcription factors, CrzA and SltA, are involved in cation homeostasis and detoxification in *Aspergillus nidulans*. *Biochemical Journal*. 414, 419-429.
- Suzuki, K., et al., 2016. In vivo genome editing via CRISPR/Cas9 mediated homology-independent targeted integration. *Nature*. 540, 144-+.
- Taheri-Talesh, N., et al., 2008. The tip growth apparatus of *Aspergillus nidulans*. *Mol Biol Cell*. 19, 1439-49.
- Treitschke, S., et al., 2010. The Myosin Motor Domain of Fungal Chitin Synthase V Is Dispensable for Vesicle Motility but Required for Virulence of the Maize Pathogen *Ustilago maydis*. *Plant Cell*. 22, 2476-2494.
- Valkonen, M., et al., 2007. Spatially segregated SNARE protein interactions in living fungal cells. *J Biol Chem*. 282, 22775-85.
- van Dam, P., et al., 2017. A mobile pathogenicity chromosome in *Fusarium oxysporum* for infection of multiple cucurbit species. *Sci Rep*. 7, 9042.
- Vlaardingerbroek, I., et al., 2016. Dispensable chromosomes in *Fusarium oxysporum* f. sp. *lycopersici*. *Mol Plant Pathol*. 17, 1455-1466.
- Wang, Q., et al., 2018. Efficient genome editing in *Fusarium oxysporum* based on CRISPR/Cas9 ribonucleoprotein complexes. *Fungal Genet Biol*. 117, 21-29.
- Wang, Q., Coleman, J. J., 2019. CRISPR/Cas9-mediated endogenous gene tagging in *Fusarium oxysporum*. *Fungal Genet Biol*.

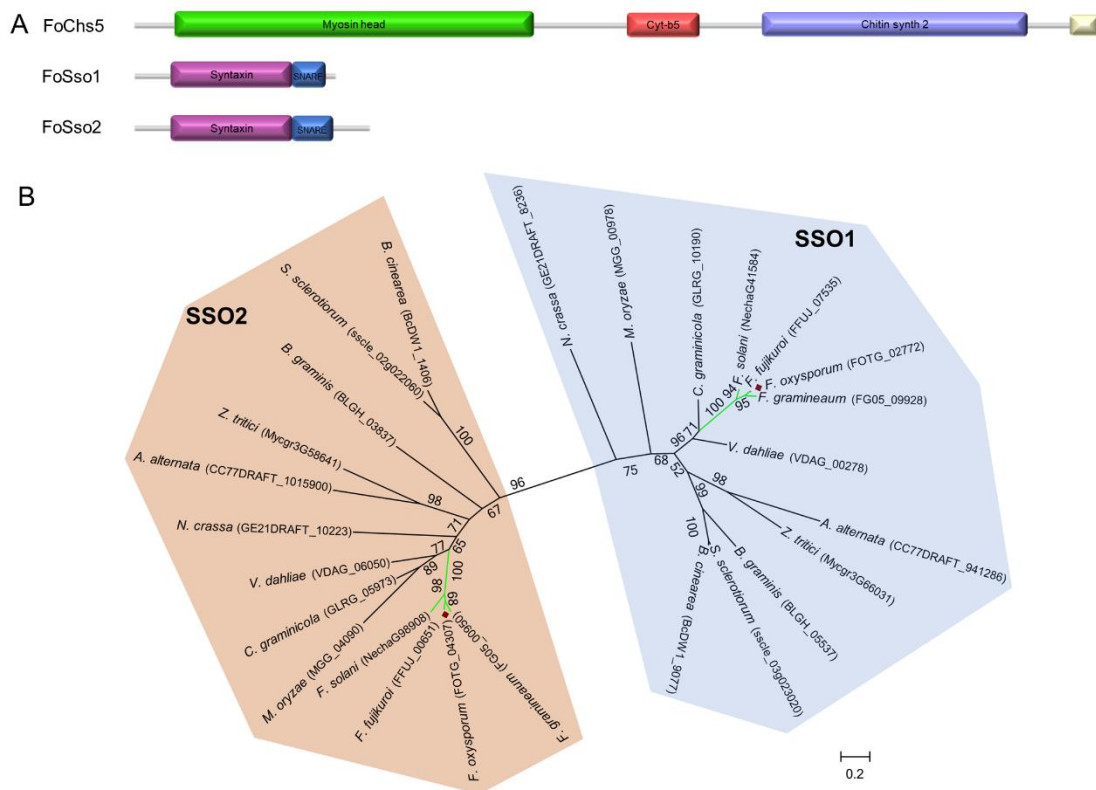


Figure 3.1 Identification of FoChs5, FoSso1 and FoSso2 proteins in *F. oxysporum*. (A) The protein domain structures of the chitin synthase FoChs5, and the two syntaxin proteins FoSso1 and FoSso2. (B) The maximum-likelihood phylogenetic tree of Sso1 and Sso2 amino acid sequences from selected filamentous ascomycete fungi. The tree was generated with a bootstrap value of 500.

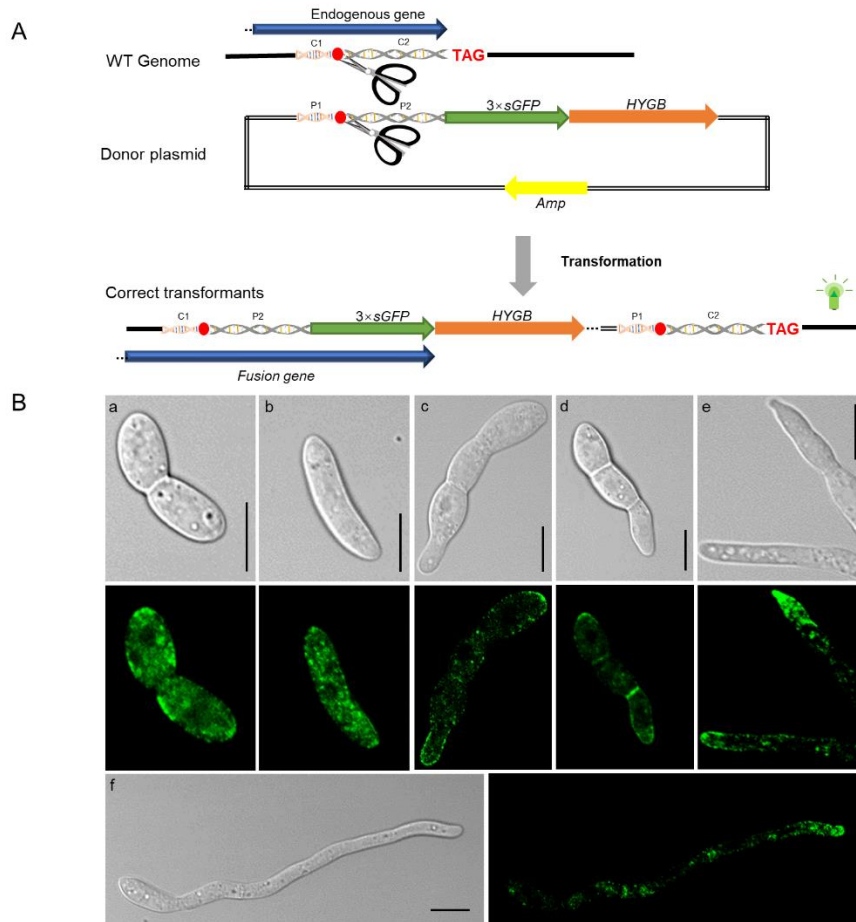


Figure 3.2 *FoCHS5* gene C-terminal tagging with a $3\times sGFP$ fluorescent marker based on the HITI strategy.

(A) The homology-independent targeted integration (HITI) strategy scheme for the C-terminal tagging of *FoCHS5* gene. A bait sequence, ~ 700 bp in length containing the sgRNA cleavage site, was cloned prior to gene stop codon and fused with a $3\times sGFP$ marker and the hygromycin resistance cassette sequences. During transformation, two DNA cross-ligation events will occur between the donor plasmid and the fungal chromosome (C1-P2 and P1-C2). The whole plasmid will be inserted into the sgRNA cleavage site on the fungal chromosome in the desired transformants. The C1-C2 fragment is homologous to the P1-P2 fragments B) *FoChs5*- $3\times sGFP$ subcellular localization in different fungal structures. a and b: conidia, c and d: conidia with the emerging germination tubes, e: fungal tips, f: hyphae, Scale bars, $10\ \mu$

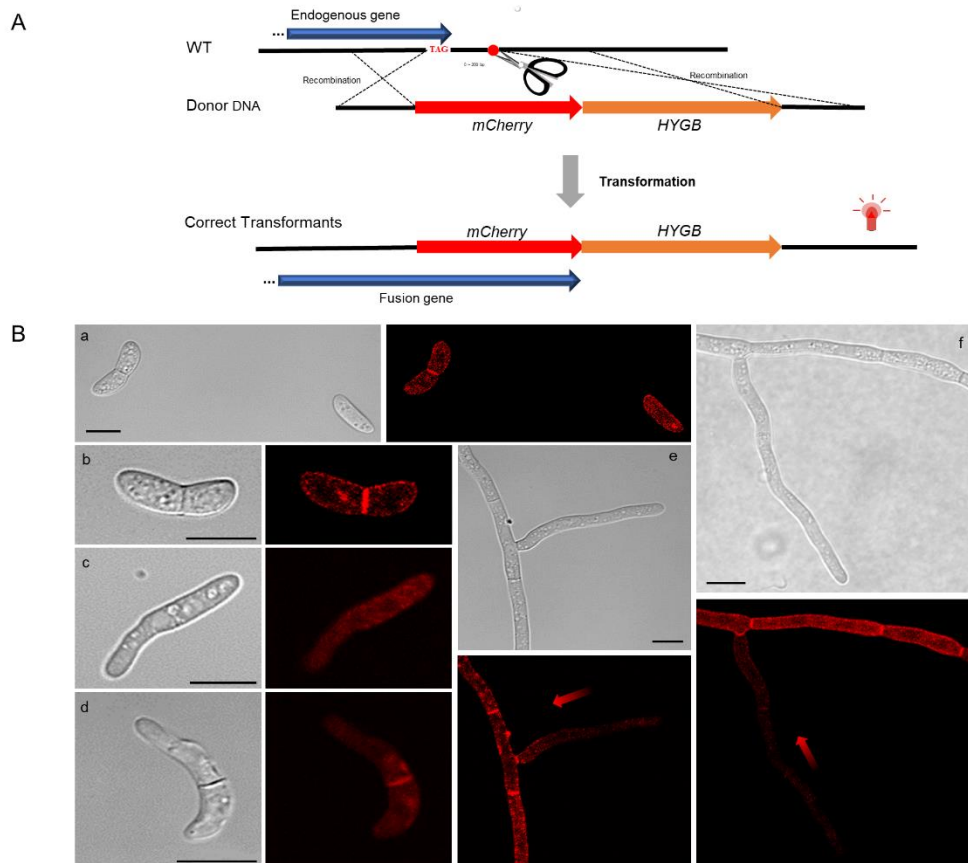


Figure 3.3 *FoSSO1* gene C-terminal tagging with a *mCherry* fluorescent marker based on the HDRI strategy.

(A) An illustration of the homology-dependent recombination integration (HDRI) strategy for the C-terminal tagging of *FoSSO1* and *FoSSO2* genes. A homologous upstream fragment was amplified prior to the gene stop codon and fused with *mCherry*, the hygromycin resistance cassette, and a homologous downstream fragment that is immediately after the sgRNA cleavage site. During the transformation, two homologous recombination events will be expected to occur and *mCherry-Tef-1-HYGB* fragment will be integrated at the 3'-terminus of the endogenous gene. (B) the FoSso1-mCherry subcellular localization in different fungal structures. a and b: conidia, c and d: germlings, e and f: fungal tips and hyphae. Gradient red arrows weaken from strong to weak, suggesting different distribution of the FoSso1 protein. Scale bars, 10 μm .

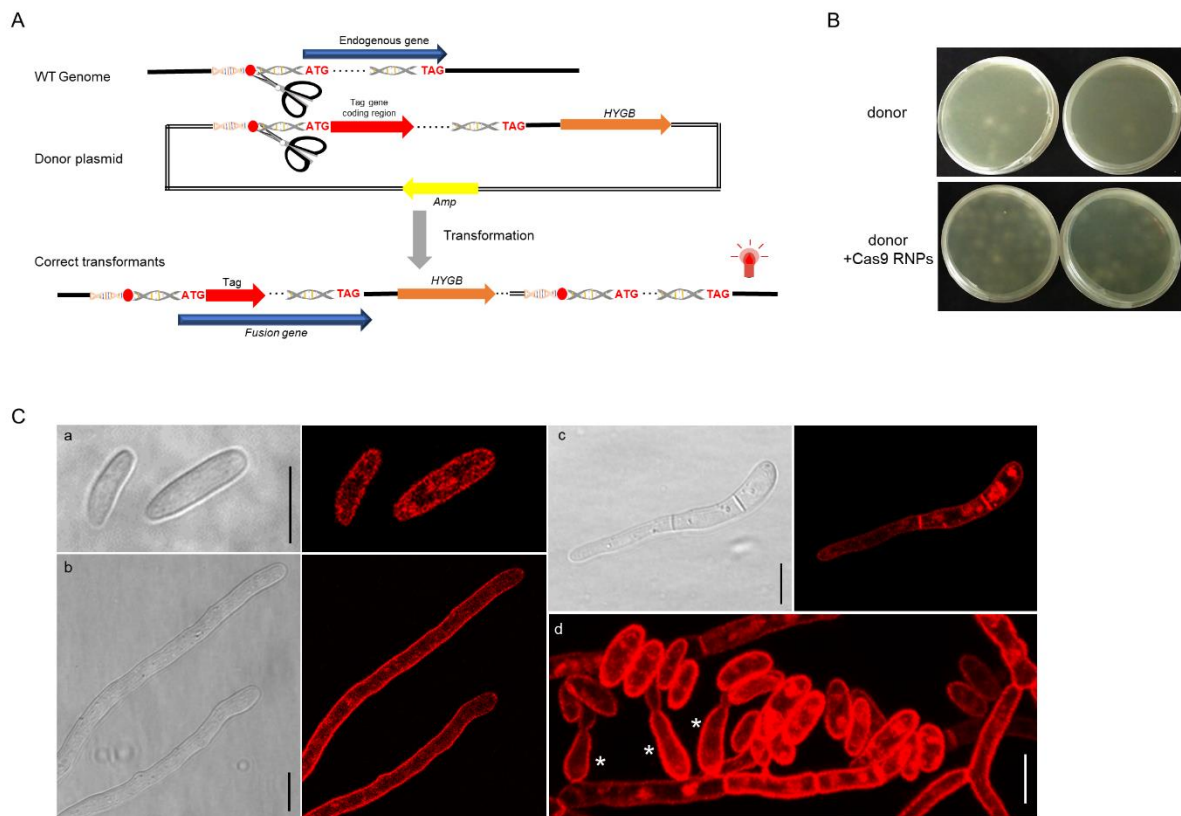


Figure 3.4 *FoSSO2* gene tagging with a N-terminal *mCherry* fluorescent marker based on the HITI strategy.

(A) a ~800 bp homologous sequence containing the sgRNA cleavage site in front of the *FoSSO2* gene start codon was cloned and fused with a 1×*mCherry* marker, *FoSSO2* endogenous gene, a 3'-UTR region of the *FoSSO2* gene and the hygromycin resistance cassette sequences. During the transformation, the whole plasmid can be inserted into the sgRNA site and a N-terminal *mCherry* fusion gene for the *FoSSO2* can be generated. (B) Comparisons of the transformation efficiency with or without Cas9 RNPs for the *FoSSO2* N-terminal tagging. (C) *mCherry*-*FoSSO2* subcellular localization in different fungal structures. a: conidia, b: fungal tips, c: a germling, d: fungal conidiation, *: phyllides Scale bars, 10 μm .

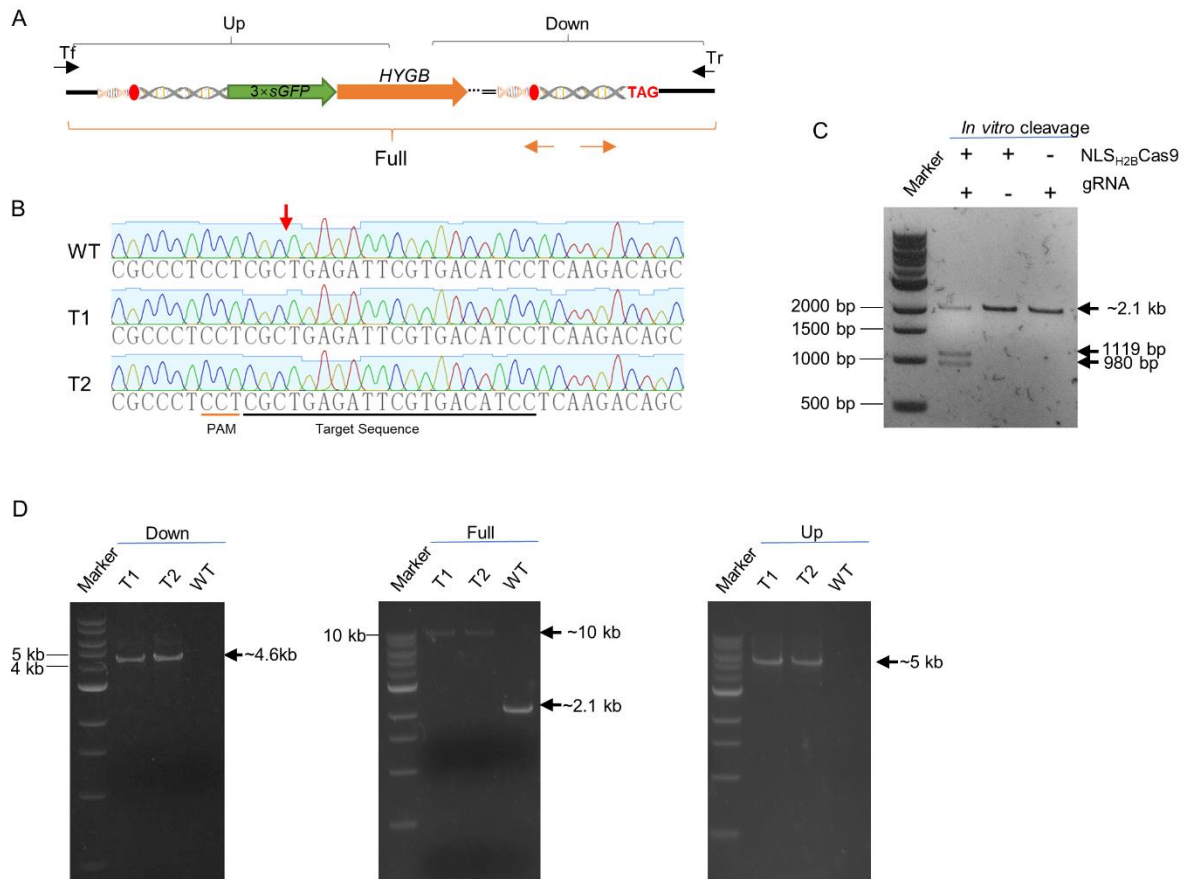


Figure 3.5 Screen of the correct HITI transformants for generation of *FoCHS5-3xsgFP*. (A) the illustration of the chromosomal region of a correct HITI transformant after the integration of the entire plasmid. Tf and Tr: a pair of primers located outside of the bait sequence and can be used to clone a ~2.1 kb fragment, from the wild-type strain DNA, which was used for the *in vitro* Cas9 nuclease assay. Three PCR products, Up, Down and Full, were used to confirm the location of the integrated plasmid at the correct target site. (B) The sequencing results of DNA fragments containing the sgRNA sites for the wild-type strain and two transformants. (C) *In vitro* Cas9 RNPs cleavage assay to assess sgRNA target sequence. (D) agarose gel electrophoresis for the three DNA fragments based on the three pairs of primers from (A).

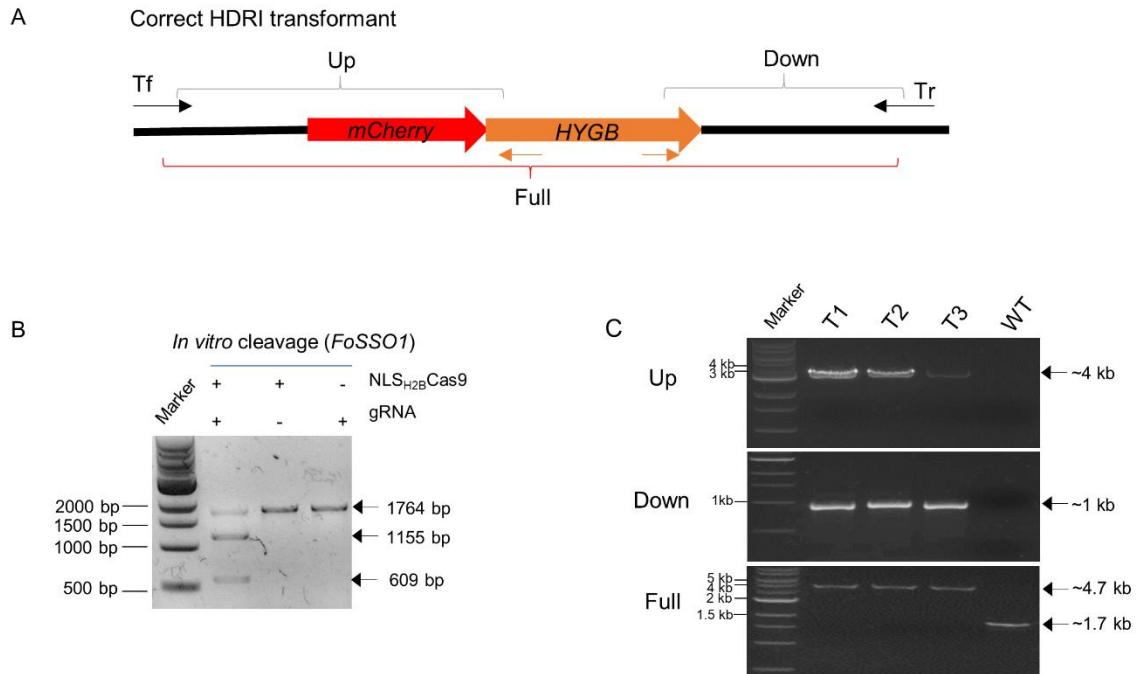


Figure 3.6 Screen of the correct HDRI transformants for generation of *FoSSO1-mCherry* (A) the illustration of the chromosomal region for correct HDRI transformants after homologous recombination. Tf and Tr: a pair of primers located outside of the homologous arms and can be used to amplify a fragment from the wild-type strain DNA for the *in vitro* Cas9 nuclease assay. Three fragments, Up, Down and Full, were used to determine the location of the integrated fragment at the desired positions. The two orange arrows represent different primers located in the region of the *mCherry-Tef-1-HYGB*. B) *In vitro* Cas9 RNPs cleavage assay for the *FoSSO1* gene. C) The results of agarose gel electrophoresis for three DNA fragments based on three pairs of primers from A).

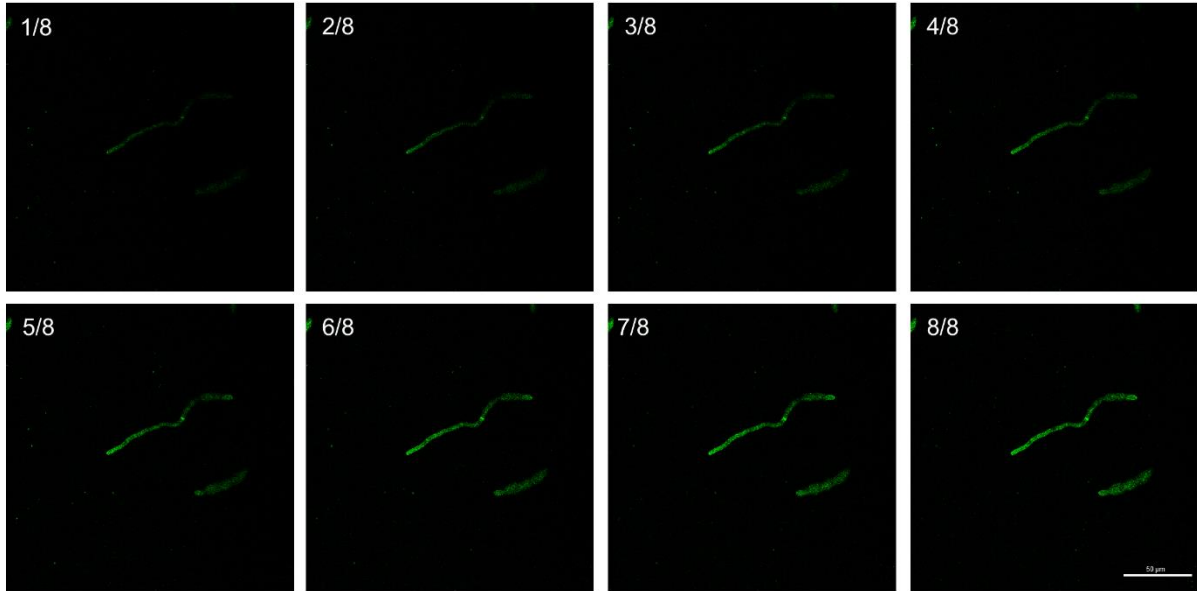


Figure 3.7 Each frame of the FoChs5-3xGFP Z-series stack

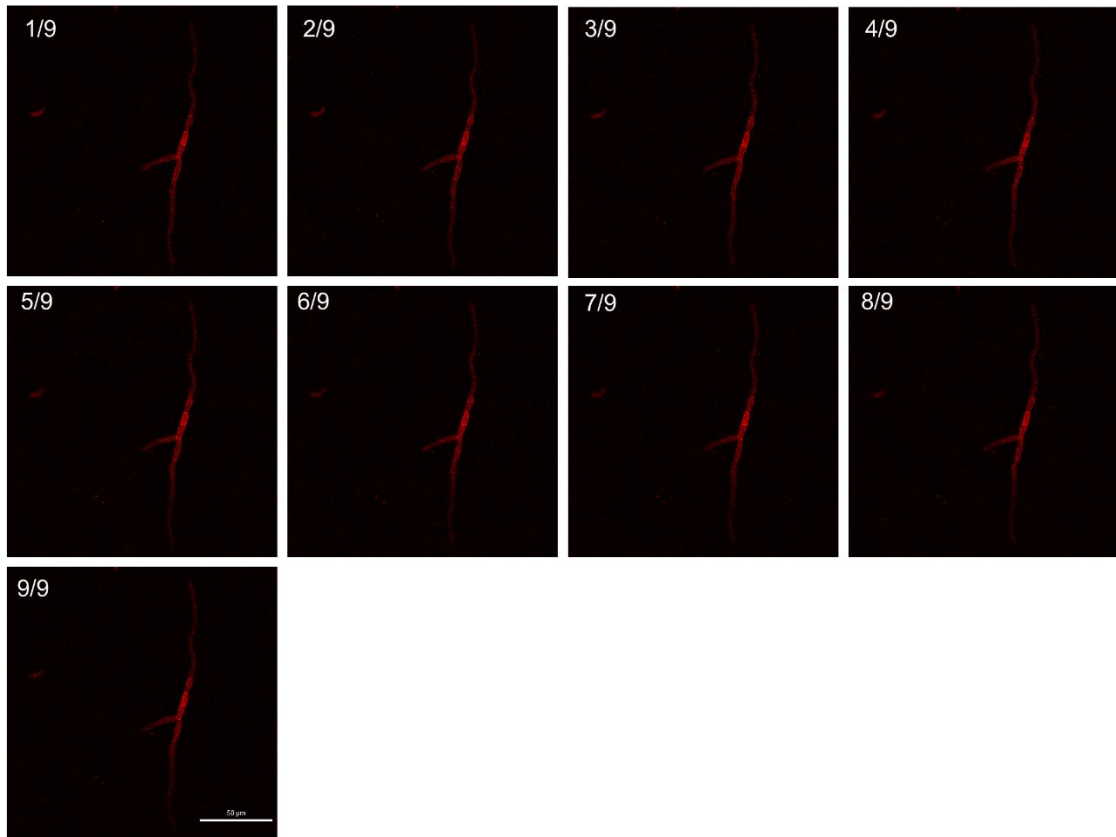


Figure 3.8 Each frame of the FoSso1-mCherry Z-series stack

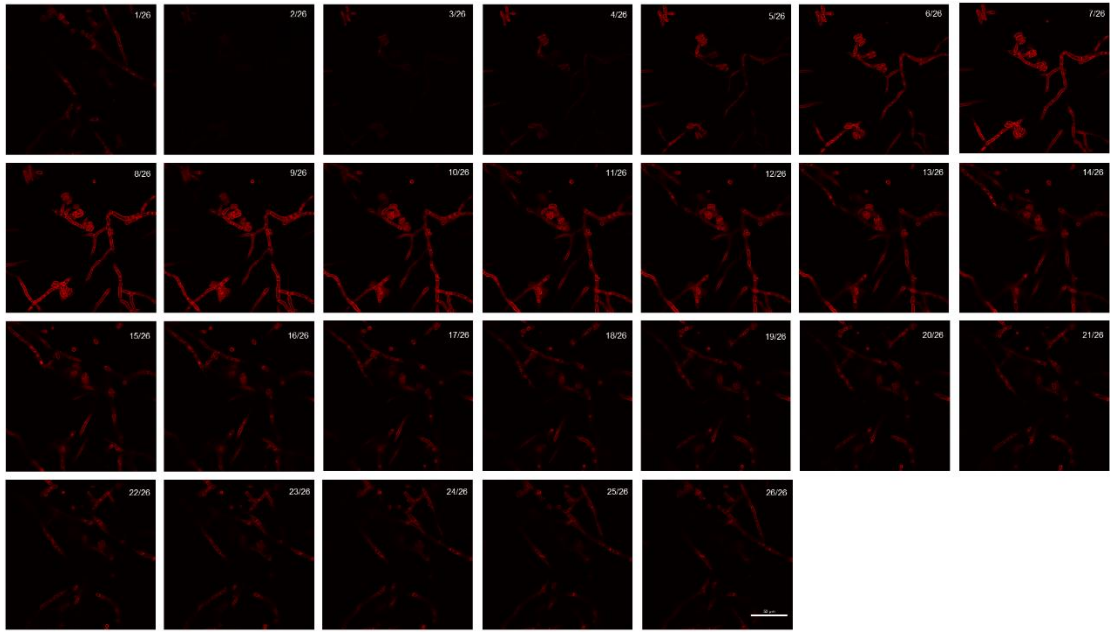


Figure 3.9 Each frame of the mCherry-FoSso2 Z-series stack

Table 3.1 The sgRNAs and associated transformants of *F. oxysporum* in Chapter 3

sgRNA	PAM	Targeted gene	Gene No.	Genotype of transformants
GGATGTCACGA ATCTCAGCG	AGG	<i>FoCHS5</i>	FOTG_09933	<i>FoCHS5-3×sGFP</i> ^{EGT} , <i>hyg</i> ^R
GAGCATCAACA TCATAACAG	CGG	<i>FoSSO1</i>	FOTG_02772	<i>FoSSO1-mCherry</i> ^{EGT} , <i>hyg</i> ^R
GATCAAAGAGA AGAATGATC ^{RCS}	GGG ^{RCS}	<i>FoSSO2</i>	FOTG_04307	<i>mCherry-FoSSO2</i> ^{EGT} , <i>hyg</i> ^R

hyg^R, hygromycin B resistance; ^{EGT}, endogenous gene tagging; ^{RCS}: reverse complement sequence.

Table 3.2 The transformant amounts of the N-terminal tagging of *FoSSO2* gene

Transformation plate	Cas9 RNPs	Transformation amounts
FoSSO2_C1	-	7
FoSSO2_C2	-	4
FoSSO2_T1	+	59
FoSSO2_T2	+	46
FoSSO2_T3	+	61
FoSSO2_T4	+	37
FoSSO2_T5	+	54
FoSSO2_T6	+	43

Table 3.3 The sequences of oligonucleotides used in Chapter 3

Primer names	Oligomer sequences	Usage
NA_PV_sGFPf	AGTGAATTCGAGCTCGGTACCCGGGA TGGTGAGCAAGGGCGAG	
NA_PV_sGFPr	ATCGAATGTCCGCTTACTTGTACAGC TCGTCCATG	The construction of the plasmid primary vector
NA_PV_Tef1f	GCTGTACAAGTAAGCGGACATTCGAT TTATGC	(<i>sGFP - Tef-1 - HYGB</i>)
NA_PV_Tef1r	TTCCATTAATATATTGGTGGCATGATG GTTG	
NA_PV_HYGBf	ATCATGCCACCAATATATTAATGGAAG GGTATATAACCACGC	
NA_PV_HYGBr (Universal)	AACAGCTATGACCATGATTACGCCAA GGGTTGCGAGGTCCAATG	
CHS5TF1	CAACGCCAAGGGCTCTTTCA	1. <i>FoCHS5</i> <i>in vitro</i> cleavage template; 2. transformant PCR detection (Full)
CHS5TR1	CGCACTCGTTTGCTACGTCT	
NA_CHS5hitiF	AGTGAATTCGAGCTCGGTACCCGGGG CCCATTACAGCTTTCTTG	
NA_CHS5hitiR	CGCCCTTGCTCACCAATTGGCCAGAA AGCAG	The construction of the plasmid pUC19-HITI-
NA_CHS5hiti- 3×egfpF1	TTCTGGCCAATTGGTGAGCAAGGGC GAGGAG	<i>FoCHS5-3×sGFP</i> . (HITI bait -3× <i>sGFP</i> - <i>Tef-1</i> - <i>HYGB</i>)
NA_CHS5hiti- 3×egfpR1	GTCGTCCTTGTAGTCCTTGTACAGCT CGTCCATGC	
NA_CHS5hiti- 3×egfpF2	GACTACAAGGACGACGTGAGCAAGG GCGAGGAG	
NA_CHS5hiti- 3×egfpR2	GTAAGCGCCAGCGCTCTTGTACAGCT CGTCCATGC	
NA_CHS5hiti- 3×egfpF3	AGCGCTGGCGCTTACGTGAGCAAGG GCGAGGAGCTG	
HyB_R3	TCCTCGGCCCAAAGCATCAG	Detection of Up fragment with TF primer (CHS5TF1 and FoSSO1TF1)
H _{out} F	GTCGATGCGACGCAATCGT	Detection of Down fragment with TR primer (CHS5TR1 and FoSSO1TR1)
FoSSO1TF1	CCCGCCATTGCTTCCTTGTT	1. <i>FoSSO1</i> <i>in vitro</i> cleavage template; 2. PCR detection (Full fragment) of the transformants;
FoSSO1TR1	TTCGTCAAGCCCTGTCCGAT	

NA_FoSSO1upF	AGTGAATTCGAGCTCGGTACCCGGGC GCTATCGCGATCAGATTG CCTTGCTCACCATCTTGTGTTGTTGG	The construction of the plasmid pUC19-HDRI- <i>FoSSO1-mCherry</i> (up arm - <i>mCherry</i> - <i>Tef-1</i> – <i>HYGB</i> – down arm)
NA_FoSSO1upR	CCAC	
NA_FoSSO1mChH YBF	CAACAACAACAAGATGGTGAGCAAG GGCGAG	
NA_FoSSO1mChH YBR	ATCAACATCATAAAGGGTTGCGAGGT CCAATG ACCTCGCAACCCTTTATGATGTTGATG	
NA_FoSSO1downF	CTCTG AACAGCTATGACCATGATTACGCCAA	
NA_FoSSO1downR	ATACCATGGAATCTCTACTC	
FoSSO2TF2	GGATAGTGCCGGTGATTGCG	1. <i>FoSSO2</i> N-terminal tagging template for <i>in vitro</i> cleavage; 2. PCR detection (Full fragment) of the transformants;
FoSSO2TR2	TCCATAACCCTGAGCGGGTG	
NA_mCS2hiti1F	AGTGAATTCGAGCTCGGTACCCGGGT CATGACGATGCGAACCTTG	The construction of the plasmid pUC19-HITI- <i>mCherry-FoSSO2</i> (HITI bait -1× <i>mCherry</i> – <i>SSO2 ORF(3-UTR)</i> - <i>HYGB</i>)
NA_mCS2hiti1R	CGCCCTTGCTCACCATTGTAGTGACT GAGCTGG	
NA_mCS2mcherryF	AGTCACTACAATGGTGAGCAAGGGC GAGGAG	
NA_mCS2mcherryR	GCAAATAAATACTCTTGTACAGCTCG TCCATGC	
NA_mCS2SSO2F	CGAGCTGTACAAGAGTGTTAGTTTGC GCCTC	
NA_mCS2SSO2R	TTCATTAATATATGGCGTATAGGTTG TCTG	
NA_mCS2HYGBf	AACCTATACGCCATATATTAATGGAAG GGTATATAACCACGC	
FoCHS5CTsgRNA	AAGCTAATACGACTCACTATAGGATG TCACGAATCTCAGCGGTTTTAGAGCT AGAAATAGCAAG	sgRNA DNA template synthesis
FoSSO1CTsgRNA	AAGCTAATACGACTCACTATAGGAGC ATCAACATCATAACAGGTTTTAGAGC TAGAAATAGCAAG	
FoSSO2NTsgRNA	AAGCTAATACGACTCACTATAGGATC AAAGAGAAGAATGATCGTTTTAGAGC TAGAAATAGCAAG	

Chapter 4.

The extracellular superoxide dismutase Sod5 from *Fusarium oxysporum* is localized in response to external stimuli and contributes to fungal pathogenicity

4.1 Introduction

The ascomycete fungus, *Fusarium oxysporum* (Fo), is an important pathogenic fungus which can infect and cause disease on a wide range of hosts including plants, animals, and humans (Gordon, 2017). Over 100 formae speciales have been described based on the ability of these fungi to cause disease on different host plants. For example, *F. oxysporum* f. sp. *lycopersici* is regarded as a tomato pathogen causing tomato wilt disease while *F. oxysporum* f.sp. *cubense* is the causal agent of banana wilt disease (Lagopodi et al., 2002; Ploetz, 2006). *F. oxysporum* f. sp. *vasinfectum* (Fov), is responsible for Fusarium wilt of cotton, a significant disease that reduces cotton yields. This soil-borne fungus invades vascular tissue via host roots and rapidly spreads to the aboveground portion of the host. Typical field symptoms of Fusarium wilt include yellowing, chlorotic leaves, dark-brown/necrotic xylem (discoloration), and wilting eventually leading to plant death (Davis et al., 2006).

Reactive oxygen species (ROS) produced by host cells play an important role in defense

against various pathogens. These small ROS molecules are highly toxic to the infective agents and are able to directly kill them. At the interaction between the host and pathogen, host cells rapidly synthesize and accumulate large quantities of ROS, during a process called the oxidative burst (Heller and Tudzynski, 2011). In plants, the oxidative burst may result in a hypersensitive response (HR) phenomenon which can inhibit the spread of the pathogen to surrounding tissue (Zurbriggen et al., 2010). Additionally, ROS serve as an important signal which can trigger a series of other plant defense responses or the production of plant hormones (Sauer et al., 2001). These processes effectively stimulate plant hosts to re-program the expression of genes involved in defense, leading to the production of antimicrobial compounds such as phytoalexins, callose deposition, and systemic acquired resistance (SAR); collectively impeding pathogens from spreading and causing disease (Forman et al., 2010; Sauer et al., 2001).

Despite the extensive production of ROS in plant defense, successful pathogens are usually able to survive in a high ROS environment and have evolved strategies to overcome these detrimental effects (Aguirre et al., 2006; Fones and Preston, 2012) as it is essential for pathogens to tolerate ROS during the infection process. The group of enzymes referred to as superoxide dismutases (SOD) are well-known to participate in catalyzing the partitioning of superoxide radicals. SOD enzymes are divided into several families according to structure of the enzymes and the binding of a metal cofactor, and include the copper and zinc SODs (Cu/Zn SOD), the iron or manganese SODs (Fe/Mn SOD), and the nickel SODs (Miller, 2012). The cytosolic Cu/Zn SODs are the most common SOD enzymes in eukaryotic cells where there is at least one Cu/Zn SOD encoding gene in a genome. In *Saccharomyces cerevisiae*, loss of

SOD1 can lead to slow growth and increased sensitivity to ROS when exposed in ROS-generating compounds (Moradas-Ferreira and Costa, 2000). Additionally, *SOD1* mutants showed attenuated virulence in some fungal pathogens. For example, the *SOD1* mutant strain of *Cryptococcus neoformans* showed less virulence than the wide-type strain and showed significantly decreased growth in macrophages (Cox et al., 2003). Additionally, loss of function of *SOD1* gene can alter normal fungal physiology. For instance, *SOD1* mutants of the ericoid mycorrhizal fungus *Oidiodendron maius* had reduced production of conidia and the capacity for mycorrhization (Abba et al., 2009). Fe/Mn SODs mainly exist in prokaryotes, protists, or mitochondria/chloroplasts, suggesting that Fe/Mn SODs are an ancient family of SODs (Miller, 2012). Only a few prokaryotic microorganisms use nickel SODs for reducing its substrates (Youn et al., 1996).

A class composed of extracellular SODs has recently been described in various pathogens (Robinett et al., 2018). In bacteria, highly virulent *E. coli* serotype O157:H7 obtained additional secreted *SodC* through horizontal prophage gene transfer and is highly resistant to degradation by host proteases (D'Orazio et al., 2008). In fungi, extracellular SODs are a typical glycosylphosphatidylinositol (GPI) protein where they usually contain an N-terminal secreted signal peptide and a C-terminal GPI anchor attachment site. The mature GPI anchor enables proteins to be located to the cell membrane or cell wall by covalent attachment (Mayor and Riezman, 2004; Robinett et al., 2018). Current experimental evidence has indicated that some fungal extracellular SODs can be secreted out of the cell and participate in catalyzing the partitioning of superoxide radicals produced by host cells allowing fungi to survive in a high ROS environment (Youseff et al., 2012). The acquirement of extracellular SODs during the

evolution of fungal pathogens largely improves their pathogenicity (D'Orazio et al., 2008; Gleason et al., 2014; Youseff et al., 2012). *Candida albicans* can secrete a SOD (Sod5), a Cu-only co-factor type, and this gene is required for pathogen defense (Gleason et al., 2014). In addition, the secreted Sod5 rapidly obtains the copper co-factor from the host to compromise the copper toxicity to *C. albicans* (Li et al., 2015). Similarly, an extracellular superoxide dismutase in the dimorphic fungus *Histoplasma capsulatum*, contributes to resistance to host-derived oxidative stress in yeast cells (Youseff et al., 2012). In *Puccinia striiformis*, the causative agent of stripe rust on wheat, a secreted extracellular Zn-only SOD contributes to enhanced resistance to oxidative stress during the interaction between the wheat host and the fungus (Liu et al., 2016). All these results showed extracellular SODs played an important role in pathogenicity to hosts and reduction of oxidative stress.

In *S. cerevisiae*, Sod1 has been shown to be localized to the nucleus when yeast cells were exposed to elevated H₂O₂ (Tsang et al., 2014). Once shuttled into the nucleus, Sod1 acts as a transcription factor binding DNA promoter regions and regulating gene expression (Tsang et al., 2014). Extracellular SODs are phylogenetically conserved throughout fungi and are predicted to have evolved from the canonical Sod1 (Robinett et al., 2018), and are therefore likely to share a similar biological function. However, little research has focused on the functional role of the homologous gene in other filamentous fungi. In this study, the extracellular SOD (FoSod5) from *Fusarium oxysporum* f. sp. *vasinfectum* was characterized and shown its subcellular localization is dependent on environmental conditions. During normal growth, FoSod5 was mainly localized to the fungal phialides. When fungi were exposed to a high ROS environment, FoSod5 was rapidly re-localized to the septum and cell wall. In a

lacZ reporter assay, the results indicate FoSod5 was a GPI protein that was rapidly induced in alkaline conditions and the GPI site was required for correct protein subcellular localization. Loss of the *FoSOD5* gene led to a reduction in fungal virulence on cotton.

4.2 Materials and Methods

***F. oxysporum* strain, *E. coli* strain, plant materials, and growth conditions**

Fusarium oxysporum f. sp. *vasinfectum* (*Fov*), a strain highly virulent on cotton, was obtained from the Fungal Genetics Stock Center (FGSC #10442) and used in this study. The wild-type *Fov* isolate and all mutant and complemented strains were cultured at room temperature (25 °C) on Potato Dextrose agar (PDA) medium or minimum nutrient medium (M-100). All *F. oxysporum* strains used in this study are listed in the Table 4.1. The mutant and complemented strains were screened on M-100 agar medium containing hygromycin B or G418 at a final concentration of 150 µg/mL or 60 µg/mL, respectively. For evaluation of fungal sensitivity to various chemical stressors, a 5 mm diameter mycelial plug was taken from the edge of a four-day-old culture grown on M-100 agar medium and put onto the new agar medium containing the chemical. The diameter of the colony was evaluated after seven days. Each treatment was repeated three times.

E. coli DH5α was used for construction and propagation of the transformation vectors. *Agrobacterium tumefaciens* strain AGL-1 was used for fungal transformation (Mullins et al., 2001). Cotton cultivar FM1944 was chosen for pathogenicity assays, and was cultured in a growth chamber with a period of 16 h light 30 °C and 8 h darkness 25 °C.

Bioinformatics analysis

The SOD protein family in *F. oxysporum* was identified using BLASTP software in the Ensembl Fungi database (<https://fungi.ensembl.org/index.html>) with several SOD query sequences (*S. cerevisiae* Sod1: YJR104C and Sod2: YHR008C; *C. albicans* Sod5: XP_719507). Protein domains were predicted using PFAM (El-Gebali et al., 2019) and BLASTP software. The subcellular localization peptide sequences were identified with SeqNLS and WoLF PSORT (Horton et al., 2007; Lin and Hu, 2013). Secreted signal peptides were predicted with SignalP 4.1 (Petersen et al., 2011). Multiple sequence alignments were conducted with the online software TCOFFEE (Notredame et al., 2000), and the phylogenetic tree was generated with PhyML 3.1 (Guindon et al., 2010). The 3D protein structure of FoSod5 was predicted by the SWISS-MODEL server (Gleason et al., 2014; Waterhouse et al., 2018).

Plasmid constructions

The *FoSOD5* gene complementary plasmid, pCom-G418^R-*FoSOD5*, was constructed based on the background plasmid of pCAMBIA1302 as the following: 1) the hygromycin cassette under the 35S promoter between the XhoI and KpnI restriction sites was replaced with a neomycin phosphotransferase II cassette (*trpC* promoter) amplified from the pII99 plasmid; 2) the *FoSOD5* gene locus, ~4 kb in length, was cloned from genomic DNA using the primers FoSOD5cassF and FoSOD5cassR, and ligated into the above constructed plasmid between the LB- and RB- T-DNA sequences with the NEBuilder[®] HiFi DNA Assembly Cloning Kit (New England Biolabs).

The HITI Cas9 RNP transformation plasmid, pUC19-HITI-*FoSOD5C2*, was constructed

using the NEBuilder[®] HiFi DNA Assembly Cloning Kit and four PCR fragments were simultaneously assembled into the pUC19 plasmid between the BamHI and the HindIII restriction sites in the following order, the first fragment contained a ~ 1kb upstream sequence and partial amino acid coding region (AA: 1-53) (primers: NA_FoSod5C1hitiF and NA_FoSod5C2uphitiR), the second fragment was the *sGFP* coding region (primers: NA_FoSod5C2midsGFPF and NA_FoSod5C2midsGFPF), the third fragment contained the partial amino acid coding region (AA: 186-end containing the GPI site) and the predicted native terminator of the *FoSOD5* gene (~800 bp) (primers: NA_FoSod5C2downF and NA_FoSod5C2downR), and the fourth fragment was the hygromycin cassette amplified from plasmid pUC19-HDRI-FoSSO1-mCherry (primers: NA_FoSod5C2HYGBF and Universal_NA_forHITITR) (Wang and Coleman, 2019). The plasmid pUC19-HITI-*FoSOD5C2* contained the *FoSOD5* gene with the catalytic SOD domain replaced by *sGFP*. The plasmids pUC19-HITI-*FoSOD5C1* and pUC19-HITI-*FoSOD5C3* were generated in a similar way. Plasmid pUC19-HITI-*FoSOD5C1* did not contain the amino acid sequences after the SOD domain, while in pUC19-HITI-*FoSOD5C3*, the ORF of the *FoSOD5* gene was completely replaced by the β -galactosidase (*lacZ*) coding region cloned from the plasmid, pCYC-*lacZ*. The three different plasmids were used to generate variants of FoSod5 enabling the study of the function of the FoSod5 protein, including protein secretion, protein subcellular localization, and protein expression. All PCR primers used are listed in Table 4.2

Target gene replacement and gene complementation

The target gene, *FoSOD5*, was replaced with the hygromycin B resistance cassette using

a previously described split-marker approach with a few modifications (Goswami, 2012). Briefly, $\sim 10^7$ conidia were inoculated into 100 mL of fresh PDB liquid medium and grown on a rotary shaker at 30 °C 180 rpm for ~ 12 -14 h. The fungal germlings were collected and treated by a mixture of protoplasting enzymes, 10 mg/mL DriselaseTM from *Basidiomycetes sp.* (Sigma), 15 mg/mL β -Glucanase from *Trichoderma longibrachiatum* (Sigma), and 5 mg/mL Lysing enzymes from *T. harzianum* (Sigma) for 2-3 h. The resulting protoplasts were filtered through Nitex Nylon mesh, centrifuged, collected, and washed with SuTC buffer. The protoplasts were suspended in SuTC buffer to a concentration of 2×10^7 protoplasts/mL. The DNA fragments were generated by overlapping fusion PCR (Goswami, 2012). The protoplast suspension (200 μ L) was mixed with a total of 10 μ g of the DNA fragments (5 μ g of the upstream fragment and 5 μ g of the downstream fragment) and were incubated at room temperature for 20 min. One mL of PSTC was slowly added to the above protoplast mixture, mixed, and left at room temperature for 20 min. After that time, 3 mL of TB3 liquid medium with 25 μ g/mL Amp antibiotics were added. The transformed protoplasts were cultured on a rotary shaker (160 rpm) for 20 h. Once the cell wall was regenerated, ~ 15 mL of melted bottom agar (~ 60 °C) with 100 μ g/mL hygromycin B were mixed with the transformed protoplasts and poured onto plates. After 10 h, a top layer of agar medium with 150 μ g/mL hygromycin B was poured over the bottom medium. Resistant colonies emerged within 3 \sim 5 days, and the resistant colonies are transferred to M-100 medium with hygromycin B for further evaluation.

For the *FoSOD5* gene complementation, a *Agrobacterium*-mediated transformation method was used according to a previous publication with a few modifications (Mullins et al., 2001). The $\Delta FoSOD5$ strain was inoculated into fresh PDB medium at 160 rpm, room

temperature (25 °C) for three to five days. *A. tumefaciens* strain AGL-1 containing the plasmid pCom-G418^R-*FoSOD5* was grown at 28 °C, 180 rpm for two days in LB liquid medium with appropriate antibiotics. The AGL-1 was diluted to an OD₆₀₀ value of 0.2 in induction medium containing 100 μM acetosyringone (Sigma) and associated antibiotics. The induction time length was about 6 h, after which a 100 μL conidial suspension (1×10^7 / mL) was mixed with an equal volume of the above AGL-1 induction medium. The total mixture was plated on the surface of a 0.45 μm nitrocellulose filter on co-cultivation medium. The plates were set in the dark at 28 °C for two days. One mL of sterile water was used to wash the conidia from the surface of the nitrocellulose filter, and each aliquot of 200 μL of the conidia-containing water mixture was plated on M100 selective medium containing 50 μg/mL of G418 and 300 μg/mL of cefotaxime (to counter select the AGL-1 cells). All selective plates were incubated at room temperature for 5-7 days. After the G418 resistant colonies appeared on the surface of selective medium, they were transferred to new selective medium for several rounds of screening. The mutants and transformants in this experiment were further confirmed by PCR and Southern blots. All PCR primers are listed in the Table 4.2.

***In vitro* Cas9 nuclease assay and Cas9 RNP transformation**

Before Cas9 RNP transformation, an *in vitro* Cas9 nuclease assay was conducted to confirm the Cas9 RNP cleavage activity. This assay was performed as described previously (Wang et al., 2018). Briefly, a total 20 μL reaction system composed of 200 ng of the Cas9 protein, 40 ng of sgRNA, 1×Cas9 Nuclease Reaction Buffer, and 50 ~ 100 ng of the DNA template, was mixed and incubated at 37°C for 1 hr. The cleaved DNA products were resolved

through a 1% agarose gel. The Cas9 RNP transformation was conducted as previously described (Wang et al., 2018), and the amount of donor plasmid did not exceed 6 µg per transformation plate. After transformation, the positive colonies were isolated on M100 selective medium containing 150 µg/mL of hygromycin. Three pairs of PCR primers were used to confirm the location of the integrated plasmids. Since three different FoSod5 variants were generated using this HITI strategy, the cleavage site at the 5'-terminus (SS, Fig. 4.3A) was sequenced.

β-Galactosidase (lacZ) activity assay

FoSOD5 expression and regulation was investigated under various conditions. For different pH values, M100 agar medium was adjusted to pH values ranging from 4 to 8 with a final X-gal concentration of 200 ng/mL. Regulation of *FoSOD5* under the influence of different carbon sources was investigated using M100 medium with the glucose replaced by 1% (w/v) of various carbon sources (glycerol, carboxymethylcellulose, starch, sucrose, sorbitol, and mannitol). Conidia ($\sim 1 \times 10^5$) were pipetted onto the center of agar plates with or without X-gal. For quantification of *β-Galactosidase* enzymatic activity, an O-Nitrophenyl-B-D-Galactopyranoside (ONPG) assay was conducted. FoSod5C3 was grown to the exponential stage in YG liquid medium and different chemicals (0.05% H₂O₂, 0.5 mM diamide, 0.2 mM menadione, 20 µg/mL xanthine oxidase/0.1mM hypoxanthomine, and 150 µM CuSO₄) were added to the YG medium with the fungi and cultured for an extra 3 hrs. Total protein was extracted under liquid nitrogen, and 5 µg of the total protein (diluted to 75 µL) from each treatment and 40 µL of 4 mg/mL ONPG was added to 700 µL of the reaction buffer (8.5 mg/mL

Na₂HPO₄, 5.5 mg/mL Na₂H₂PO₄·H₂O, 750 ng/mL KCl and 246 ng/mL MgSO₄·7H₂O, pH 7.0) and incubated at 30 °C for 25 min. After which, 100 µL of 1M Na₂CO₃ was used to stop the above reaction. The *β-Galactosidase* enzymatic activity was determined by spectroscopy at an absorbance of 420 nm (Cytation 3, BioTek).

RNA extraction of *Fov*-infected cotton roots and qRT-PCR

Cotton seedlings that were ~10-days-old were uprooted from soil, washed with sterile water, placed in a water-culturing box containing ~ 500 mL of nutrient buffer (1/10 Murashige & Skoog basal medium with vitamins (MS) with 0.1% sucrose, PhytoTechnology Laboratories), and allowed to acclimate for 3 days in a growth chamber. Conidia (~ 2×10⁷) were inoculated into the nutrient buffer in a water-culturing box and mixed well by gently shaking. The *Fov*-infected cotton roots were collected at different time-points (0h, 4h, 12h, 24h, 36h, 2d, 3d, 5d and 7d post inoculation) for total RNA extraction. Total RNA of the cotton roots was extracted using the E.Z.N.A.[®] Total RNA Kit I (OMEGA, Bio-tech), according to the manufacturer's instructions. Reverse transcription was immediately conducted to generate first-strand cDNA using the RETRO Script kit (Ambion) with the random oligos. The transcript expression of *FoSOD5* was determined by qRT-PCR on a Bio-Rad CFX96 instrument for the different time points of fungal infection using the primers qFoSOD5F and qFoSOD5R. The *F. oxysporum* elongation factor 1 alpha gene (*EF1α*) was used as the internal reference gene using the primers qEF1αF and qEF1αR. The relative expression levels were calculated by the $\Delta\Delta Ct$ method (Livak and Schmittgen, 2001). Three cotton roots were combined for extracting total RNA and three technical replicates were performed in this experiment. The genes and primers sequences

are listed in Table 4.2.

6 × His-FoSod5 protein purification and SOD activity assay

The 6×His-FoSod5 protein purification was conducted using a previously published method (Gleason et al., 2014). Briefly, the signal peptide (N-terminus) and GPI-anchor sites (C-terminus) of the *FoSOD5* gene sequence were removed and the middle amino acid sequence was inserted into the pHis-Parallel1 vector (Sheffield et al., 1999). The recombinant plasmid was transformed into *E. coli* Rosetta™(DE3) competent cells. Protein production was induced by the addition of 0.5 mM IPTG to a culture at an OD₆₀₀ value between 0.5 and 0.6 and allowed to grow for 4 h at 37 °C. Protein purification was performed under denaturing conditions with the prepared denaturing buffer (50 mM Tris-HCl (pH 8.0), 8 M urea, and 1.5 mM reduced glutathione) using a Ni-NTA Purification System (Thermo Fisher). A series of dialysis buffers with different concentrations of urea (50 mM Tris-HCl (pH 8.0), 6/4/2/0 M urea and 0.25 mM oxidized glutathione) were used for FoSod5 protein refolding with a 10 kDa dialysis tube. SOD proteins usually require different metals to fold into the correct structure for function. Different metal ions (ZnCl₂, FeCl₃, CuSO₄, and MnSO₄) were provided to the 6×His-FoSod5 at the final dialysis overnight. The final 6×His-FoSod5 protein was concentrated to 2 mg/mL with 3K protein concentrator tubes (Millipore Sigma).

Two methods, the nitro-blue tetrazolium (NBT) method and the SOD-WST assay, were used for assessing the enzymatic activity of the purified 6×His-FoSod5. The NBT method reflects SOD enzyme efficiency through inhibition of the reduction of NBT when superoxide is present. When NBT is reduced by superoxide, formazan is produced causing a proportional

color change to dark blue that can be monitored. Three mL of the freshly prepared reaction buffer (10 μ M riboflavin, 45 μ M EDTA, 350 μ M NBT, 60 μ M methionine, and potassium phosphate with a pH value of 7.8) was mixed to obtain different concentrations (0, 4, 10, 20 and 40 μ g) of the purified 6 \times His-FoSod5 protein and immediately incubated under the light (\sim 4000 Lx) for 20 min at 28°C. The color change of the reaction solution is an indication of formazan production, and is proportional to the amount of SOD enzyme activity. The SOD-WST assay was conducted using the EnzyChromTM Superoxide Dismutase Assay Kit (BioAssay Systems) and conducted according to the manufacture instructions. One μ g of the FoSod5 protein that was reconstituted in the presence of different metal cations was added to the WST-1 reaction buffer and incubated at room temperature for 1 h. The results were measured by spectroscopy at the the absorbance $A_{440\text{ nm}}$.

Secreted protein extraction and western blotting

A trichloroacetic acid (TCA) precipitation method was used to extract fungal secreted proteins. The fungal isolates were cultured in YG liquid medium for three days at room temperature. The resulting fungal culture was centrifuged at 13000 g for 10 min and filtered through a 0.22 μ m filter to remove hyphae and conidia. TCA was added to a final concentration of 10%, and the mixture chilled at 4 °C overnight. The solution was centrifuged at 13000 g for 10 min, and the resulting pellets were washed with ice-cold acetone at least twice. The final protein pellets were dissolved in 50 mM Tris-HCl buffer (pH=7.5), and the protein concentration was determined using a Qubit 3.0 Fluorometer with the QubitTM Protein Assay Kit (Thermo Fisher Scientific).

The western blotting was conducted with a total of 5 µg of the secreted proteins which were separated by 10% sodium dodecyl sulfate polyacrylamide gel electrophoresis (SDS-PAGE) and stained with Coomassie blue staining solution (0.1% Coomassie Brilliant Blue R-250, 50% methanol and 10% glacial acetic acid). The proteins in the SDS-PAGE gel were transferred to a nitrocellulose filter membrane (GE Healthcare) using the Mini Trans-Blot[®] Electrophoretic Transfer Cell (BioRad). Anti-GFP (Rockland Immunochemicals) and the ECL chemiluminescent detection kit (GE Healthcare) were used to detect the resulting proteins.

Confocal microscopy observation

Confocal microscopy was conducted with a Nikon A1 Confocal Microscope with an excitation wavelength of 488 nm for detecting the sGFP fluorescence. The observation was performed according to a previously described protocol (Wang and Coleman, 2019). For different chemical treatments, a mixture of hyphae and conidia was inoculated into YG medium and cultured for three days. One mL of the hyphal-conidial mixture was transferred into fresh YG medium and cultured on a rotary shaker at 18 °C at 220 rpm for 16 h. Different chemicals (0.03% H₂O₂ and 20 µg/mL xanthine oxidase/0.1mM hypoxanthomine) were added to the YG medium and cultured for an additional 2 h. At this time, samples were aliquoted, fixed with 4% paraformaldehyde, and observed by confocal microscopy using an inverted agar method (Hickey and Read, 2009).

Pathogenicity assay

Two different infection assays were used to assess fungal virulence. In the cotton root

lesion assay, cotton seeds (cultivar FM1944) were washed and surface sterilized with 20% bleach followed by 75% ethanol, washed in sterile water, and germinated on wet filter paper for 3~5 days. Cotton seedlings with cotton roots 4~6 cm in length were chosen for the infection assay and at least ten cotton roots were used for evaluating the virulence of a single fungal strain. Conidia were collected and dispersed into sterile water at a concentration of 1×10^6 per mL. Ten μ L were dropped onto the root surface and incubated in a dark, wet box for 48 h. Virulence was quantified by the length of the lesions caused by *F. oxysporum*.

For the cotton root infection assay, cotton seeds (cultivar FM1944) were planted in sterile soil and placed in a growth chamber with a 16 h 28 °C light / 8 h 24 °C dark cycle. After 2 weeks, cotton plants at a two-to-three true leaf stage were used for the infection assay, where the cotton seedlings were carefully uprooted and immersed in sterile water to remove adhering soil from the root. A set of eight seedlings were transplanted to a water-culturing box which contained nutrient solution (1/10 MS with 0.1% sucrose) to sustain the growth of the cotton plant and allowed to acclimate for four days in the growth chamber. During this time, the wild-type and mutant strains of *Fov* were inoculated to PDB and allowed to grow at room temperature for 5 days on a rotary shaker. The conidia were collected from the cultures, washed in sterile water, and suspended at a concentration of 1×10^7 conidia/mL in sterile water. Two mL of the conidia were pipetted into the water-culturing box containing the cotton plants and mixed well with gentle shaking. Each week the remaining nutrient solution in the plant culturing box was replaced with fresh nutrient solution. After 5-8 weeks, disease symptoms were recorded by photo and the cotton vascular tissue was evaluated. Based on *F. oxysporum* disease symptoms on cotton, four disease index categories were developed: 0 – no symptoms,

1 – light yellowing of the leaves and black root tips, 2 – extensive yellowing of the leaves, wilting evident, and brownish discolored vascular tissue, 3 – severely wilted plant with dark discolored vascular tissue or whole plant death. Pathogenicity assays for each strain were repeated at least twice.

4.3 Results

4.3.1 Identification of an extracellular GPI SOD protein (FoSod5) from *F. oxysporum*

Sod proteins from different fungal species were used as queries to identify five Sod proteins encoded in the *F. oxysporum* genome, which included two Fe/Mn SOD genes (*FoSOD3*: FOTG_10379; *FoSOD4*: FOTG_02058) and three Cu/Zn SOD genes (*FoSOD1*: FOTG_01421; *FoSOD2*: FOTG_16882; *FoSOD5*: FOTG_08628) (Fig 4.1A). Subcellular localization prediction analysis indicated these five Sod proteins had varied in subcellular localization where FoSod1 (a Cu/Zn SOD) was localized to the fungal cytosol while FoSod3 (a Fe/Mn SOD) was localized to the mitochondrion, in agreement with the subcellular localization of homologous proteins from other fungi (Luk et al., 2003; Yao et al., 2016). However, FoSod2 (a Cu/Zn SOD) was predicted to be localized to the peroxisome or the nucleus while FoSod4 (a Fe/Mn SOD) contains a predicted secretion signal peptide and could represent a secreted SOD enzyme. FoSod5, the final SOD in *F. oxysporum*, contains a N-terminal secreted signal (AA: 1-21) and a C-terminal glycosylphosphatidylinositol (GPI) attachment site (AA: 240), which suggests that this protein is secreted and anchored to the fungal cell wall or membrane (Fig. 4.1A). Sequence alignment of select Cu/Zn SODs revealed that like CaSod5, FoSod5 lacked two histidine sites involving in zinc binding, suggesting

FoSod5 was a Cu-only SOD enzyme (Fig. 4.8) (Gleason et al., 2014). Although the amino acid sequence similarity between CaSod5 and FoSod5 was only 33%, the predicted structure of FoSod5 was highly similar to the Cu-only CaSod5, suggesting functional similarities between the two proteins (Fig. 4.1B). Phylogenetic analysis showed that most fungi in the Ascomycota phylum contained a single ortholog of the *SOD5* gene (Fig. 4.1C). Interestingly, all the isolates of *Aspergillus* lost the GPI anchor site in the Sod5 protein during their evolution. Isolates within *Fusarium* carried a single phylogenetically conserved copy of the *SOD5* gene, which likely had diverged from the well-characterized extracellular SOD from *C. albicans*, *CaSOD5* (Fig. 4.1C).

4.3.2 FoSod5 was a functional SOD protein.

To assess the SOD activity for FoSod5, the N-terminus secretion signal peptide and the C-terminus GPI site were removed, and the middle amino acid sequence harboring the SOD domain was fused with a N-terminus 6 × His tag for protein purification using *E. coli* *Rosetta*TM(*DE3*) (Fig. 4.2B). Two SOD activity detection methods, the nitro-blue tetrazolium (NBT) method and the SOD-WST1 assay, were used for determining the enzymatic activity of the purified 6 × His-FoSod5 and the specificity for different metal ions to serve as a cofactor for FoSod5 activity.

In the SOD-WST1 assay, of all the heavy metals tested, only copper could efficiently confer SOD activity, demonstrating that FoSod5 was a copper-only SOD (Fig. 4.2D), consistent with a previous publication (Gleason et al., 2014). The traditional NBT-riboflavin method was also used to confirm SOD activity of the 6 × His-FoSod5. Under illumination, the riboflavin-methionine mixture was able to produce superoxide, and NBT was reduced to blue formazan

which can be inhibited by SOD activity. A series of the $6 \times$ His-FoSod5 protein at an increasing quantity (0 to 40 μ g) were added to the reaction buffer, and as the concentration of the $6 \times$ His-FoSod5 protein increased, a decrease in the production of formazan was evident (Fig. 4.2C) indicating that FoSod5 was a SOD enzyme able to inhibit NBT reduction. In addition, a radial growth ROS stress assay showed the $\Delta FoSOD5$ mutant had increased sensitivity to hydrogen peroxide and diamide, a ROS-generating compound (Fig. 4.1D). Collectively, these results indicate that FoSod5 is a functional copper specific SOD enzyme that may have an important role in overcoming ROS damage.

4.3.3 *FoSOD5* is up-regulated during infection of cotton.

Many fungal virulence factors have increased expression during the infection of host plants. For example, two LysM effectors from *Zymoseptoria tritici* are expressed during infection of wheat where they protect fungal hyphae against plant-derived hydrolytic enzymes (Marshall et al., 2011). In addition, the effector *SIX6*, a virulence factor from *Fusarium oxysporum* f. sp. *lycopersici*, is expressed during the early and late stages of infection of tomato and its expression is triggered by living host cells (Gawehns et al., 2014). As FoSod5 is a SOD and many of these enzymes are known to be involved in virulence in other fungal pathogens, the expression profile of *FoSOD5* during infection of cotton was investigated by qRT-PCR. The expression of *FoSOD5* was low over the initial 12 hours of infection, but this gene was drastically induced and expressed from 24 h to 7 d after infection (Fig. 4.2A). At all-time points 36 hr after infection, there was at least a >50 fold increase in *FoSOD5* transcripts, peaking at 3 d dpi (Fig. 4.2A).

4.3.4 *FoSOD5* was required for full virulence of *Fov*

The WT, *FoSOD5* mutant ($\Delta FoSOD5$), and complemented ($\Delta FoSOD5/FoSOD5$) isolates were used to investigate the role of FoSod5 in pathogenicity on cotton. In a cotton root lesion assay, *Fov* conidia inoculated on the surface of the cotton seedlings are able to infect the root tissue and cause a lesion within 48 h. While the *FoSOD5* mutant was able to cause a lesion, it was significantly smaller in size than the lesions formed by the wild-type isolate (Fig. 4.7A and 4.7 B), supporting the involvement of *FoSOD5* in pathogenicity. As *Fov* is responsible for wilting symptoms, a second virulence assay was conducted on whole plants to confirm the role of FoSod5 in infection. While the wild-type isolate was able to colonize the xylem tissue in the roots and cause some necrosis, the $\Delta FoSOD5$ mutant had reduced necrosis (Fig. 4.7C). Overall, the cotton plants inoculated with the *FoSOD5* mutant displayed less wilting symptoms, had less yellowing of the leaves, and there was less necrosis of the root xylem when compared to cotton plants inoculated with the WT and the $\Delta FoSOD5/FoSOD5$ complement isolates (Fig 4.7C and 4.7D).

4.3.5 Expression of *FoSOD5* is regulated by various carbon sources and repressed in a nutrient rich-medium.

The function of cell wall proteins (CWPs) can vary and sometimes be species-specific, as they contribute to the diverse properties of the cell wall and enable fungi to adapt to harmful environments (Gow et al., 2017). The expression of these CWPs is highly regulated; for example, *C. albicans* significantly alters the composition of CWPs in response to the availability of a carbon source, iron limitation, or hypoxia (Chaffin, 2008; Ene et al., 2012;

Sorgo et al., 2013). A *lacZ* reporter construct was generated under the control of the native *FoSOD5* promoter to further investigate the expression of *FoSOD5* in various environments. The *lacZ* gene, encoding the beta-galactosidase protein converting X-gal to the blue product which was easily seen by naked eyes, is commonly used as a reporter gene for the *in vivo* analysis of gene regulation in various organisms. After transformation, eight independent colonies were selected for analysis, and seven of these transformants produced the blue pigment when grown on M100 medium containing X-gal, indicating the *lacZ* gene can be a suitable reporter for the *in vivo* analysis of gene regulation in *F. oxysporum*. Sequencing results of six of the seven transformants revealed that error free DNA repair occurred at the sgRNA cleavage region without any nucleotide additions or deletions (Fig 4.3A, SS sites), whereas the remaining transformant had a 77 bp nucleotide deletion (Fig. 4.10).

The *FoSOD5-lacZ* reporter was used to investigate the expression pattern of *FoSOD5* when grown on various carbon sources. LacZ activity was evident using this strain when the fungus was grown on a minimal nutrient medium (M-100) for four days. When a agar plug (5 mm in diameter) was removed from the *lacZ* inducing M-100 plate and placed on a rich nutrient medium (TB3), the resulting hyphae that grew on the TB3 medium failed to have significant LacZ activity after 4 days, and the hyphae were primarily white in color (Fig. 4.4C). Even after one week, there was no significant color change of the mycelia on TB3 media. When an agar plug of the *FoSOD5-lacZ* reporter mycelia that was grown on TB3 was placed on the minimal M-100 medium, the mycelia had LacZ activity. This regulation of LacZ activity by the *FoSOD5* promoter indicates that the superoxide dismutase is dependent on the available nutrient(s).

Since the available carbon sources between the M-100 and TB3 media were different, it

was hypothesized that the carbon source in the medium may regulate *FoSOD5* gene expression. The 1% (w/v) glucose content in the M-100 agar medium was replaced with 1% (w/v) of various other carbon sources (sucrose, mannitol, glycerol, CMC, starch, and sorbitol). Four days after inoculation the mycelia of the *FoSOD5-lacZ* reporter indicated LacZ activity was evident for all carbon sources investigated, but there was a clear difference between nutrients. Interestingly, the LacZ activity of the mycelia in the presence of CMC and starch were higher than those for the other carbon sources (Fig. 4.4B), suggesting that plant-derived carbon sources may facilitate *FoSOD5* gene expression. In addition, *FoSOD5* gene regulation was investigated when in the presence of different chemical stimuli. After the addition of different chemicals including hydrogen peroxide and the ROS generating compounds diamide and menadione, the LacZ activity of the mycelia was increased to various levels, suggesting *FoSOD5* expression is up-regulated under different stimuli (Fig. 4.4D).

4.3.6 *FoSOD5* is rapidly induced under an alkaline environment.

Many virulence factors of phytopathogenic fungi, including those in *F. oxysporum*, are dependent on the pH of the surrounding environment, and therefore, we hypothesized that the pH of the medium may play a role in the regulation of *FoSOD5*. Conidia of the *FoSOD5-lacZ* reporter strain were placed on M-100 plates that have been adjusted to pH's ranging from 4 to 8 and monitored over time. In a neutral or alkaline environment (pH= 7 or 8), *FoSOD5* was induced within the first 24 hours; however, mycelia at a pH 6 did not display LacZ activity until 48 hours, and at a pH of 4 or 5 it required 3 days for LacZ activity to be evident (Fig. 4.4A).

4.3.7 FoSod5 is only associated with fungal cells

Typical glycosylphosphatidylinositol (GPI) proteins contain both the N-terminus secreted signal peptide and the C-terminus GPI site (Mayor and Riezman, 2004). These GPI proteins are attached to either the fungal cell wall or the plasma membrane. Previously Sod3, a homologous GPI protein from *H. capsulatum*, could be associated with yeast cells and secreted into the culture medium (Youseff et al., 2012). To assess the N-terminal secretion signal peptide of FoSod5, two FoSod5 variants under the control of the native promoter were generated (Fig. 4.3B). The homologous-independent targeted integration (HITI) strategy was used to insert an entire plasmid at the *FoSOD5* endogenous gene locus (Fig. 4.3A). The FoSod5C1 variant was constructed by replacing the nucleotide sequences coding for the SOD domain and GPI site (AA: 53 - 263) with sGFP; while the FoSod5C2 variant replaced the internal catalytic SOD domain (AA: 53 - 186) with sGFP (SP+sGFP+GPI) (Fig. 4.3B). After transformation, the loci of interest of three FoSod5C1 and two FoSod5C2 transformants were sequenced, confirming that all five transformants do not contain indels or other undesired alterations (Fig. 4.10). These FoSod5 variants and the wild type isolate were grown in liquid culture and after several days the supernatant analyzed for the presence of sGFP by western blot. Using anti-GFP antibody only the sGFP of FoSod5C1 was able to be detected in the liquid culture medium (Fig. 4.3C), confirming FoSod5 contained a N-terminal functional secretion peptide. When the GPI anchor is included (FoSod5C2) the protein is unable to be detected in liquid culture medium, even when up to 25 µg of the extracted protein was used for the western blot and increasing the exposure time for detection. Therefore, unlike Sod3 from *H. capsulatum*, FoSod5 was only associated with the fungal cells and was not secreted into the liquid medium.

4.3.8 Subcellular localization of FoSod5

Bioinformatic analysis of FoSOD5 indicates a GPI anchor resides after the SOD catalytic domain towards the C-terminus, and therefore this protein could be attached to the cell wall although little is known about the subcellular localization of this protein in detail. Two different modifications, a sugar modification or a lipid modification, can occur at GPI sites, and the mature protein will be sorted with a C-terminal attachment to the vesicle membrane (Mayor and Riezman, 2004). GPI proteins can be secreted and attached to the fungal cell wall under the direction of a N-terminal cleavable secreted signal peptide. Since mature proteins pass through the secretory pathway, the SOD domain was replaced with a sGFP coding sequence (FoSod5C2) which was used for subcellular localization studies (Fig. 4.3B). Surprisingly, most of FoSod5 protein were specifically localized to the fungal phialides in YG medium, a medium that is less rich in nutrients than TB3 (Fig. 4.5A). However, a weak fluorescent signal was present in conidia, fungal tips, septa, and hyphae indicating that FoSod5 also accumulated in these structures (Fig. 4.5A and 4.5B). When this isolate was grown in minimal nutrient M-100 medium, FoSod5 was localized to the conidia, hyphae, and septa, indicating a significant alteration of the subcellular localization (Fig. 4.5C and 4.5D). Interestingly, large amounts of FoSod5 was accumulated in the hyphal tips (Fig. 4.5E). The *in vivo* FoSod5 protein regulation appears to be more complex in YG medium when compared to growth in M-100 medium. A Z-series stack using confocal microscopy indicated that strong fluorescence was present in the cell wall of conidia, hyphae, and phialides (Fig. 4.11).

4.3.9 The GPI anchor is required for proper FoSod5 subcellular localization

The GPI anchor is known to play an important role in subcellular localization for many proteins. Comparison of the two sGFP constructs, FoSod5C1 and FoSod5C2 which only differed by the presence of the GPI site in FoSod5C2, demonstrated that the FoSod5C1 transformants without the GPI site had no fluorescent signal at the phialides under confocal microscopy (Fig. 4.6A and 4.6C). This finding, in conjunction with the previous result that sGFP was detected by western blot of the supernatant of the FoSod5C1 transformant, confirms that the GPI site of FoSod5 is required for proper physiological localization (Fig. 4.6A and 4.6C).

4.3.10 FoSod5 could be localized to the cell wall and septum in the presence of ROS

Increased expression of FoSOD5 was observed when the fungus was treated with various chemicals, including H₂O₂ and ROS generating compounds. Since FoSod5 preferentially accumulates to the phialides in YG medium but accumulates at the fungal cell walls/septa in M-100 media, we hypothesized that some FoSod5 proteins would be localized to the cell wall after the fungal cell recognizes the appropriate stimuli. Two different ROS-generating chemicals, H₂O₂ and xanthine oxidase/ hypoxanthine, which generates superoxide, were used to treat the FoSod5C2 transformants in YG medium. While the sGFP localization was previously found primarily at the phialides (Fig. 4.5A), in the presence of H₂O₂ and xanthine oxidase/ hypoxanthine treatments the sGFP fluorescent signal accumulated at the cell walls and septa of the FoSod5C2 transformants (Fig. 4.6A and 4.6B), suggesting that FoSod5 was localized to the fungal cell wall and septa when challenged with ROS. Statistical analysis

indicated that the frequency of FoSod5 localization to the septa was significantly different between the two treatments ($P= 0.002$ and 0.021 ; Fig. 4.6D).

4.3 Discussion

A vast amount of evidence supports the importance of ROS in fungal-host interactions. Successful fungal pathogens must overcome the cellular damage from ROS during infection (Heller and Tudzynski, 2011). In the present study, the GPI-protein Sod5 from *F. oxysporum* was shown to be a virulence factor. *FoSOD5* was gradually up-regulated during infection, suggesting that the FoSod5 protein may participate in ROS scavenging during the infection process. Mutation of *FoSOD5* led to increased sensitivity to ROS and attenuated virulence on cotton.

In fungi, the number of *SOD* encoding genes in a genome varies greatly. For example, *Saccharomyces cerevisiae* only encodes two *SOD* genes (Sod1 and Sod2) while some filamentous fungi, including *F. oxysporum*, encode five or more *SOD* encoding genes, suggesting that the expansion of the *SOD* gene family was a complex, selective process. Usually protein family expansion leads to divergence of protein function. Bioinformatic analysis indicated that the five SOD enzymes of *F. oxysporum* have a different subcellular localization. FoSod2 and FoSod5 are predicted to have evolved from FoSod1 (a Cu/Zn SOD), but they are hypothesized to be localized to the peroxisome/nucleus and cell wall, whereas FoSod1 is in the cytosol. FoSod4, which is most closely related to the mitochondrial localized SOD FoSod3, has a secretion signal peptide at its N-terminus. These results indicate that Sod proteins are translocated into different organelles/localizations which may have an influence

on the enzymatic function. Increasing evidence has shown that Sod proteins have various subcellular localizations and are re-localized under stressful conditions. In *S. cerevisiae*, the Cu/Zn SOD enzyme (Sod1) is mainly distributed in the cytosol and the Mn SOD enzyme is localized in the mitochondrion. Interestingly, Sod1 could rapidly relocate into the nucleus in response to high endogenous and/or exogenous ROS, aiding to maintain genomic stability (Tsang et al., 2014). In addition, Sod1 as a nuclear transcription factor is able to bind DNA promoter regions of oxidative resistance and repair genes and regulate the gene expressions. These results clearly indicate that the function of Sod1 is far more complex than only a ROS scavenging enzyme. In addition, some Sod1 proteins are able to be localized into the mitochondrial intermembrane space and the peroxisome (Fischer et al., 2011).

The FoSod5 protein accumulates to high levels at the fungal phialides in YG medium, suggesting that a large amount of ROS might be produced at the phialides and FoSod5 might act as a ROS scavenging enzyme during *F. oxysporum* conidiation. In addition, regulation of FoSod5 appears to be more complex in M100 medium as it was found in many locations. Although the FoSod5 protein was localized to the cell walls of conidia and hyphae in M100 medium, a strong accumulation of FoSod5 was present at the fungal tip. As rapidly growing regions, fungal tips have been shown to produce large amounts of ROS in *M. oryzae* (Egan et al., 2007). Fungal tip-localized FoSod5 might cooperate with other cytosol Sod proteins to scavenge ROS. Interestingly, when *F. oxysporum* was treated with superoxide and hydrogen peroxide in YG medium, FoSod5 was translocated to the hyphal cell wall and septa, indicating FoSod5 was not restricted to a single location in the fungal cell for function, but instead it could be translocated into other cellular regions in response to environmental stimuli.

Usually multiple virulence factors from a pathogen might cooperate to facilitate the infection process of a host plant. Other isolates of *F. oxysporum* secrete peptides which induce alkalization in plants and enhance fungal virulence during infection (Fernandes et al., 2017; Masachis et al., 2016). MAPK-mediated fungal growth on cellophane is more invasive at pH 7 than that at pH 5 (Masachis et al., 2016). In addition, alkaline treatment can increase root damage and inhibit seedling growth inhibition with ROS accumulation (Masachis et al., 2016). As the infection process is dynamic, fungi must evolve relevant strategies to overcome these pressures. *FoSOD5* was rapidly induced under an alkaline environment, suggesting that an alkaline condition may be a key induction factor during early fungal infections. The alkalization-inducing expression profiles might help fungi to overcome ROS damage at the alkaline environments.

The *SOD5* gene regulation in *F. oxysporum* was different than the regulation of homologous genes of human pathogenic fungi including *C. albicans*. For instance, the *SOD5* gene in *C. albicans* was shown to be a hyphae-induced factor and was gradually up-regulated during the hyphal induction (Heilmann et al., 2011; Martchenko et al., 2004). However, the *SOD5* gene from *F. oxysporum* was found to be regulated by external environments, since the *lacZ* assay showed there was nearly no expressions of *FoSOD5* under the rich-nutrient medium TB3. When cultured in minimum nutrient medium, the fungus showed high expression of *FoSOD5*. These results indicated that *SOD5* gene regulations largely diverged during fungal evolution. In addition, *FoSOD5* was involved in fungal pathogenicity during the infection. However, the previous evidence showed that *FgSOD5* from the closely-related fungus, *F. graminearum*, did not contribute to fungal infection (Rittenour and Harris, 2013). qRT-PCR results showed that

FgSOD5 was expressed at a low level and could not be highly induced during the infection of wheat (Yao et al., 2016). This divergence may suggest the various Sods have a different importance in virulence and could be dependent on fungus and/or host plants. Above all, *FoSOD5* expression is highly regulated by environmental factors rather than fungal development, and could be highly up-regulated during infection and contribute to virulence on cotton.

References

- Abba, S., et al., 2009. SOD1-Targeted Gene Disruption in the Ericoid Mycorrhizal Fungus *Oidiodendron maius* Reduces Conidiation and the Capacity for Mycorrhization. *Molecular Plant-Microbe Interactions*. 22, 1412-1421.
- Aguirre, J., et al., 2006. Fungal responses to reactive oxygen species. *Med Mycol*. 44, S101-S107.
- Chaffin, W. L., 2008. *Candida albicans* cell wall proteins. *Microbiol Mol Biol Rev*. 72, 495-544.
- Cox, G. M., et al., 2003. Superoxide dismutase influences the virulence of *Cryptococcus neoformans* by affecting growth within macrophages. *Infection And Immunity*. 71, 173-180.
- D'Orazio, M., et al., 2008. Regulatory and structural properties differentiating the chromosomal and the bacteriophage-associated *Escherichia coli* O157:H7 Cu, Zn superoxide dismutases. *BMC Microbiol*. 8, 166.
- Davis, R. M., et al., 2006. Fusarium wilt of cotton: Population diversity and implication for management. *Plant Disease*. 90, 692-703.
- Egan, M. J., et al., 2007. Generation of reactive oxygen species by fungal NADPH oxidases is required for rice blast disease. *Proceedings Of the National Academy Of Sciences Of the United States Of America*. 104, 11772-11777.
- El-Gebali, S., et al., 2019. The Pfam protein families database in 2019. *Nucleic Acids Res*. 47, D427-D432.
- Ene, I. V., et al., 2012. Carbon source-induced reprogramming of the cell wall proteome and secretome modulates the adherence and drug resistance of the fungal pathogen *Candida albicans*. *Proteomics*. 12, 3164-79.
- Fernandes, T. R., et al., 2017. How alkalization drives fungal pathogenicity. *Plos Pathogens*. 13.
- Fischer, L. R., et al., 2011. SOD1 targeted to the mitochondrial intermembrane space prevents motor neuropathy in the *Sod1* knockout mouse. *Brain*. 134, 196-209.
- Fones, H., Preston, G. M., 2012. Reactive oxygen and oxidative stress tolerance in plant pathogenic *Pseudomonas*. *FEMS Microbiol Lett*. 327, 1-8.
- Forman, H. J., et al., 2010. Signaling Functions of Reactive Oxygen Species. *Biochemistry*. 49, 835-842.
- Gawehns, F., et al., 2014. The *Fusarium oxysporum* effector Six6 contributes to virulence and suppresses I-2-mediated cell death. *Mol Plant Microbe Interact*. 27, 336-48.
- Gleason, J. E., et al., 2014. *Candida albicans* SOD5 represents the prototype of an unprecedented class of Cu-only superoxide dismutases required for pathogen defense. *Proc Natl Acad Sci U S A*. 111, 5866-71.
- Gordon, T. R., 2017. *Fusarium oxysporum* and the Fusarium Wilt Syndrome. *Annu Rev Phytopathol*. 55, 23-39.

- Goswami, R. S., Targeted gene replacement in fungi using a split-marker approach. *Plant fungal pathogens*. Springer, 2012, pp. 255-269.
- Gow, N. A. R., et al., 2017. The Fungal Cell Wall: Structure, Biosynthesis, and Function. *Microbiol Spectr*. 5.
- Guindon, S., et al., 2010. New Algorithms and Methods to Estimate Maximum-Likelihood Phylogenies: Assessing the Performance of PhyML 3.0. *Systematic Biology*. 59, 307-321.
- Heilmann, C. J., et al., 2011. Hyphal induction in the human fungal pathogen *Candida albicans* reveals a characteristic wall protein profile. *Microbiology*. 157, 2297-2307.
- Heller, J., Tudzynski, P., 2011. Reactive oxygen species in phytopathogenic fungi: signaling, development, and disease. *Annu Rev Phytopathol*. 49, 369-90.
- Hickey, P. C., Read, N. D., 2009. Imaging living cells of *Aspergillus* in vitro. *Med Mycol*. 47 Suppl 1, S110-9.
- Horton, P., et al., 2007. WoLF PSORT: protein localization predictor. *Nucleic Acids Res*. 35, W585-7.
- Lagopodi, A. L., et al., 2002. Novel aspects of tomato root colonization and infection by *Fusarium oxysporum* f. sp. *radicis-lycopersici* revealed by confocal laser scanning microscopic analysis using the green fluorescent protein as a marker. *Mol Plant Microbe Interact*. 15, 172-9.
- Li, C. X., et al., 2015. *Candida albicans* adapts to host copper during infection by swapping metal cofactors for superoxide dismutase. *Proc Natl Acad Sci U S A*. 112, E5336-42.
- Lin, J. R., Hu, J., 2013. SeqNLS: nuclear localization signal prediction based on frequent pattern mining and linear motif scoring. *PLoS One*. 8, e76864.
- Liu, J., et al., 2016. An extracellular Zn-only superoxide dismutase from *Puccinia striiformis* confers enhanced resistance to host-derived oxidative stress. *Environ Microbiol*. 18, 4118-4135.
- Livak, K. J., Schmittgen, T. D., 2001. Analysis of relative gene expression data using real-time quantitative PCR and the 2^(-T)(-Delta Delta C) method. *Methods*. 25, 402-408.
- Luk, E., et al., 2003. Manganese activation of superoxide dismutase 2 in *Saccharomyces cerevisiae* requires MTM1, a member of the mitochondrial carrier family. *Proc Natl Acad Sci U S A*. 100, 10353-7.
- Marshall, R., et al., 2011. Analysis of two in planta expressed LysM effector homologs from the fungus *Mycosphaerella graminicola* reveals novel functional properties and varying contributions to virulence on wheat. *Plant Physiol*. 156, 756-69.
- Martchenko, M., et al., 2004. Superoxide dismutases in *Candida albicans*: transcriptional regulation and functional characterization of the hyphal-induced SOD5 gene. *Mol Biol Cell*. 15, 456-67.
- Masachis, S., et al., 2016. A fungal pathogen secretes plant alkalizing peptides to increase infection. *Nature Microbiology*. 1.
- Mayor, S., Riezman, H., 2004. Sorting GPI-anchored proteins. *Nat Rev Mol Cell Biol*. 5, 110-20.
- Miller, A. F., 2012. Superoxide dismutases: ancient enzymes and new insights. *FEBS Lett*. 586, 585-95.
- Moradas-Ferreira, P., Costa, V., 2000. Adaptive response of the yeast *Saccharomyces cerevisiae* to reactive oxygen species: defences, damage and death. *Redox Report*. 5, 277-285.
- Mullins, E. D., et al., 2001. Agrobacterium-Mediated Transformation of *Fusarium oxysporum*: An Efficient Tool for Insertional Mutagenesis and Gene Transfer. *Phytopathology*. 91, 173-80.
- Notredame, C., et al., 2000. T-Coffee: A novel method for fast and accurate multiple sequence alignment. *Journal Of Molecular Biology*. 302, 205-217.
- Petersen, T. N., et al., 2011. SignalP 4.0: discriminating signal peptides from transmembrane regions. *Nat Methods*. 8, 785-6.
- Ploetz, R. C., 2006. Fusarium wilt of banana is caused by several pathogens referred to as *Fusarium oxysporum* f. sp. *cubense*. *Phytopathology*. 96, 653-656.
- Rittenour, W. R., Harris, S. D., 2013. Glycosylphosphatidylinositol-Anchored Proteins in *Fusarium graminearum*:

- Inventory, Variability, and Virulence. *Plos One*. 8.
- Robinett, N. G., et al., 2018. Eukaryotic copper-only superoxide dismutases (SODs): A new class of SOD enzymes and SOD-like protein domains. *J Biol Chem*. 293, 4636-4643.
- Sauer, H., et al., 2001. Reactive oxygen species as intracellular messengers during cell growth and differentiation. *Cellular Physiology And Biochemistry*. 11, 173-186.
- Sheffield, P., et al., 1999. Overcoming expression and purification problems of RhoGDI using a family of "parallel" expression vectors. *Protein Expression And Purification*. 15, 34-39.
- Sorgo, A. G., et al., 2013. Iron restriction-induced adaptations in the wall proteome of *Candida albicans*. *Microbiology*. 159, 1673-82.
- Tsang, C. K., et al., 2014. Superoxide dismutase 1 acts as a nuclear transcription factor to regulate oxidative stress resistance. *Nature Communications*. 5.
- Wang, Q., et al., 2018. Efficient genome editing in *Fusarium oxysporum* based on CRISPR/Cas9 ribonucleoprotein complexes. *Fungal Genet Biol*. 117, 21-29.
- Wang, Q., Coleman, J. J., 2019. CRISPR/Cas9-mediated endogenous gene tagging in *Fusarium oxysporum*. *Fungal Genet Biol*.
- Waterhouse, A., et al., 2018. SWISS-MODEL: homology modelling of protein structures and complexes. *Nucleic Acids Research*. 46, W296-W303.
- Yao, S. H., et al., 2016. A cytoplasmic Cu-Zn superoxide dismutase SOD1 contributes to hyphal growth and virulence of *Fusarium graminearum*. *Fungal Genet Biol*. 91, 32-42.
- Youn, H. D., et al., 1996. A novel nickel-containing superoxide dismutase from *Streptomyces* spp. *Biochem J*. 318 (Pt 3), 889-96.
- Youseff, B. H., et al., 2012. Extracellular superoxide dismutase protects *Histoplasma* yeast cells from host-derived oxidative stress. *PLoS Pathog*. 8, e1002713.
- Zurbriggen, M. D., et al., 2010. ROS signaling in the hypersensitive response: when, where and what for? *Plant Signal Behav*. 5, 393-6.

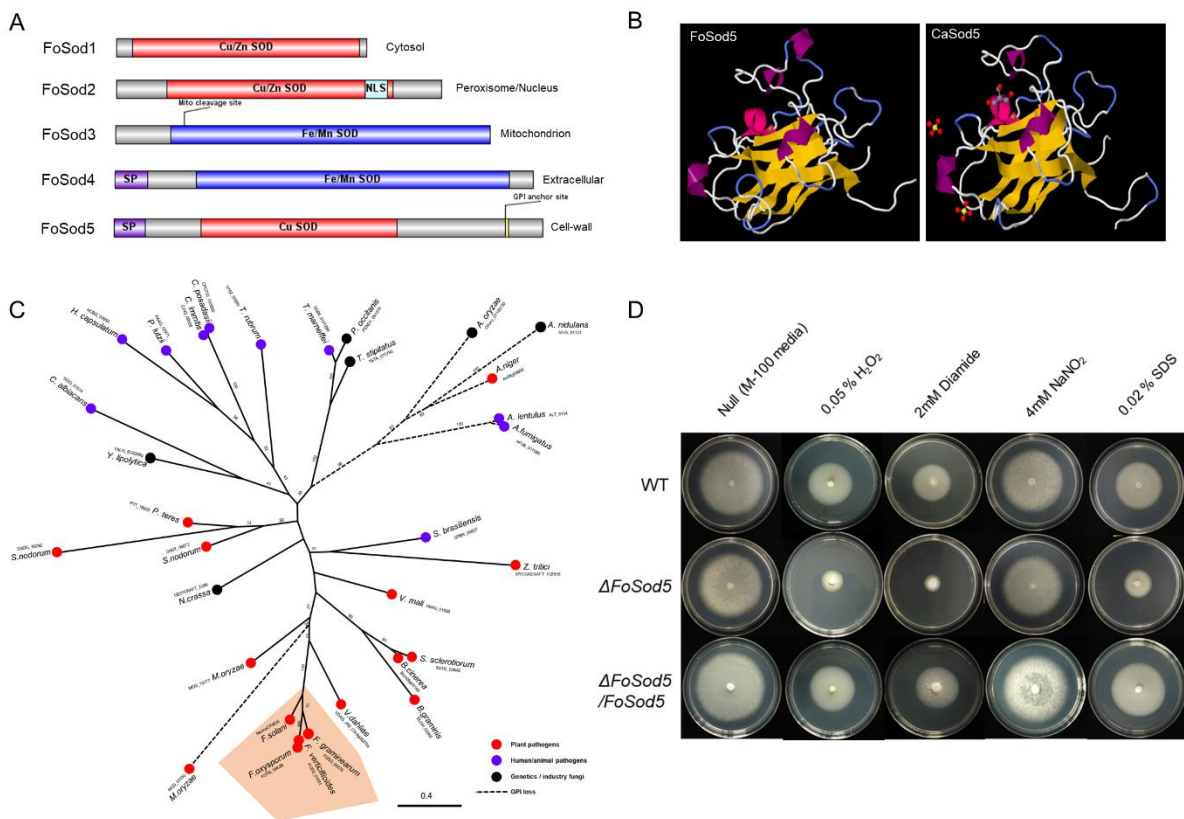


Figure 4.1 Bioinformatic analysis of the FoSod5 protein and stress assay

A) Identification of the Sod protein family in *F. oxysporum* and subcellular localization predictions of FoSod proteins. NLS: nucleus localization sequence; SP: secreted peptide B) The predictive structure of FoSod5 and comparison with that of CaSod5. C) The maximum-likelihood phylogenetic tree of Sod5 amino acid sequences from the ascomycete fungi. The tree was generated with a bootstrap value of 500. D) The evaluation of fungal sensitivity to different chemical stresses. The indicated strains were inoculated on the minimal medium (M-100).

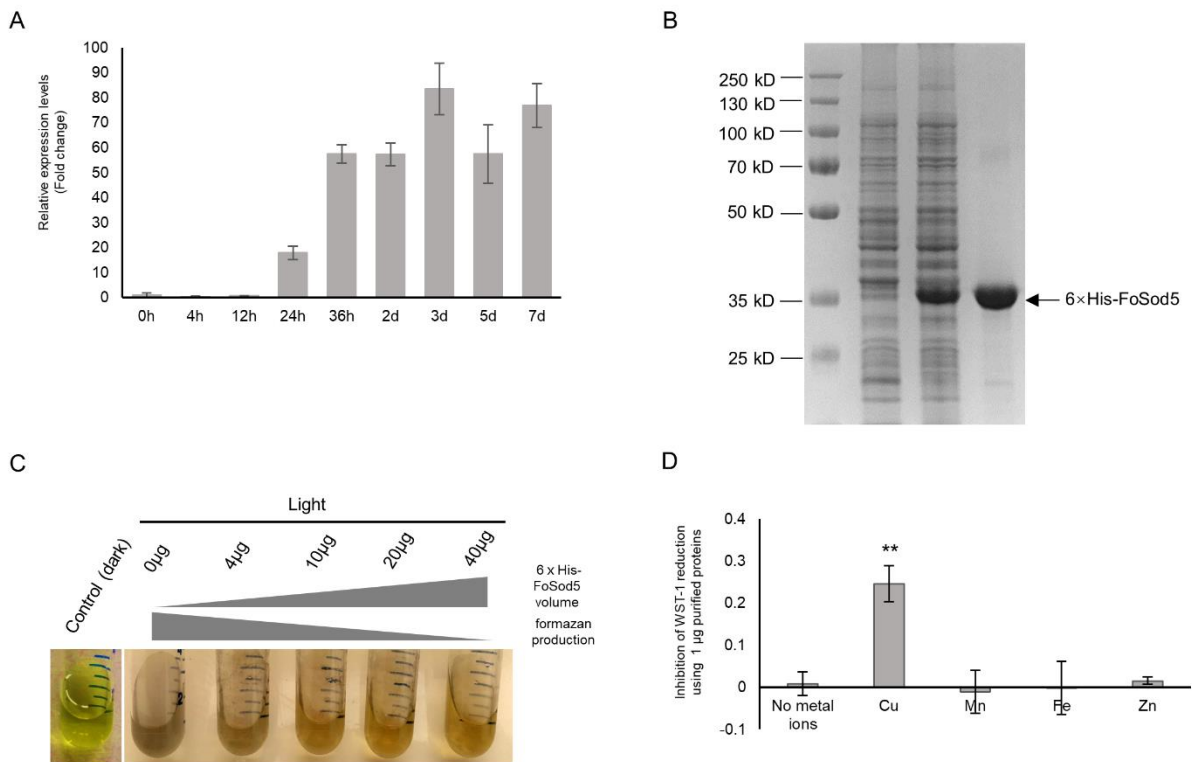


Figure 4.2 *FoSOD5* gene was up-regulated during infection and FoSod5 was a functional SOD protein.

A) The expression of *FoSOD5* during infection was measured by quantitative real-time RT-PCR (qRT-PCR) using cDNA from infected plant tissue. B) SDS-PAGE gel depicting protein expression and purification conditions. Lane 1 represents total protein before inducing; Lane 2 total protein after addition of 0.5 mM IPTG for 4 h; Lane 3 represents purified 6xHis-FoSod5 protein C) the nitro-blue tetrazolium (NBT) method was used for testing purified 6xHis-FoSod5 enzyme activity. The production of formazan decreases as the 6xHis-FoSod5 protein increases. D) Statistics analysis of 6xHis-FoSod5 enzyme activity with different metal ions using SOD-WST assay.

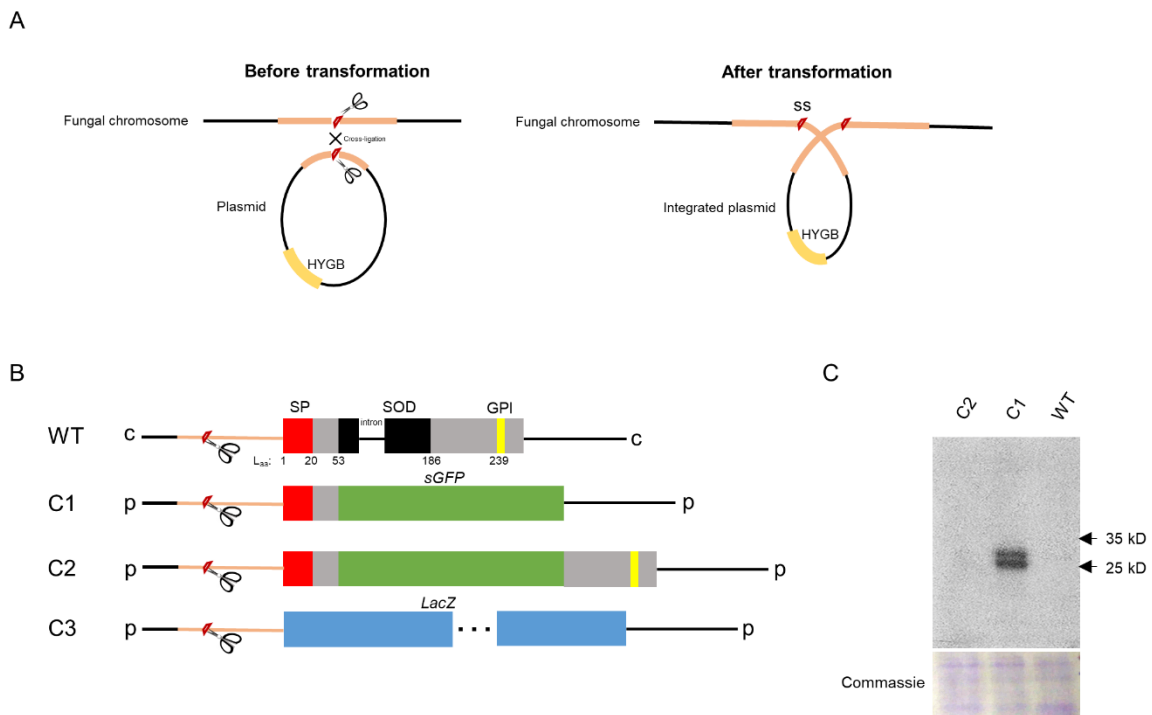


Figure 4.3 CRISPR/Cas9 RNPs-based transformant generation

A) The homologous-independent targeted integration (HITI) strategy was illustrated and the desired transformant contained the donor plasmid integrated into endogenous *FoSOD5* locus with the hygromycin cassette as the selective marker B) Schematic diagram of three different FoSod5 constructs. C1: using *sGFP* to replace the SOD domain and GPI site (SP+sGFP); C2: using *sGFP* to replace the SOD domain (SP+sGFP+GPI); C3: using *lacZ* to replace the whole ORF of *FoSOD5* gene. C) Western blotting analysis showed that FoSod5 could be only associated with fungal cells. Coomassie protein staining indicated the same volume of loading samples.

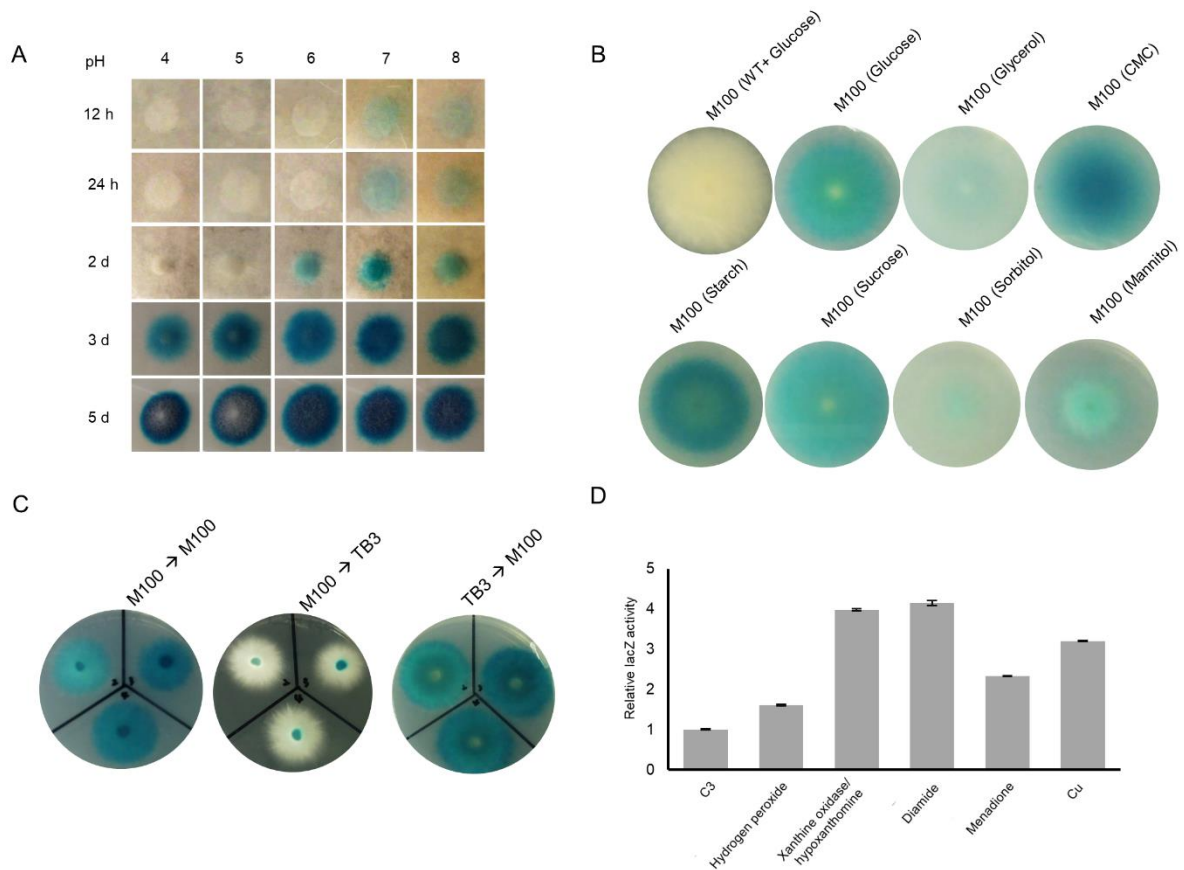


Figure 4.4 *lacZ* as a suitable reporter gene was used for *in vivo* analysis of *FoSOD5* expression under different environments in *F. oxysporum*

A) The pH value influences *FoSOD5* gene expression. The minimum medium (M-100) with X-gal and a series of different pH values were used and *FoSod5C3* transformant conidia were dropped onto the M-100 medium. The agar color changes were monitored. Under the alkaline environment (pH= 7 or 8), was *FoSOD5* gene could be rapidly induced. B) Expression of *FoSOD5* was regulated by various carbon sources C) the nutrient medium TB3 could repress *FoSOD5* gene expression. D) the *lacZ* gene showed variously up-regulated expression under different chemical stimuli.

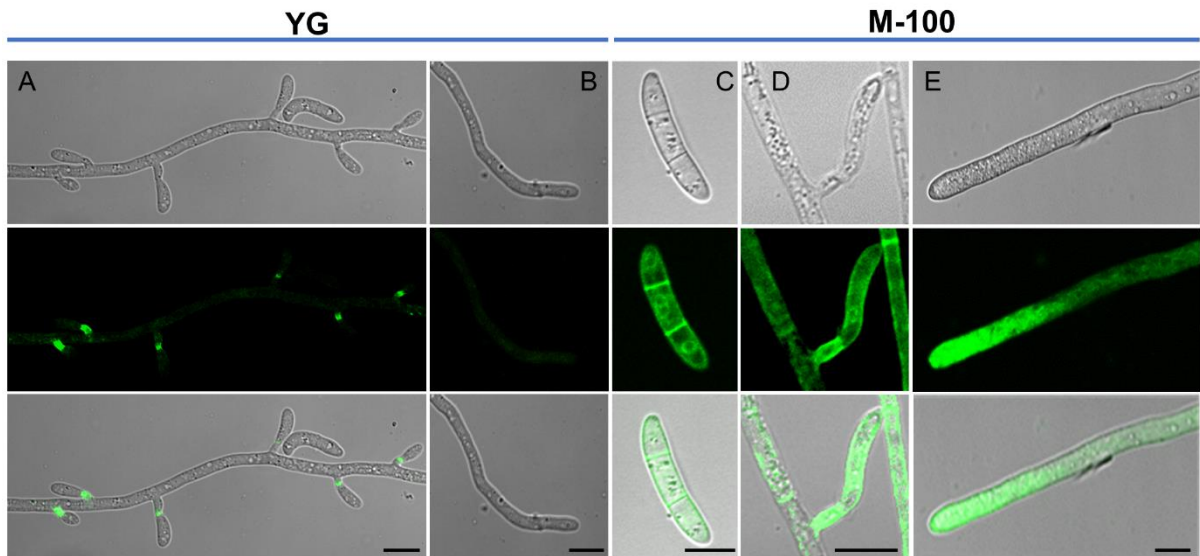


Figure 4.5 FoSod5C2 subcellular localization under confocal microscopy
 A-B) FoSod5C2 subcellular localization in YG medium C-E) FoSod5C2 subcellular localization in M-100 medium.

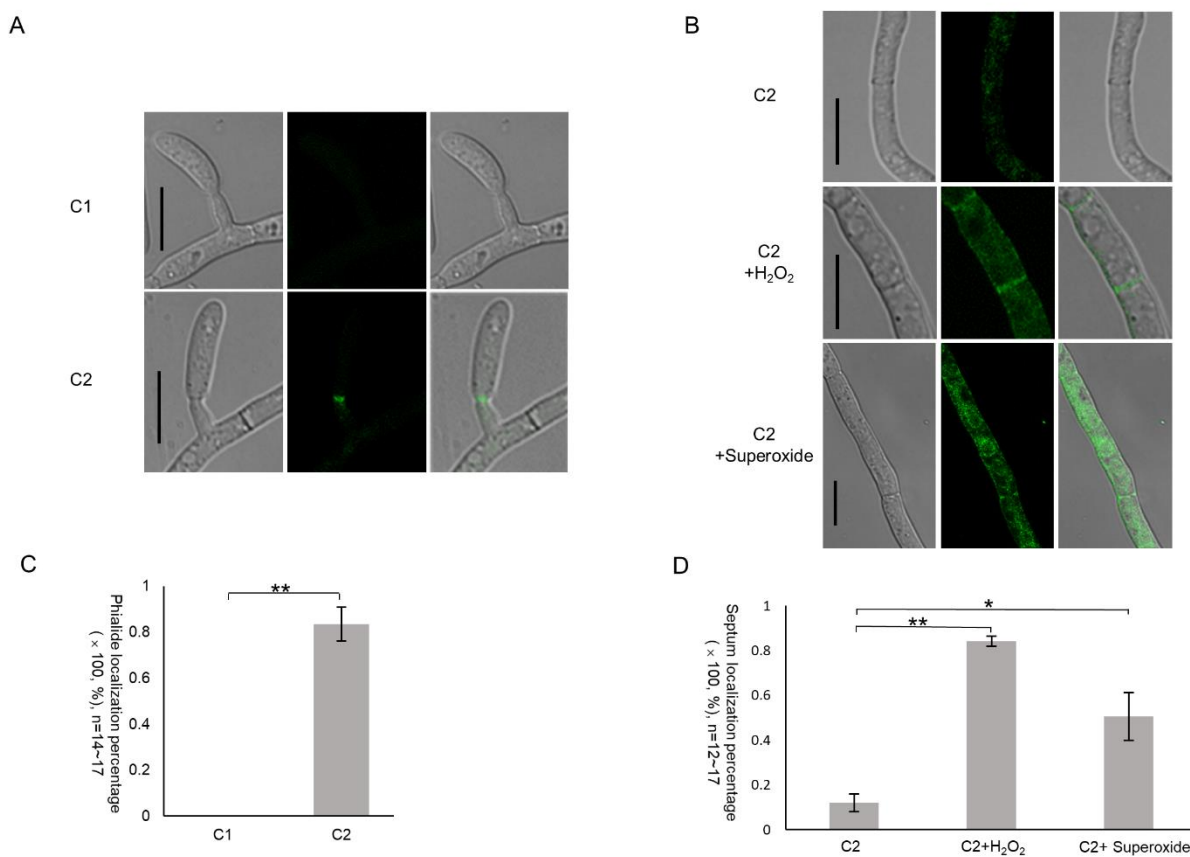


Figure 4.6 GPI site was required for FoSod5 subcellular localization and ROS treatments allowed FoSod5 to localize to cell walls and septa in YG medium.

A) phialide localization of FoSod5C1 and FoSod5C2; B) septum localization of FoSod5C2 and FoSod5C2 with treatments of H₂O₂ and superoxide (xanthine oxidase / hypoxanthine); C) Statistical analysis of phialide localization among FoSod5C1 and FoSod5C2; D) Statistical analysis of septum localization among FoSod5C2 and FoSod5C2 with treatments of H₂O₂ and superoxide (xanthine oxidase / hypoxanthine)

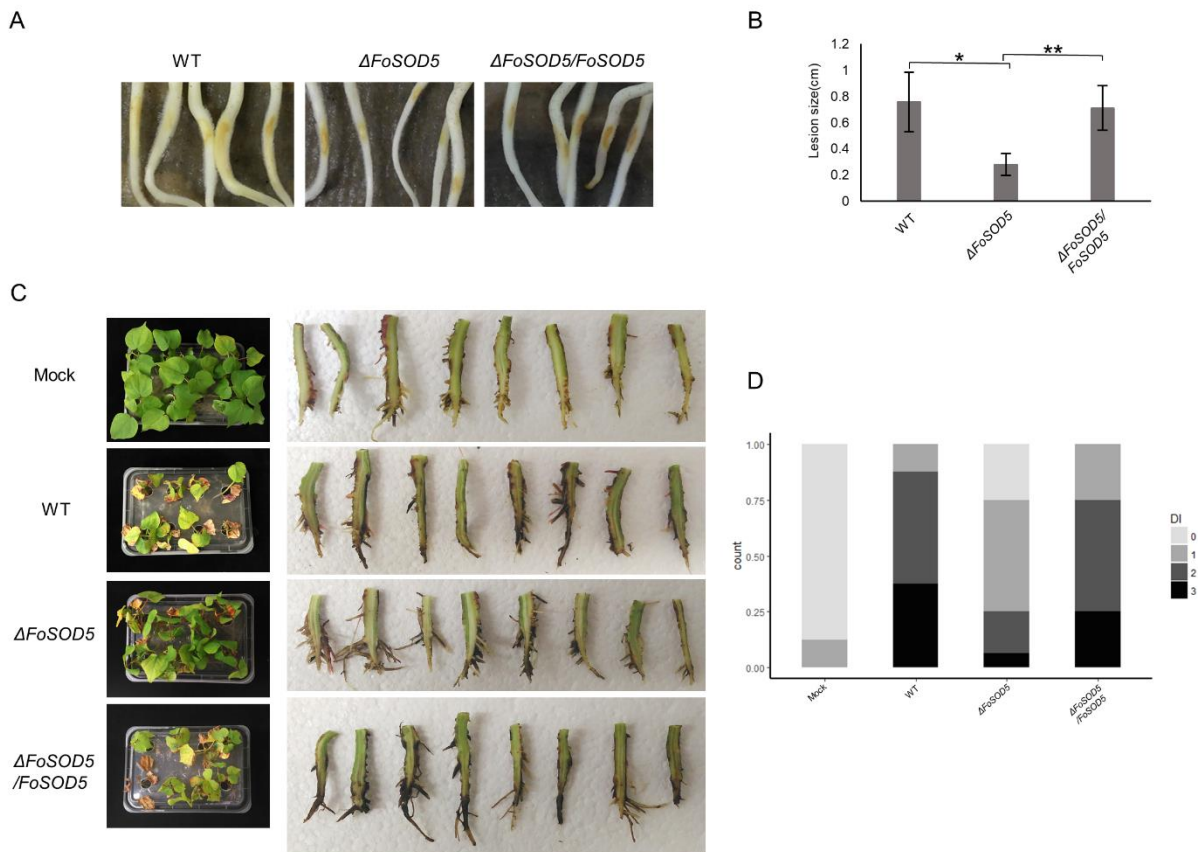


Figure 4.7 Assessment of the role of the *FoSOD5* gene in virulence on the natural host. A) Pathogenicity assay using cotton seedlings B) Statistical analysis of the size of lesions caused by *WT*, $\Delta FoSOD5$, and $\Delta FoSOD5/FoSOD5$ strains. C) The cotton symptoms caused by infections of *WT*, $\Delta FoSOD5$, and $\Delta FoSOD5/FoSOD5$ strains and control group (Mock) D) Statistical analysis of the disease index for *WT*, $\Delta FoSOD5$, and $\Delta FoSOD5/FoSOD5$ strains.

```

FoSod5  NVKGFIIQAEAPSDGHGVQFKVQFSNLPKEGGPFTYHΔHHVEPVPDNGNCTA 107
CaSod5  NIEGTIKFT-PANNGTVSVSVDLKGLPSDIGPPYHΔHVHEKVPVASKNCSA 90
CaSod1  KVQGTVHFEQESSEAPTTISWEIEGNDPNAL-RGFHΔHHΔHQFGDNTN-GCTS 61
FoSod1  KVSΔHGTVIFEQESSEAPTTITWDITGNDPNAK-RGFHΔHHΔHIFGDNTN-GCTS 61
ScSod1  -VSGVVKFEQASESEPTTVSYEIAGNSPNAE-RGFHΔHHΔHIEFGDATN-GCVS 61

TLAHLDE FARGΔHEEPPCDPEKΔHPASCQVGDNSGKHKGITSDPFTADYIDYYA 157
TENHFNΔHFYNGTVRAATPAAH----EΔHVGDLAGKHGNIMGESYKTEYDDSYI 136
AGPHFNΔHFGKQHGAPEDDER----HVGDLGNISTDGNΔHGVAK-GTKQDLLI 106
AGPHFNΔHFHNKTHGAPSDETR----HVGDLGNLETΔHDGQGNΔHAK-GSVTDSLΔHI 106
AGPHFNΔHEFKΔHKTHGAPTDEVR----HΔHVGDΔHMGNVKTDEΔHNGVAK-GSFKDSLΔHI 106

STKEGIGAYFGNRSFVΔHLHY-----ANKTRLTΔHCANF 187
SLNEKRSRYIGGLSIVIHA-----NNGTRLNΔHCANI 166
KLIGKDS--ILGRTIVVHAGTDDYGKGGFEDSKTTGHAGARPACGVI 151
KLIGPHS--IIGRTVVVHAGTDDLKGDNEESLKTGNAGPRPACGVI 151
KLIGPTS--VVGRSVVIHAGQDDLKGDTEESLKTGNAGPRPACGVI 151

```

Figure 4.8 Amino acid multiple sequence alignment of the SOD domain from FoSod5, CaSod5, CaSod1 (*C. albicans*), FoSod1, and ScSod1 (*Saccharomyces cerevisiae*).

Two ΔH sites represented the missing zinc binding histidine residues and the Δel represents the missing Sod1 electrostatic loop, suggesting FoSod5 is a Cu-only binding enzyme. R181 is a conserved site required for the activity of SODs.

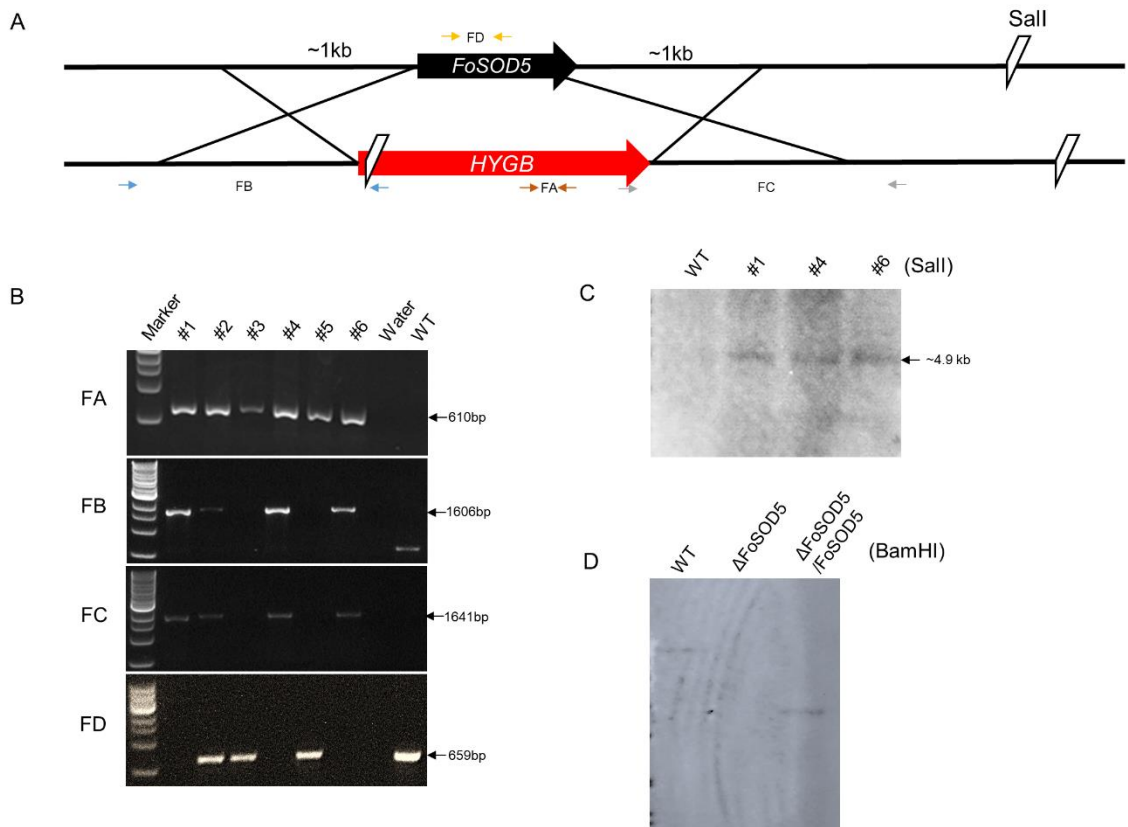


Figure 4.9 The *FoSOD5* gene replacement and complementation.

A) The ~1 kb upstream and ~1 kb downstream flanking sequences of *FoSOD5* were amplified. These two fragments were then ligated adjacent to the hygromycin phosphotransferase (*HPH*) by overlapping PCR. B) Four pairs of primers were used to assess the correct inserted position of the *HPH* cassette. C) Southern blotting was used to confirm a single integration event occurred of the *HPH* cassette in the *F. oxysporum* genome. D) Southern blotting was used to confirm the single *FoSOD5* gene cassette integrated into a $\Delta FoSOD5$ strain.

	Target	↓	PAM	
Fungal chromosome	GCTGCACAAATTCATATCAGGCTTTGCCCAACACGGATT		GGGGACTTTAGCATTTCTCG	
Donor plasmid	GCTGCACAAATTCATATCAGGCTTTGCCCAACACGGATT		GGGGACTTTAGCATTTCTCG	
Desired transformant	GCTGCACAAATTCATATCAGGCTTTGCCCAACACGGATT		GGGGACTTTAGCATTTCTCG	
FoSod5C1T	GCTGCACAAATTCATATCAGGCTTTGCCCAACACGGATT		GGGGACTTTAGCATTTCTCG	x3
FoSod5C2T	GCTGCACAAATTCATATCAGGCTTTGCCCAACACGGATT		GGGGACTTTAGCATTTCTCG	x2
FoSod5C3T	GCTGCACAAATTCATATCAGGCTTTGCCCAACACGGATT		GGGGACTTTAGCATTTCTCG	x6
	----- -77bp deletion -----		ATTGGGGACTTTAGCATTTCTCG	x1

Figure 4.10 The DNA sequences of the target region of FoSod5C1, FoSod5C2, and FoSod5C3 transformants.

The red arrow represents the cleavage site of the Cas9 RNP.

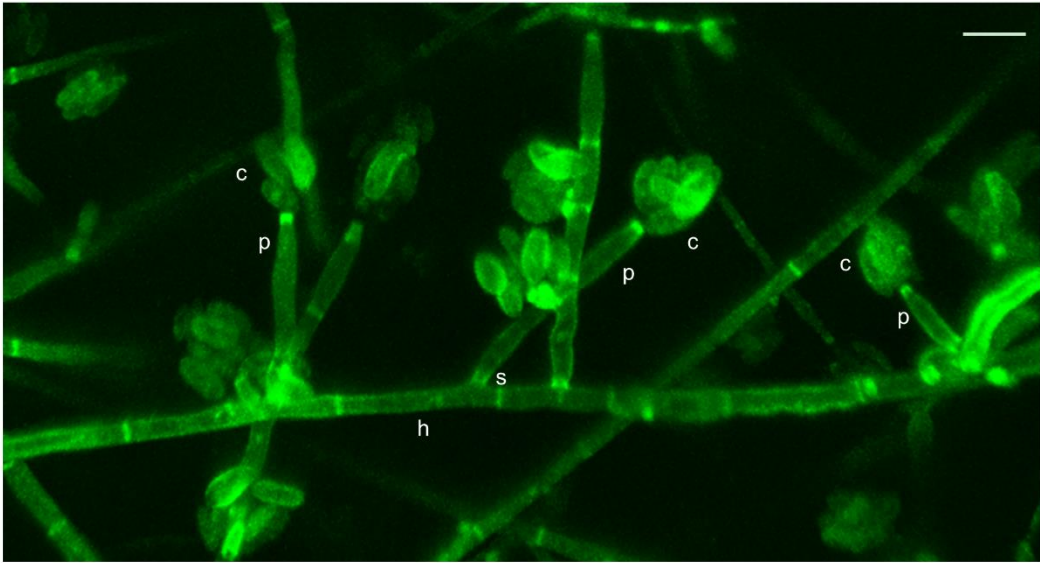


Figure 4.11 The Z-stacks analysis of FoSod5C2 on M-100 medium under confocal microscopy.

c: conidia; p: phialide; h: hyphae; s: septum

Table 4.1 Strains of *F. oxysporum* used in Chapter 4

Strain	Genotype description
10442	Wild type (WT)
<i>ΔFoSOD5</i>	<i>FoSOD5</i> gene deletion from WT
<i>ΔFoSOD5/FoSOD5</i>	The complementation strain for <i>ΔFoSOD5</i>
FoSod5C1	EGT ^{CRISPR} -based transformation of WT expressing SP+sGFP
FoSod5C2	EGT ^{CRISPR} -based transformation of WT expressing SP+sGFP+GPI
FoSod5C3	EGT ^{CRISPR} -based transformation of WT expressing <i>lacZ</i> under the native <i>FoSOD5</i> promoter

SP: secreted peptide; GPI: glycosylphosphatidylinositol sites; EGT^{CRISPR}: CRISPR/Cas9-mediated endogenous gene tagging system.

Table 4.2 The sequences of oligonucleotides used in Chapter 4

Primer names	Oligomers sequences	Usage
oIFoSOD51F	ACGGAGGGTTCCATTCCGT CA	<i>FoSOD5</i> gene replacement (knock-out) using a previously described split- marker approach
oIFoSOD52R	TTGACCTCCACTAGCTCCA GCCAAGCCTGACCACTAGG GCCCGACAGA	
oIFoSOD53F	GAATAGAGTAGATGCCGAC CGCGGGTTCGGCGGTTAGG GGTAACGGG	
oIFoSOD54R	TCCTCGGCTTGGCCTGCAT C	
HYGF1	GGCTTGGCTGGAGCTAGTG GAGGTCAACGGGGATCCTC TAGAGTCGACGG	
HYGR2	GTATTGACCGATTCCCTTGCG GTCCGAA	
HYGF3	GATGTAGGAGGGCGTGGAT ATGTCCT	
HYGR4	AACCCGCGGTCGGCATCTA CTCTATTC	
oIFoSOD57F	CGGAATCCGGGCTCGGAG AA	Detection of <i>HYH</i> cassette integration locus in potential $\Delta FoSOD5$ mutants
oIFoSOD58R	GCAAGCGTCAGCGGATCTG G	
oIFoSOD55F	GCCGCAATCGACGGCAATG T	
oIFoSOD56R	GGGAGCGTAGCAGACGAG GC	
H _{out} R	GGTCGAGCGTGGTGGCTTG A	
H _{out} F	GTCGATGCGACGCAATCGT	
NeoF_KpnI	CGGGGTACCACCCCGAA AAGTATCGACT	<i>FoSOD5</i> gene complementation for Δ <i>FoSOD5</i> mutants using the <i>Agrobacterium</i> -mediated transformation method
NeoR_XhoI	CCGCTCGAGTAATGCATTG CAGATGAGCTGTAT	
pCom_FoSOD5R	AGATTGAATCCTGTTGCCG GT	
pCom_FoSOD5F	ACACCCGAAAAGTATCGAC TC	
FoSOD5cassF	CAAGACCGGCAACAGGAT TCAATCTCTGCTCGCTGGT CGATAG	
FoSOD5cassR	GCCGGAGTCGATACTTTTC	

	GGGTGTGATTTGGGGGCAG AAGTG	
FoSod5domBamHf	CGCGGATCCGGATGACTCT CACGATGCTCC	6 x His-FoSod5 protein expression
FoSod5domHindIIIr	CCCAAGCTTTTAGGGACTA ACAACGCTAGTCTC	
qEF1 α F	CATCGGCCACGTCGACTCT	The transcript expression of <i>FoSOD5</i> by qRT-PCR
qEF1 α R	AGAACCCAGGCGTACTTGA A	
qFoSOD5F	GTCCAGTTCAAGGTCCAGT TC	
qFoSOD5R	GGCGGTACAGTTGCCATTA T	
FoSod5sgRNA1	AAGCTAATACGACTCACTA TAGGCTTTGCCAACACGG ATTGTTTATAGAGCTAGAAA TAGCAAG	CRISPR/Cas9-mediated endogenous gene tagging system was used to generate three FoSod5 variants
gRNAR	AAAAGCACCGACTCGGTG CCACTTTTTCAAGTTGATA ACGGACTAGCCTTATTTTAA CTTGCTATTTCTAGCTCTAA AAC	
FoSod5TF	CGGGCTCGGAGAAGTGTA AC	
FoSod5TR	TCGGAGCTTCAGCCTGGAT A	
NA_FoSod5C1hitiF	AGTGAATTCGAGCTCGGTA CCCGGGGCACTCGTTTTGC TTGTTG	
NA_FoSod5C1hitiR	CGCCCTTGCTCACTGCGGC ATCTTTGAAGAAAG	
NA_FoSod5C1sGFPHY GBF	CAAAGATGCCGCAGTGAG CAAGGGCGAGGAG	
NA_FoSod5C2uphitiR	CGCCCTTGCTCACTGCGGC ATCTTTGAAGAAAG	
NA_FoSod5C2midsGFP F	CAAAGATGCCGCAGTGAG CAAGGGCGAGGAG	
NA_FoSod5C2midsGFP R	CCGGGTTCAAGTTCTTGTA CAGCTCGTCCATGC	
NA_FoSod5C2downF	CGAGCTGTACAAGAACTTG AACCCGGGTGTTATC	
NA_FoSod5C2downR	GGCATGATGGTTGTCGACT GATTGCGCTACTC	
NA_FoSod5C2HYGBF	CGCAATCAGTCGACAACCA	

	TCATGCCACCAATATATTAA
	TG
NA_Psod5R	CGACGGGATCCATCTTGAG
	TGAGATGGTAAAGC
NA_lacZF	CATCTCACTCAAGATGGAT
	CCCGTCGTTTTAC
NA_lacZR	TCATTCAACCCCCTTATTTT
	TGACACCAGACCAAC
NA_Tsod5_HYGBF	GTGTCAAAAATAAGGGGGT
	TGAATGATGAAACTG
Universal_NA_forHITIT	AACAGCTATGACCATGATT
R	ACGCCAAGGGTTGCGAGG
	TCCAATG